Aalto University
School of Science

Pekka Kupiainen

Simplified concepts in modelling a multi-barrier radioactive waste disposal system and biosphere using probabilistic methods

Master´s thesis submitted in partial fulfillment of the requirements for the degree of Master of Science in Technology in the Degree Programme in Engineering Physics and Mathematics.

Espoo, September 16, 2014

Supervisor: Professor Filip Tuomisto

Instructors: Olli Nummi M. Sc. (Tech)
Tapani Eurajoki M. Sc. (Tech), M. A.

Aalto University
School of Science

ABSTRACT OF THE MASTER'S THESIS

Author: Pekka Kupiainen

Title: Simplified concepts in modelling a multi-barrier radioactive waste disposal system and biosphere using probabilistic methods

Title in Finnish: Moniesteperiaatteeseen perustuvan radioaktiivisten jätteiden loppusijoitusjärjestelmän ja biosfäärin yksinkertaistettu mallintaminen tilastollisilla menetelmillä

Degree Programme: Degree Programme in Engineering Physics and Mathematics

Major subject: Engineering Physics

Minor subject: Strategic Management

Chair (code): TFY-56

Supervisor: Professor Filip Tuomisto

Instructors: Olli Nummi M. Sc. (Tech)
Tapani Eurajoki M. Sc. (Tech), M. A.

In Finland, the disposal system for spent nuclear fuel is based on a nested barrier system where barriers are designed to confine and limit possible radionuclide release rates into the biosphere. A postulated leak in a waste canister is used to assess the performance of the individual barriers. The radionuclide migration is depicted by using a simplified solute transport model that is an alternative approach compared to numerical modelling used largely in the performance assessments.

An earlier simplified model is extended by introducing both a simplified biosphere analysis and a probabilistic simulation in order to estimate the radiological consequences of the disposal. In the simplified model, the radionuclide migration is calculated by using an analogy to a branching radioactive decay chain. The time constants of the model are solute half-times and delay times in the release barriers and biosphere compartments. A dose assessment is performed based on the resulting radionuclide inventories in the biosphere compartments. With a probabilistic simulation, initial data can be distributed and confidence levels for the release rates or dose rates can be determined.

A simulation with seven nuclides (C-14, Cl-36, Se-79, Mo-93, Nb-94, Ag-108m, I-129) using the simplified model and chosen parameter distributions and correlations reveal that the distributions for results (time constants, dose rates, release rates) are roughly log-normal or log-uniform. The median total dose rate (50 % confidence level) and cautious 95 % confidence level have about two orders of magnitude difference at most during the 10 millennia time scope. The parameters with the largest uncertainty do not affect the final result if they are not related to the most significant barriers of the system (canister or buffer). The simplified model performs well for the geosphere transport but overestimates the results of the biosphere analysis compared to earlier results with similar parameters.

Date: September 16, 2014 | Language: English | Number of pages: viii+119

Keywords: nuclear waste, disposal system, radionuclide migration, biosphere, dose assessment, probabilistic simulation, performance assessment

Aalto-yliopisto Perustieteiden korkeakoulu	DIPLOMITYÖN TIIVISTELMÄ
Tekijä: Pekka Kupiainen	
Työn nimi: Moniesteperiaatteeseen perustuvan radioaktiivisten jätteiden loppusijoitus-järjestelmän ja biosfäärin yksinkertaistettu mallintaminen tilastollisilla menetelmillä	
Title in English: Simplified concepts in modelling a multi-barrier radioactive waste disposal system and biosphere using probabilistic methods	
Tutkinto-ohjelma: Teknillisen fysiikan ja matematiikan tutkinto-ohjelma	
Pääaine: Teknillinen fysiikka	Sivuaine: Strateginen johtaminen
Opetusyksikön (ent. professuuri) koodi: TFY-56	
Työn valvoja: Professori Filip Tuomisto	Työn ohjaajat: Diplomi-insinööri Olli Nummi Diplomi-insinööri, Filosofian maisteri Tapani Eurajoki

Suomessa loppusijoitusjärjestelmä käytetylle ydinpolttoaineelle perustuu sisäkkäisiin vapautumisesteisiin, jotka on suunniteltu pidättämään ja rajoittamaan mahdollisia radionuklidien päästöjä biosfääriin. Vapautumisesteiden toimintakykyä arvioidaan olettamalla vuoto loppusijoituskapselin seinämässä. Työssä käytetty radionuklidien yksinkertaistettu kulkeutumismalli on vaihtoehtoinen lähestymistapa toimintakykyanalyyseissä laajalti käytettyyn numeeriseen mallinnukseen verrattuna.

Aiempaa yksinkertaistettua kulkeutumismallia on laajennettu sekä yksinkertaistetulla biosfäärianalyysillä että tilastollisella simuloinnilla, jotta loppusijoituksen radiologisten seurausten arviointi on mahdollista. Mallissa radionuklidien kulkeutuminen lasketaan käyttämällä analogiana haarautuvaa radioaktiivista hajoamisketjua. Mallin aikavakiot ovat kompartmenttien viipymäajat ja nuklidien pitoisuuden puoliintumisajat. Säteilyannosten arviointi tehdään pohjautuen saatuihin radionuklidien inventaareihin biosfäärin kompartmenteissa. Tilastollisessa analyysissa lähtötiedot voivat olla jakautuneita ja vapautumisnopeuksien sekä annosnopeuksien luottamustasot voidaan määrittää.

Simulointi seitsemällä nuklidilla (C-14, Cl-36, Se-79, Mo-93, Nb-94, Ag-108m, I-129) valituilla parametrien jakaumilla ja korrelaatioilla osoittaa, että tulosten jakaumat (aikavakiot, annosnopeudet, vapautumisnopeudet) noudattavat karkeasti logaritmista normaali- tai tasajakaumaa. Kokonaisannosnopeuden mediaanin (50 % luottamustason) ja 95 % luottamustason ero on suurimmillaan noin kaksi kertaluokkaa ensimmäisen 10 000 vuoden aikana. Parametrien epävarmuudet eivät vaikuta lopputulokseen, jos ne eivät liity merkittävimpiin vapautumisesteisiin (loppusijoituskapseli tai puskuri). Yksinkertaistettu malli kuvaa hyvin kulkeutumista teknisten vapautumisesteiden ja kallion läpi, mutta yliarvioi biosfäärianalyysin tuloksia verrattuna aiempiin tuloksiin samanlaisilla parametreilla.

Päivämäärä: 16. syyskuuta 2014	Kieli: englanti	Sivumäärä: viii+119

Avainsanat: ydinjäte, loppusijoitusjärjestelmä, radionuklidien kulkeutuminen, biosfääri, annoslaskenta, tilastollinen simulointi, toimintakykyanalyysi

ACKNOWLEDGEMENTS

This thesis study was carried out in the Nuclear Waste department at Fortum as a co-operation between Posiva and Fortum. After joining the department in 2013, the learning process could not have been more fruitful. The career at this point has given me significant competence in long-term safety issues and deep understanding of the whole energy industry. I am truly grateful to all my colleagues and people that I have met through my work.

I want to thank to my supervisor, professor Filip Tuomisto, for having a supportive and positive attitude towards my thesis. I am thankful for the feedback and I hope this thesis will bring new information in the field of the spent nuclear fuel disposal. Special thanks to my colleagues in the Nuclear Waste department, especially Jari Tuunanen and my instructors Tapani Eurajoki and Olli Nummi who have helped me throughout the process. Big thanks belong to also Lasse Koskinen, Kirsi Riekki and Lauri Parviainen at Posiva Oy as without you this thesis would not exist as such. I am also grateful to Thomas Hjerpe and Robert Broed at Facilia Ab for excellent guidance and feedback. Thanks everyone for the meetings, discussions and comments on the thesis drafts, they have been crucial.

The support from family and friends at all times is important in achieving anything. My parents, brothers and other family have offered great support and home in Kuopio is always a relaxing place to visit. My mother Arja has always tried to calm me down and watched over her shoulder that extends to anywhere I go. With my father Pertti, I have had many meaningful conversations that have helped me significantly in life. My brothers Juho and Matti have always been supportive and I will continue to depend on you.

I want to also show my appreciation and gratitude towards to all great people I have met during my years of studying. After all, you have had significant effect on my motivation and desire to pursuit the challenging degree. Thanks to my friends for great times in all various occasions from course projects to rock festivals. Having friends like Antti, Ville or Martti has brought me great doses of positive energy in everyday life. Friendships are golden now and they will continue to be. After this checkpoint in life, life continues, new challenges appear and I could not be more excited to do my best. There are still legendary moments to come and getting to be involved in those is definitely worth the effort.

Espoo, September 16, 2014

Pekka Kupiainen

TABLE OF CONTENTS

LIST OF ABBREVIATIONS AND SYMBOLS

AM	Arithmetic mean
BSA-2012	Biosphere Assessment 2012 by Posiva in TURVA-2012 portfolio
BSA-RC	Reference case of BSA-2012 assessment
BP	Before present
BSO	Biosphere object
BWR	Boiling water reactor
CDF	Cumulative distribution function
FGR	Fission gas release
GM	Geometric mean
GSD	Geometric standard deviation
IMS	Intermediate sediment in a lake
IRF	Instant release fraction
KBS-3V	KBS-3 repository concept based on vertical deposition holes and vertical emplacement of the waste canisters (KBS - kärnbränslesäkerhet)
K-S test	Kolmogorov-Smirnov test for testing goodness-of-fit against empirical distribution
MLE	Maximum-likelihood estimate
NORTA	Method used for sampling correlated random numbers (NORmal to Anything)
NPP	Nuclear power plant/net primary production as a parameter
PDF	Probability density function
PSA	Probabilistic sensitivity analysis
PWR	Pressurized water reactor
RCCA	Rod Control Cluster Assembly in spent nuclear fuel
RNT-2008	An interim safety case report of Posiva on the radionuclide release and transport analysis, reported in 2008
SKB	Svensk Kärnbränslehantering Ab
STD	Standard deviation
STUK	Radiation and Nuclear Safety Authority (in Finnish Säteilyturvakeskus)
TDZ-path	A flow path in the floor of the deposition tunnel ("Tunnel Damaged Zone")
TEM	Ministry of Employment and the Economy (in Finnish Työ-ja elinkeinoministeriö)
TR	Triangular distribution
TS	Top sediment in a lake
tU	Tons of uranium
TURVA-2012	Safety case portfolio on disposal of spent nuclear fuel by Posiva
YEA	Nuclear Energy Decree (in Finnish ydinenergia-asetus)
YEL	Nuclear Energy Act (in Finnish ydinenergialaki)
YVL Guides	Regulatory Guides on Nuclear Safety by STUK
cb	Notation for the canister to buffer interface

bf	Notation for the buffer to fracture interface
bt	Notation for the buffer to tunnel interface
tf	Notation for the tunnel to fracture interface
cbf	Release path via canister-buffer-fracture
cbtf	Release path via canister-buffer-tunnel-fracture
f	Notation for the fracture to biosphere interface
δ	Dirac Delta function $\delta(t)$
δ_τ	$\delta(t-\tau)$
m_c	Solute mass in the canister
m_b	Solute mass in the buffer
m_t	Solute mass in the section of tunnel above the deposition hole
m_f	Solute mass in the geosphere
N_i	Nuclide amount of nuclide *i*
$f_{r,n}$	Response function of compartment *n* in the transport chain (1/a)
f_t	Total response function for a nuclide (1/a)
f_{cd}	Source function for gradual leaching (Bq/a)
f_{csl}	Source function for solubility limited release rate (Bq/a)
A_{max}	Solubility limited volumetric activity of a nuclide (Bq/m^3)
c_{0n}	Coefficient for the total response function due to branching(s) of transport chain (-)
r	Release rate of a nuclide (Bq/a)
$H(t-t_0)$	Heavyside step function
λ	Mass transfer coefficient (1/a)
$t_{1/2}$	Solute half-time in a compartment (i.e. compartment half-time) corresponding
λ_c	Mass transfer coefficient from canister to buffer (1/a)
λ_{bf}	Mass transfer coefficient from buffer to fracture (1/a)
λ_{bt}	Mass transfer coefficient from buffer to tunnel (1/a)
λ_{tf}	Mass transfer coefficient from tunnel to fracture (1/a)
λ_f	Mass transfer coefficient from fracture to biosphere (1/a)
λ_a	Mass transfer coefficient due to advection, runoff or infiltration in biosphere (1/a)
λ_D	Mass transfer coefficient due to diffusion in biosphere (1/a)
λ_{dis}	Mass transfer coefficient due to outflow (discharge) from a BSO (1/a)
$\lambda_{IRR,i}$	Mass transfer coefficient due to irrigation to target *i* (1/a)
$t_{d,cb}$	Delay time from canister to buffer (a)
$t_{d,bf}$	Delay time from buffer to fracture (a)
$t_{d,bt}$	Delay time from buffer to tunnel (a)
$t_{d,f}$	Delay time in geosphere (a)
t_s	Duration of the solubility limited source (a)
q	Equivalent flow rate (m^3/a)
q_c	Equivalent flow rate from canister to buffer (m^3/a)
q_{bf}	Equivalent flow rate from buffer to fracture (m^3/a)
q_{bt}	Equivalent flow rate from buffer to tunnel (m^3/a)
q_{tf}	Equivalent flow rate from tunnel to fracture (m^3/a)

q_f	Equivalent flow rate in geosphere (m^3/a)
R_i	Retardation factor (-)
V_p	Pore volume (m^3)
Kd	Distribution coefficient (m^3/kg)
CR	Concentration ratio ((Bq/l)/(Bq/d), (Bq/kg_{fresh})/(Bq/d), (mg/kg)/(mg/kg), (µg/kg)/(µg/m^3) or (µg/kg)/(µg/kg))
E_{dw}	Effective dose rate due to ingestion of contaminated water (drinking) (Sv/a)
$E_{f,i}$	Effective dose rate due to ingestion of contaminated foodstuff (Sv/a)
$E_{milk-water}$	Effective dose rate due to ingestion of contaminated milk that is contaminated due to ingestion of contaminated water (drinking) (Sv/a)
$E_{milk-pasture}$	Effective dose rate due to ingestion of contaminated milk that is contaminated due to ingestion of contaminated pasture (Sv/a)
$E_{meat-water}$	Effective dose rate due to ingestion of contaminated meat that is contaminated due to ingestion of contaminated water (drinking) (Sv/a)
$E_{meat-pasture}$	Effective dose rate due to ingestion of contaminated meat that is contaminated due to ingestion of contaminated pasture (Sv/a)
E_{inh}	Effective dose rate due to inhalation of air containing contaminated dust (Sv/a)
E_{ext}	Effective dose rate due to external irradiation (Sv/a)
$R_{C-14/C-12}$	Excess C-14/C-12 ratio (specific activity) (Bq/kg_C)
$E_{ing,i}$	Effective dose rate from C-14 due to ingestion of foodstuff (Sv/a)
p	Probability level [0,1], also denotes p-value for statistical testing when non-italic
ρ	Correlation coefficient [-1, 1]
ρ_i	Density (kg/m^3)
N(0,1)	Standard normal distribution with mean value 0 and standard deviation/variance of 1
ϕ(x)	CDF of a standard normal distribution at x
erf(x)	Error function at x
rv	Realistic value for a parameter
cv	Conservative value for a a parameter
$Var(X)$	Variance of random variable X
$Cov(X,Y)$	Covariance between random variables X and Y
$\log X$	Logarithm of variable X (10-based)
C	Constant value
LU	Log-uniform distribution
$N(\mu,\sigma)$	Normal distribution with mean value μ,
N_{log}	Log-normal distribution
U	Uniform distribution
$p_{X,Y}$	Joint PDF for random variables X and Y
min	Minimum value
max	Maximum value

1 INTRODUCTION

1.1 Background

Due to increased awareness of risks related to commercial nuclear energy, the support functions, such as nuclear waste management, have developed to form a substantial part of the industry. During the recent decades, the investments of electricity producers in nuclear waste management have increased because of regulation development and increasing waste amounts. Finding a sustainable solution for different types of wastes is partly an open issue because of extremely long time scales needed to take into consideration.

In Finland, the spent nuclear fuel originating from nuclear power plants (NPPs) in Loviisa and Olkiluoto is planned to be disposed of in a repository located in Olkiluoto. The repository is managed by Posiva and it is to be constructed as an extension to ONKALO research facility. In the current design, the capacity of the repository is 9000 tons of uranium (tU) and it is planned to start its operation in early 2020s. (Posiva, 2012a)

The use of nuclear energy and nuclear waste management in Finland is controlled by a framework of legal and regulatory requirements. The obligations for management of nuclear materials and wastes are in line with all relevant international treaties and agreements. The basis for the use of nuclear energy in Finland is given in the Nuclear Energy Act (YEL 990/1987) and Nuclear Energy Decree (YEA 161/1987). Already in the Nuclear Energy Act, the disposal of the nuclear waste is to be intended as permanent and safe so that long-term safety does not require surveillance of the disposal site. The legislation concerning nuclear energy was updated in 2008. Government Decree 736/2008 replaced Government Decision 478/1999 and it sets the legal requirements regarding the safety of disposal of spent nuclear fuel. According to the law, the Ministry of Employment and the Economy (TEM) decides on the principles to be followed regarding nuclear waste.

The regulator when considering safety of the nuclear waste management in Finland is the Radiation and Nuclear Safety Authority (STUK). The practical fulfilment of the legal requirements set out in Government Decree 736/2008 are issued in guidance documents by STUK. The guidelines for nuclear waste management are set in Regulatory Guides on Nuclear Safety (YVL Guides) and the requirements are to be met in the safety analyses for the disposal facilities.

This study is related to the KBS-3V disposal concept that is chosen for the spent nuclear fuel repository in Olkiluoto. The concept has been introduced by Svensk Kärnbränslehantering Ab (SKB) that is responsible for the disposal radioactive waste, including spent nuclear fuel, in Sweden and it has been developed in co-operation. The KBS-3V concept is based on a nested barrier system consisting of copper canisters, bentonite buffer and the tunnel backfill (containing bentonite) forming the engineered barrier system and host bedrock forming the natural barrier system.

The safety of any radioactive waste disposal facility is based on release barriers. The safety of a disposal facility depends primarily on how effectively the barriers can confine or limit the release of radionuclides over relevant time scales. In the KBS-3V concept, the safety primarily relies on total confinement of the copper canister. The bentonite buffer around the canister limits the groundwater movement around the canister, protects the canister from rock movements, limits the microbial activity at the canister surface and limits the radionuclide transport in case of canister leak. A leak in a disposal canister poses a risk as the groundwater flow could transport the radionuclides to the surface environment. Radionuclide release in the biosphere may pose a risk to humans that needs to be minimized with careful planning of the waste disposal system.

The safety analysis concept has been developed over the recent decades to assess the risks related to the geological disposal of nuclear waste. Extensive research has been conducted in order to clarify the safety aspects and uncertainties related to different concepts of geological radioactive waste disposal systems. The information is combined with the estimated radiological risks in analyzing the safety of the disposal systems. In principle, the geological disposal should not pose a significant threat to future generations living at the disposal site and to estimate the risk in the future, various modelling is required. The modelling of performance of the release barriers consists typically of a chain of consequent models. The reason behind many models is that the physical and hydrological processes that determine the performance of safety functions are complex in nature. The safety analysis considers all the related safety functions of a repository and assesses the safety of the whole disposal system.

Due to complex processes that determine the performance of safety functions in a repository, a cautious (also called conservative) approach is used in determining the simplifications and parameter data for the models. Cautious means that the decisions made in the modelling process should neither overestimate nor overly underestimate the performance of the safety functions. In practice, the decisions in the modelling process preferably result in a slight overestimation of the radiological consequences for humans or other biota. This principle is in line with the YVL Guide D.5 requirements set in paragraph A06 (STUK, 2013).

For radionuclide transport modelling, different types of numerical compartment models are used commonly. Numerical models are a necessity when geometrically, physically and chemically detailed and complicated systems are modelled. Based on an integrated model response of the whole system, it is difficult to estimate the importance of transport barriers on the performance of the repository system. In addition, in many cases, several codes are applied for different parts of the nested compartment system. As a result, the transparency in the analysis suffers and the significance of an individual barrier in the system is not clear to resolve. Understanding the relative importance of the different barriers helps in judging, for example, the impact of various uncertainties on the release rates and dose rates.

A recently developed simplified model of nuclide transport in geosphere (Poteri et al., 2012) is used as a basis of developing the model to be used in this thesis. The benefits of the simplified concepts are a simple description of the nested compartment system and surface environment as well as a straightforward way to identify the most

significant barriers and parameters in the system. The results obtained for the geosphere release rates with the simplified model are not significantly different from comparable numerical results (Poteri, 2013). The biosphere analysis was not originally included in the simplified model. However, in performance assessments the biosphere has been extensively analyzed with sophisticated numerical models and with cautious, more simple screening models (Posiva, 2012a).

1.2 Objectives of the study

In this study, the simplified model of geosphere transport (Poteri et al., 2012) is extended to include a simplified biosphere analysis. The radionuclide migration in the biosphere and dose assessments are also performed based on likely projections of the surface environment evolution and present-day human habits. The performance of the spent fuel repository is assessed by using the Posiva's reference scenario where a single canister with an initial defect is emplaced in the repository. Due to the simplified nature of the analysis, time-dependent phenomena such as permafrost and glaciation are not considered. The modelling of such a leak is one way to demonstrate the safety features of the disposal system and estimate the radiological risk related to the disposal system. The efficient retardation of radionuclides forms the basis of the safe and secure waste disposal system. The focus in this study is on the uncertainties of the physical quantities and their effect on the results of the modelling process.

Simplified modelling concepts with larger transparency in the analysis can be used to highlight the main aspects of the safety of a disposal concept. The reduced accuracy and improved computational performance in the analysis can still produce valuable information and often provide a new redundant analysis method for use. In general, the modelling of the nuclide transport in the geosphere and biosphere includes processes and data with large uncertainties. By identifying the most significant uncertainties and assessing their importance, the research resources can be better allocated. The information achieved helps focusing on areas that are important and significant in respect to the long-term safety of the disposal system.

Generally, the modelling of the radionuclide transport from the repository includes parameters that can be considered stochastically distributed due to uncertainty. Therefore, a Monte Carlo simulation is implemented in order to extend the concept to cover also different types of realizations of the system. Instead of obtaining only one realization of the modelled disposal system, a large number of realizations are used. For a single realization, the parameters for the system are randomly sampled from distributions that are determined beforehand using available knowledge and expert judgment. The resulting dose rates from a simplified model with parameter uncertainties included are also compared to the Posiva's reference scenario results.

The significance of the release barriers and biosphere compartments in the radionuclide transport may vary between the different realizations. By obtaining a large number of simulated realizations, confidence levels can be determined for the release rates to biosphere and dose rates to an exposed individual. In this study, effect of parameter uncertainty on the total result of the calculation is examined. This includes the

significance of distribution selections for the parameters and dependencies (correlations) between the parameters.

The objectives of the study can be summarized as follows:

- Extending the simplified model with a simplified biosphere analysis.
- Developing the model into a probabilistic Monte Carlo simulation.
- Determining distributions for the parameters of the model.
- Determining the results including distributions of time constants, release rates to biosphere and total dose rates and comparing them to earlier results
- Identifying key uncertainties and parameters regarding the final results.

1.3 Structure

The structure of the thesis covers the description of the KBS-3V disposal system and of the Olkiluoto site evolution in Section 2. The modelling concepts on a general level for the geosphere and biosphere analysis are largely based on earlier research. The mathematical formulation of the simplified model regarding the geosphere and biosphere is presented in Section 3. The geosphere transport model is adapted from the study in (Poteri et al., 2012). The biosphere model is developed for the needs in this study based on a cautious screening model by Posiva (Posiva, 2014b). The biosphere modelling includes also dose assessment calculations for a member of the most exposed group.

Probabilistic calculation methods used in the analysis are introduced in Section 4. The use of the Monte Carlo simulation in obtaining the confidence levels is similar to the approach in (Nummi et al., 2012). The sampling procedure from various distributions used in the simulations is also presented using a mathematical approach.

The parameter selections for the base case in this study are also presented in Section 4. The most of the data are adapted from Posiva reports (Cormenzana, 2013b) and (Posiva, 2014a) but also some processing of data is conducted. The determination of parameter correlations is also presented and hypothetical calculation cases varying the base case assumptions are presented.

The calculated results are presented in Section 5. The simulated time constants, which determine the radionuclide transport in the model, are studied first. Then, the results from a base case are presented. The last results are calculated by varying the base case assumptions in order to determine the significance of decisions related to parameter selections and dependencies. The thesis ends with discussion and conclusions in Section 6 and a summary of the study in Section 7.

2 MODELLING CONCEPTS

The radionuclide transport modelling is based on simplified modelling of known processes that transport contaminated solutes (via groundwater) in the geosphere and surface environment. The chemical reactions are excluded with the radionuclides (except all C-14 converting cautiously to CO_2) in the biosphere and geosphere as little knowledge is available. The development of the surface environment (i.e. biosphere) is approximated in the analysis in this study based on site-specific data.

The time scope regarding the performance of the repository system (biosphere not included) is assumed to be 100 000 years in this thesis. This differs from one-million-year time scope in Posiva's in TURVA-2012 safety case portfolio regarding spent nuclear fuel disposal. The assessment period is limited to 100 000 years because the simplifying assumptions (presented in Section 3.2) are assumed to hold up for the 100 000 years. For example, time-dependent phenomena occurring at later stage, such as a permafrost or a glaciation period, are not included in the study. For the biosphere part and dose assessment (Biosphere Assessment 2012, BSA-2012), the analysis is performed for the next 10 000 years during which also the assumptions regarding biosphere are assumed to hold up. The requirement of the assessment period for the biosphere analysis is presented in the YVL Guide as a minimum of several millennia (STUK, 2013) which is interpreted as 10 000 years by Posiva (Posiva, 2012a).

To perform the radionuclide transport calculations, an initial undetected defect is assumed in one of the canisters in the repository. With the continuing development of the canister manufacturing methods it is possible to show that the probability of more than one initially defective canister in the repository is less than one percent (Posiva, 2014b). Therefore, at the moment, one out of 4500 canisters has a defect in the reference scenario chosen by Posiva.

The groundwater can enter the canister through the hole and dissolved radionuclides contaminate the water. A leak out from the canister to the surrounding barriers and flowing groundwater in the bedrock fractures can establish migration paths for radioactive substances in the geosphere. Finally, the radionuclides may migrate in the biosphere possibly ending up to exposed human beings. Simplifications are needed to be made in the modelling process in order to estimate the radiation doses but a cautious approach provides a safety margin for the most possible scenarios.

2.1 KBS-3V repository system

The spent nuclear fuel is planned to be disposed of according to the KBS-3 (KBS - kärnbränslesäkerhet) method (Posiva, 2012a). The method consists of engineered barriers and host rock as a natural barrier. These also form the part of the disposal system that is located in the geosphere (i.e. the repository system). The KBS-3V design is based on a multi-barrier principle where copper-iron canisters containing the spent fuel are placed vertically in deposition holes in the deposition tunnels in the repository. The schematic of the method is presented in Figure 1. The location of the repository is in Olkiluoto.

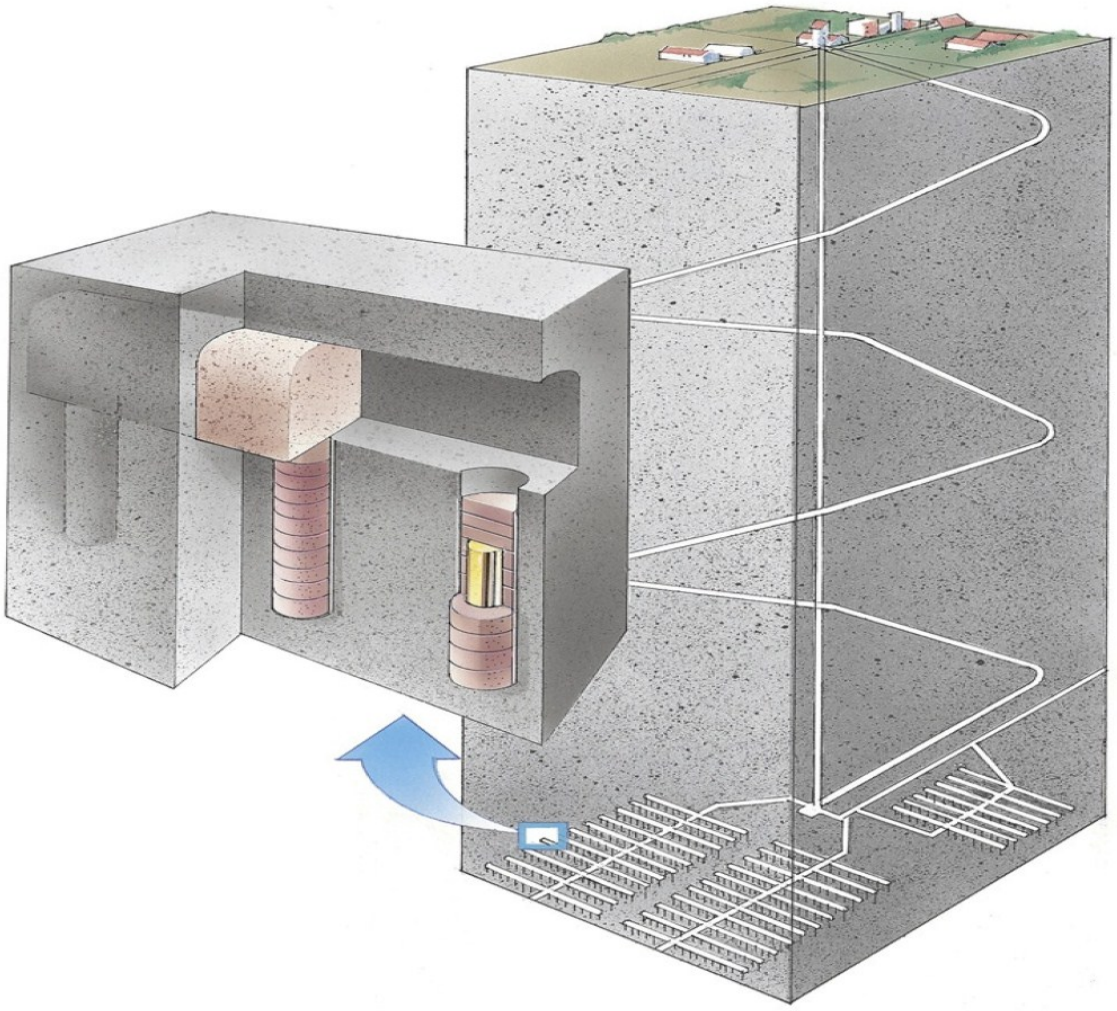

Figure 1. *The schematic presentation of the KBS-3V method. (Posiva, 2014a)*

In the KBS-3 method, the spent, sufficiently cooled-down nuclear fuel is encapsulated in water-tight and gas-tight sealed copper canisters with an iron insert (Posiva, 2014a). The copper used in the canisters is highly corrosion resistant under various conditions expected to be met at the disposal depth. Each canister is designed to contain about 2 tons of the spent nuclear fuel and in the current plans, the repository holds up about 4500 canisters. The canisters are placed in deposition holes that are drilled in the crystalline bedrock at the minimum depth of 400 m. In the KBS-3V concept, the deposition holes are vertical in respect to the deposition tunnel floor.

Swelling bentonite clay is used as a buffer to separate the canister from the bedrock. The bentonite protects the canister against minor rock movements in the deposition hole and its low hydraulic conductivity reduces groundwater flow around the canister. The hydraulic conductivity of bentonite is reported to be 10^{-13} m/s or less so the diffusion is the main transport mechanism for the solutes (Poteri, 2013).

The deposition tunnels are backfilled with a material with low permeability. In the current design, the tunnel backfill consists of bentonite and other minerals (Keto et al., 2013). The backfill is constructed by using specifically manufactured blocks and pellets that significantly prevent groundwater flow in the tunnels and provide mechanical

stability for the deposition holes. The hydraulic conductivity depends on the bentonite content of the backfill and the design basis value under expected conditions is less than 10^{-10} m/s (Keto et al., 2013). The tunnels are finally closed with a specifically designed closure structures ("plugs") that prevent the groundwater flow from the tunnels until the repository can be finally sealed. One goal for the backfill is to restore the natural conditions in the host rock. At the same time, the backfill and the sealing structures should decouple the repository from the surface environment.

The host bedrock is crystalline rock, mainly granite and has a geologically stable nature. The bedrock provides a stable environment for the repository and separates it from the surface and near-surface environment (biosphere) (Poteri, 2013). The groundwater movement in the bedrock is slow but the groundwater flowing in the bedrock proposes a transport path for solutes in the bedrock fractures. These fractures may finally end up in the biosphere. The bedrock is a natural barrier in the disposal concept and its properties need to be understood in extensively. With the information, criteria for the deposition tunnels and holes can be set with justified safety margins avoiding bedrock zones with major fractures.

The components of the geological disposal system are summarized in Figure 2. In addition to the components of the repository system, the surface environment is a part of the disposal system (Posiva, 2012a). Surface environment (regarded as biosphere) is presented in Section 2.2.

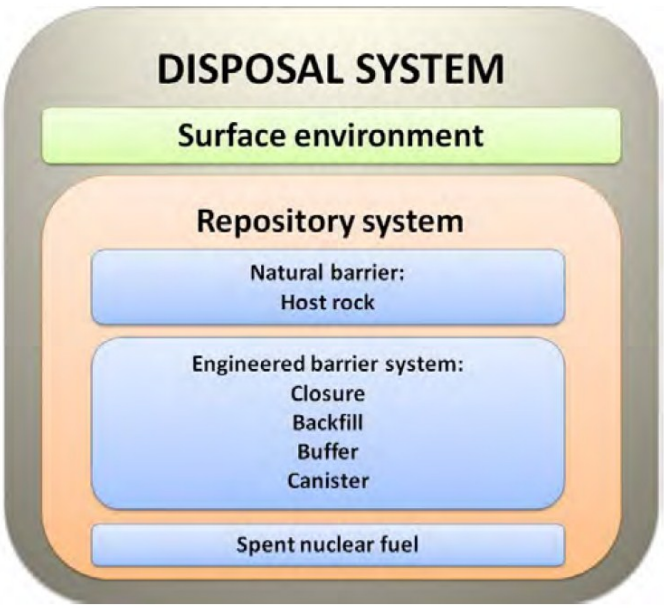

Figure 2. *The components of the disposal system in the KBS-3 method. The surface environment is regarded as biosphere. (Posiva, 2012a)*

2.2 Biosphere

The biosphere includes the surface environment from the bedrock to the lowest layers of the atmosphere. It is not considered to have such transport barriers (except sediments sometimes act as barriers) as the geosphere. Biosphere is a part of the disposal system because in the biosphere, the potential harmful risks may occur to humans and other biota. The surface environment is an open and varying system that evolves in time. In this respect, explicit time dependent analysis is recommended for better accuracy. On the other hand, the evolution of the surface environment includes large uncertainties. The processes, which include land uplift, sedimentation, water advection and erosion etc., are researched but large uncertainty is related to the properties of the surface environment as a system.

The justifications for the simplifying assumptions are critical in the sense that the results may vary and be sensitive to different parameters of the model. The aim is to make cautious assumptions regarding the radionuclide migration in the biosphere but to keep parameters related to the model as realistic as possible and avoid overconservatism. The avoidance of overconservatism is difficult due to generally inherently cautious determination of "best-estimate" values for parameters. Ideally, with realistic, more or less site-specific parameter choices, only the conceptual conservatism is left in the system.

The model for the biosphere is formulated by using compartments that represent various objects in the biosphere. The most sophisticated modelling of the Olkiluoto biosphere migration is currently conducted in the BSA-2012 where several thousands of compartments are used in the radionuclide transport modelling (Posiva, 2014b). In this thesis, a much simplified model is used to describe biosphere and formulate the most significant transport and dose paths.

The location of the repository for the spent nuclear fuel is in Olkiluoto, near the current Olkiluoto 1 and 2 NPPs. The site evolution during recent history has included a glacial period during which an ice sheet has covered the area (at around 10 000 years BP) (Posiva, 2014a). As a result of post-glacial rebound, the land uplift is a major process changing the surface environment. In Olkiluoto, the rate of the land uplift is about 6-7 mm/year, which means during the next millennia the land uplift will continue shaping the surface environment. As a result, more land emerges from below the sea surface, current lakes may dry and new ones form. Thus, the land use changes in the area.

The development of the coastal area at Olkiluoto at three projected time points is shown in Figure 3. The area around the repository forms into inland area with a few larger lakes and some rivers. During the first millennia, the large water masses around the repository decrease as the land uplift draws the coastline further west from the current location. Therefore, the mixing water volumes for possible leaks from the spent nuclear fuel repository will tend to decrease. Of course, the position of the release location affects much the resulting risks as the for example, the dilution of the substances varies. For example, the size of the largest lake that develops to the west from the repository changes little until about 12 000 years. Therefore, the mixing water volume for the

radioactive releases remains large for the dose assessment period if the release location is in the lake. The resulting doses are then likely lower than with a decreasing, smaller water volume at a different release location.

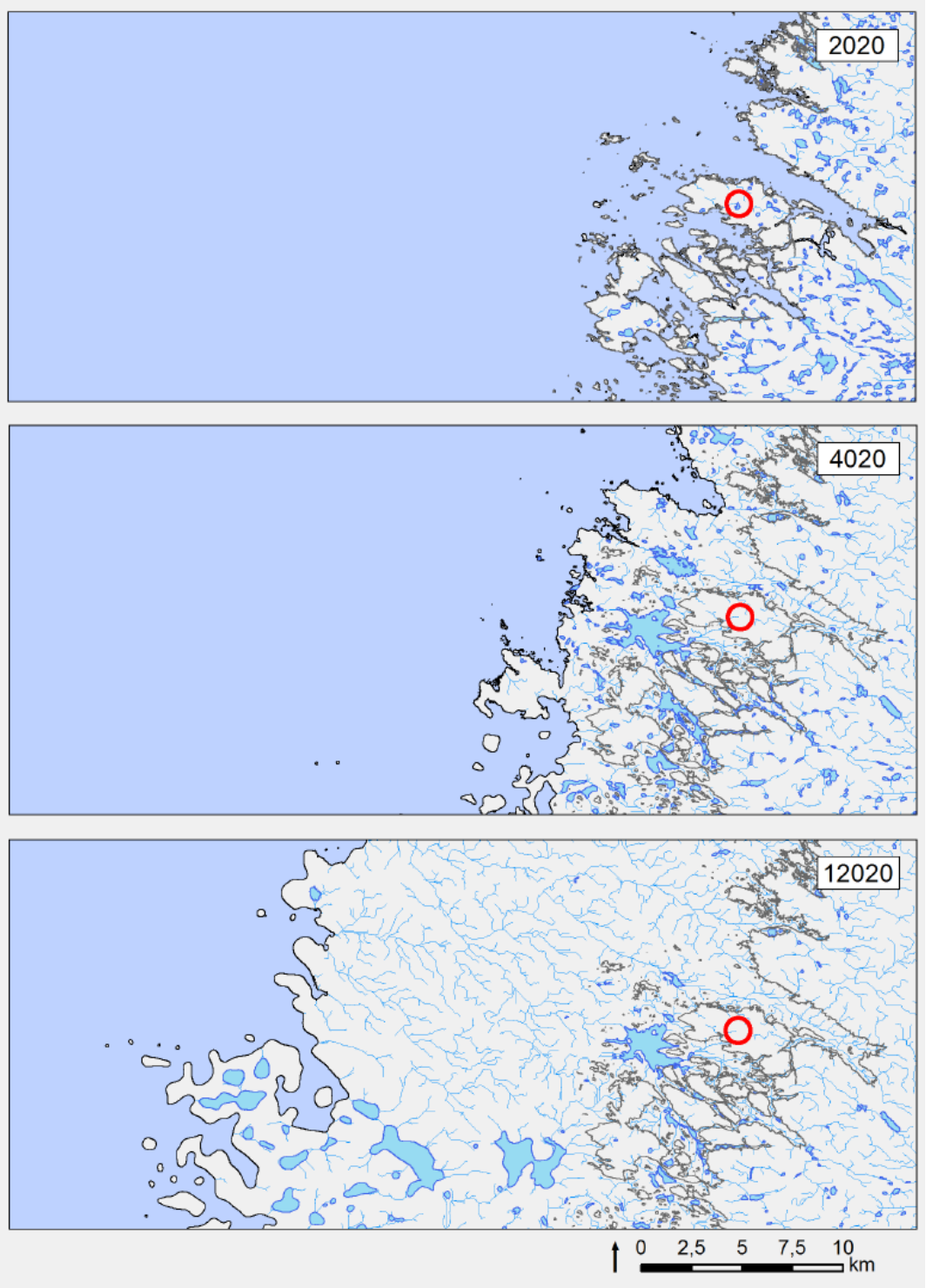

Figure 3. *The repository site and modelling area development calculated by Posiva. The red circle indicates the repository area. (Posiva, 2013a)*

The characteristics of the surface environment with the most general domains, which form around the repository, are stylistically depicted without time-development in Figure 4. It is notable that the repository is located on a growing island that already is almost connected to the mainland. Lakes or rivers are predicted to form around the island at all sides except the eastern side. Therefore, the site development suggests that the repository area and its surroundings would provide suitable conditions for human activities of various form.

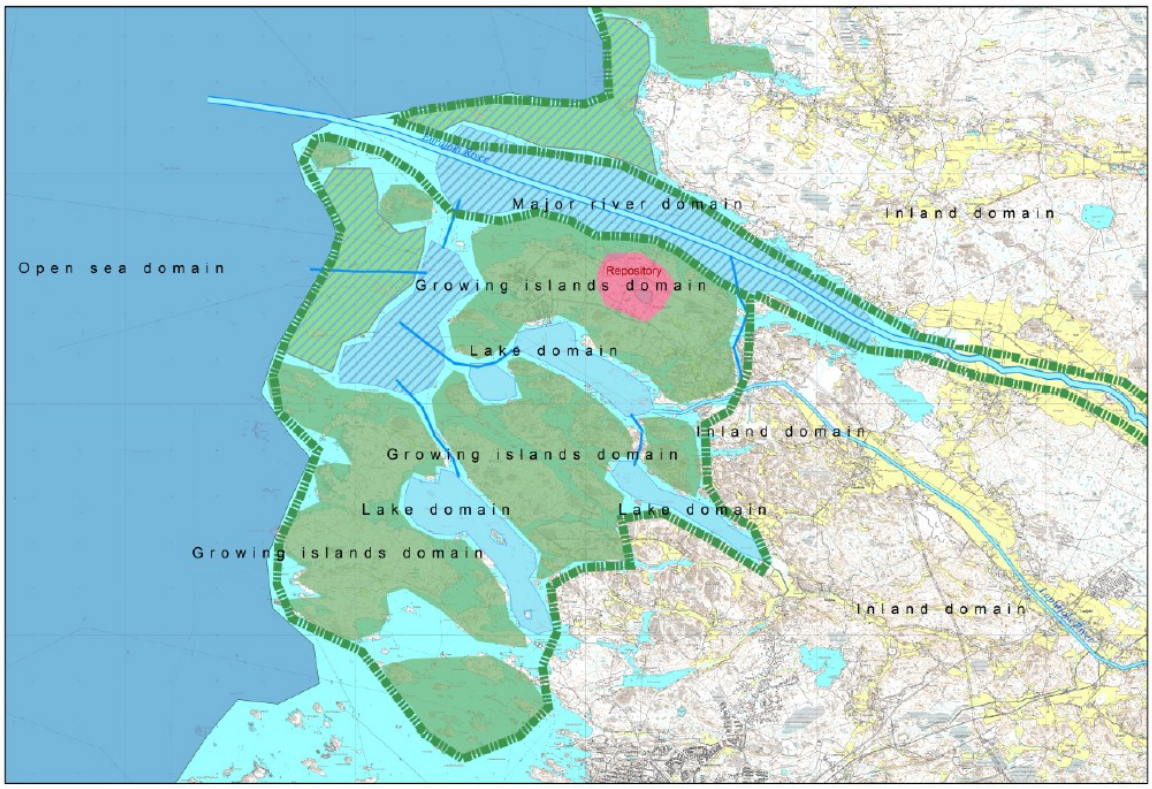

Figure 4. *The conceptual site development model by Posiva. The illustration includes the main areas around the repository in a stylistic manner without time reference. The repository area is shown in red. (Posiva, 2013a)*

The repository area, which contains the modelled release points for the radionuclides from the geosphere, is depicted in Figure 5. The release locations at 3000 and 5000 years are overlaid on the modelled biosphere development at 5020 years. In principle, the geosphere retards the radionuclides for a long time due to slow groundwater flow and good stability. At some point, it is assumed that contaminated groundwater transported by bedrock fractures may finally end up in the predicted locations.

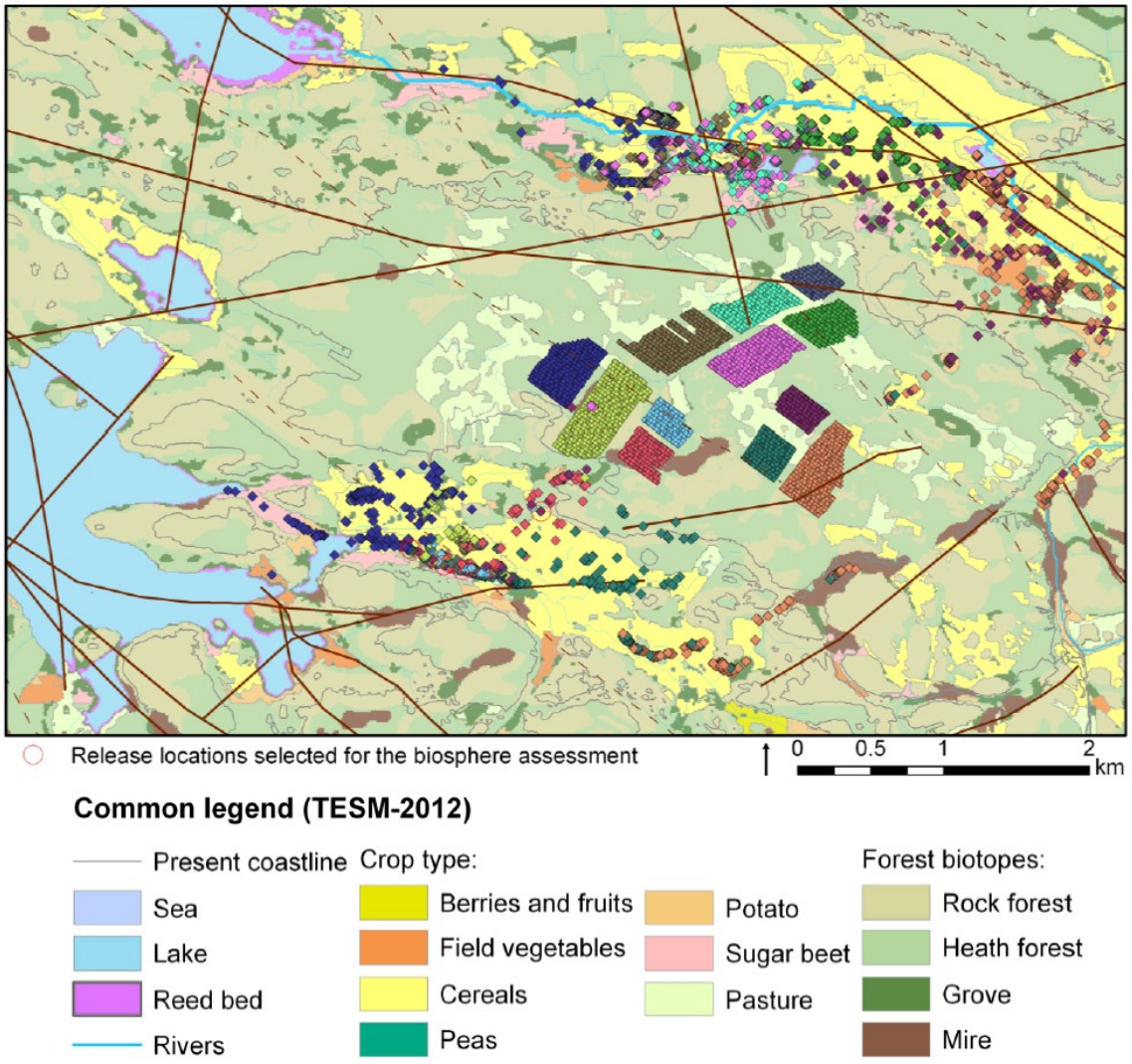

Figure 5. *The release paths from the geosphere calculated by Posiva for years 3000 and 5000 overlaid on the reference case of biosphere development at 5020 years. The brown lines depict the main bedrock lineaments. The origin of the points of the paths (canister positions) are shown in the middle colored by repository panel. The colors are the same as the respective release points and the present coastline is indicated by the grey contour. The legend to the background map is presented below the map. (Posiva, 2013a)*

The predicted biotopes are presented also in Figure 5 and, for example, most suitable crop types can be seen on the map at various locations. In practice, the area comprising the release locations may be used for various human activities in the future, which can be seen from the numerous possible locations in areas that are suitable for different crop types, forests or lakes. In this thesis, the human activities and properties of the biosphere are cautiously modelled but in practice, this leads to a generic model that is not completely site-specific (realistic). However, the site-specific parameters attempt to fix the problem to some extent and aim is to estimate a cautious average dose for an exposed individual. Following the regulations, it can be assumed that the human behavior in respect to agricultural land use and diet remains similar as currently in agricultural societies (STUK, 2013).

The biosphere model built for purposes of this thesis consists of biosphere objects that have one or more soil sediments or water volumes as compartments. The choices of objects are largely based on the biosphere assessment (BSA-2012) by Posiva and its screening model Tier 2[1] (Posiva, 2014b) (see next Section for more information). The structure and properties of the compartments in the model are decided by a credible development of the surface environment at the release site. The results from the surface hydrology modelling and terrain and ecosystems modelling by Posiva are taken into account when deciding compartments for the transport modelling. With probabilistic modelling, some variations in the biosphere objects and their properties are used to extend the coverage of the assumed biosphere objects over the time scope of the calculation.

As the last part in the biosphere assessment, the dose assessment is performed for the radionuclide release scenario from the repository. The total dose is estimated based on relevant exposure pathways for an exposed individual. A cautious principle is used to obtain conservative results for the total dose. The average total dose exposure to an exposed individual is the final quantity used to quantify potential radiological impact related to a release scenario. STUK has also set constraints for the total dose rate that are applicable to safety assessments. The constraints are also set for the release rates of the radionuclides to the surface environment.

2.3 The scope of biosphere analysis by Posiva

The research conducted by Posiva has been from the beginning aimed at a safe and secure disposal of spent nuclear fuel. The safety assessment methodology and parameter data have been developed in planned steps during recent decades. The safety case for the geological disposal facility has developed to a report portfolio called TURVA-2012 (Posiva, 2012a) and it forms a substantial part of the construction license application which was submitted in 2012. The TURVA-2012 safety case portfolio documents the scientific and technical understanding of the disposal system, including for example the release barriers and the surface environment and results of a quantitative safety assessment together with a reliability analysis. The summary of the safety case is provided in the synthesis report (Posiva, 2012a).

The biosphere analysis by Posiva has been developed to an own assessment consisting of seven reports inside the TURVA-2012 safety case portfolio. The biosphere assessment 2012 (BSA-2012) forms a significant portion of the safety case portfolio and it includes for example an assessment of environment scenarios, synthesis of site understanding and scientific methodology and input data for the assessment (with justifications). From the main reports, the data basis report (Posiva, 2014a) is widely used in this study.

[1] The screening evaluation consists of three phases named Tier 1-3. In Tier 1, all activity is assumed to end up in a 1 m^2 area where an exposed individual stays in place receiving annual dose from inhalation, external exposure or ingestion, whichever is the highest. In Tier 2, a generic biosphere model is used with maximum release rates as constant input in the system. In Tier 3, a complex, time-dependent landscape model is performed to obtain radionuclide inventories in site-specifically defined ecosystems.

The essential modelling regarding biosphere analysis is conducted in four reports. The evolution of the biosphere including the terrain and ecosystems development modelling (Posiva, 2013a), geosphere-to-biosphere interface including the surface and near-surface hydrological modelling (Posiva, 2013b), radionuclide transport in the biosphere including the dose assessment for humans (Posiva, 2014b) and for plants and animals (Posiva, 2014c) form the extensive research conducted by Posiva during recent years.

The radionuclide transport in biosphere is analyzed in BSA-2012 by conducting a screening evaluation for all the radionuclides that are possibly released to the biosphere. The radionuclides are screened out in consequent phases by ending up in Tier 3 and a landscape model of the radionuclide migration in biosphere. The biosphere model in this study is modified from Tier 2 screening model to be more realistic. In the screening model Tier 2, a cautious screening of radionuclides is conducted before the Tier 3 and landscape model calculation. In Tier 2, the maximum release rates are used as constant input in the model. The biosphere is described with small water volumes and cropland sizes in order to maximize the resulting activity concentrations. The whole release is also assumed to enter both the well and a lake to ensure a very cautious result that is sometimes beyond physical possibility.

The landscape model used for Tier 3 analysis is a complex, time-dependent and site-specific compartment model that handles thousands of compartments in order to cover many soil and sediment layers in different evolving ecosystems in Olkiluoto. The Tier 3 analysis is a sophisticated model of radionuclide migration in the biosphere that takes into account the evolution of the many possible ecosystems including mires, croplands, forests etc. Due to screening evaluation at earlier phases only a handful of nuclides are analyzed in landscape model. These nuclides are also the ones analyzed in this study.

3 SIMPLIFIED SOLUTE TRANSPORT MODELLING OF A GEOLOGICAL DISPOSAL SYSTEM

3.1 A multi-compartment model of the repository system

In this thesis, a simplified approach presented in (Poteri et al., 2012) is used to model the geosphere part of the disposal system. The nested barriers of the system are described as compartments that retard or limit the release of the radionuclides from the repository. Retardation means in this case that a release beginning at some time at the inner part of a release barrier appears later at the outer boundary of the barrier (Poteri et al., 2012). Limitation means that the maximal release rate is lowered but the duration of the release is lengthened.

The components of the repository system are presented in Figure 6. The processes, which transport the solutes containing radionuclides from the canister, are also presented with the relevant transport paths illustrated by arrows. The spent fuel is enclosed in a canister with an initial defect (hole). The buffer around the canister is assumed to be fully saturated with groundwater. The groundwater is expected to enter the canister through the initial defect as a part of the formation of the transport path from the canister into geosphere. In the scenario of the simplified model, the reference groundwater type is brackish groundwater and it is expected to prevail at least the temperate climate period, i.e. the next 50 000 years (Posiva, 2013c). Nevertheless, since the saline groundwater is also observed at depth of -400 m (Figure 7-8 in (Posiva, 2012c)) it is judged that the saline groundwater should also be considered. The presence of other groundwater types is unlikely or they are expected at a later stage.

At some point, the groundwater is able to enter the canister through the initial defect and the source term from the spent nuclear fuel consists of two parts. First, an instant release fraction (IRF) is released almost immediately after the contact with water from different parts of the fuel depending on the nuclide. The parts of the spent fuel considered in this study are the fuel matrix, zirconium alloys and other metal parts. The IRF is an assumed form of release due to dissolved nuclides that are released rapidly upon contact with water. Secondly, the degradation of different parts of the fuel occurs gradually. The gradual degradation is assumed to occur at constant speeds for different parts of the fuel. A part of the inventory could be released in gas phase instantly after the integrity of the canister is lost but the gaseous transport of nuclides in geosphere is not considered in this thesis. In the long-term analysis, the gaseous transport in spent nuclear fuel concerns only C-14 (other nuclides screened out as non-significant) and recent calculations have shown that the cautious release gaseous release rates are under the regulatory constraints (Posiva, 2012b).

From the canister defect, the radionuclides are able to enter the buffer surrounding the canister. The nuclides must pass the buffer to reach the possible bedrock fractures on the outer boundary of the buffer. The molecular diffusion is the dominant transport process in the buffer. A possible fracture intersecting the deposition hole at the position of the initial defect in the canister forms a transport path for the solute. The groundwater flow in the fracture transports the solute further in the bedrock towards the surface environment. The deep location of the repository means sparse fracturing in the bedrock

and low groundwater flow rates. Therefore, the transport distance from the repository to biosphere is long and transport slow. In the surface environment, the contaminated groundwater may be used as a water source for human activities.

Another transport branch from the buffer enters the deposition tunnel from the buffer material. The diffusion is the transfer process in the tunnel backfill as well. Hydraulic conductivity in the backfill is about the same of order of magnitude as the average hydraulic conductivity in the surrounding bedrock so the tunnel does not collect water from large area and form fast flow paths for the radionuclides. A bedrock fracture crosses the tunnel section and groundwater flow in the fracture transports the solute further in the bedrock. Again, the groundwater migrates through the bedrock and may enter the surface environment.

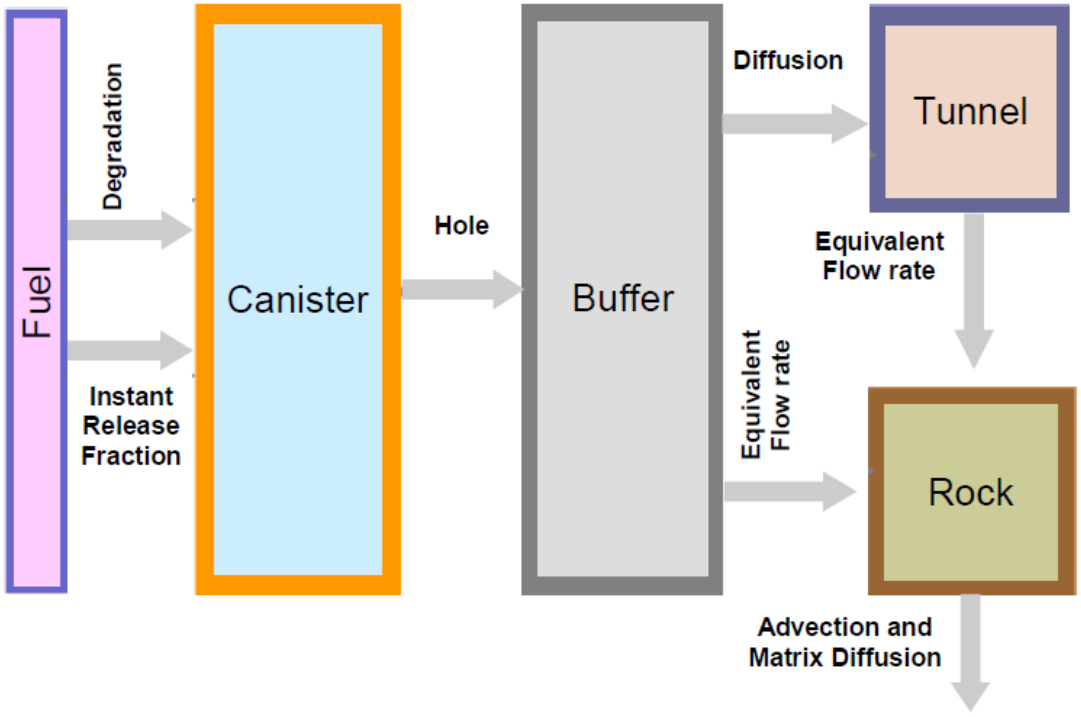

***Figure 6**. The illustration of the nested multi-barrier repository system and transport paths. Due to nested structure there are few paths for solute transport. (Poteri, 2013)*

Solute transport in the geosphere barriers is modelled with simplified concepts in (Poteri et al., 2012). In the model, the solute transport of the multi-barrier system is modelled based on nested compartments that depict the release barriers. The main features of the model include the following assumptions (Poteri et al., 2012):

- All the barriers are fully saturated with water.
- Mass transfer between barriers occurs only to one direction from inner barriers to outer barriers meaning that the mass flux between two barriers is determined by assuming a zero concentration in the target barrier (i. e. there is no counter pressure caused by the target barrier).
- The system consists of reservoirs in which capacities are connected by resistances that limit the mass fluxes.

The mathematical description of the system and solute transport can be simplified by taking the characteristic behavior of mass transfer into consideration. The mass transfer between successive barriers is strongly restricted by the interfaces between the barriers. These interfaces are for example a small hole in the canister or a thin fracture intersecting the deposition hole. Thereby, the diffusive mixing leads to a homogenous concentration profile of the solute in the pore volumes of individual transport barriers and a well-mixed state is reached in every compartment.

The well-mixed barrier volumes allow to assume that the mass outflow from a compartment depends linearly on the concentration. The behavior of a single barrier is described by equivalent flow rate of the solute that essentially depends on the volume of pore space of a barrier and mass flow out of that barrier. Because of the design of the repository system, the pore volume of the succeeding barrier in the system is usually much larger than the volume of the previous one. Also, mass transfer coefficient into a barrier is usually much smaller than the one out of the barrier. Therefore, the back coupling of the solute transport is weak and zero concentration in the target barrier can be assumed. This assumption is also conservative regarding mass fluxes.

The well-mixed state of the compartments means there is not assumed to exist any concentration gradients in the volumes where the transport occurs. The effect of the barriers can be described with two parameters:

1) half-time of the solute in the barrier and

2) delay time of the barrier.

The half-time of the solute describes how the barrier attenuates (limit) the release rate and disperses the release pulse. The inverse of the lifetime multiplied with $\ln(2)$ is called the solute decay constant or a mass transfer coefficient. The delay time describes the time interval that is needed for the transport path to form. The delay occurs due to retardation of the solute in the barrier volumes. This time elapses until the compartments are in a well-mixed state and it is a translation in time for the release pulse.

Because the individual barriers are represented by the half-times of the solute and sequential topology of the barriers, the system is analogous to a radioactive decay chain. The time behavior of a radioactive decay chain with branches can be solved with a straightforward way and an analytical solution for the system is obtained. The benefits of the model are that the functionality of individual barriers can be assessed using response functions and results are usually comparable to actual numerical modelling results of the repository system.

The release paths described above are based on the assumption that different components of the engineered barrier system perform as designed. The changes in the physical or chemical conditions cannot be completely ruled out but some amount of variability of the conditions may be taken into account by introducing a simulation where parameters have pre-set distributions from which the values for each realization

are picked. Also, uncertainty in the models parameters needed for the calculation supports the probabilistic approach.

The nuclides considered in this report are listed in Table 1. The chosen nuclide set is based on the biosphere analysis in TURVA-2012 safety case by Posiva. In the BSA-2012, the chosen nuclides are considered to be the most critical in terms of long-term safety of the disposal of spent nuclear fuel during the assessment period. The inventories are calculated using 2 tU per canister (Cormenzana, 2013a). The selected inventories are based on obtained inventories in (Cormenzana, 2013a) that take into account different types of spent nuclear fuel and burnup. In the calculations, each part in the inventory have specific IRF portions and rest of the inventory dissolutes at a constant rate. With the inventories, the source terms for the simplified model can be established to obtain release rates and perform dose assessment. In the calculations, Cl, Se and I are assumed to be present in anionic form and the rest of the elements transport as cationic or neutral species.

Table 1. *Radionuclide inventories and half-lives used in this thesis. (Cormenzana, 2013a)*

Nuclide	**Half-life (a)**	**Inventory of 2 tU**		
		Fuel matrix (GBq)	**Zirconium alloys (GBq)**	**Other metal parts (GBq)**
C-14 (neutral)	5700	67	49	1.9E+02
Cl-36 (anion)	301 000	2.8	9.6E-01	0.0
Se-79 (anion)	327 000	9.2	0.0	0.0
Mo-93 (cation)	4000	6.6E-01	8.6E-02	44
Nb-94 (cation)	20 300	3.6E-02	6.4E+02	8.6E+02
Ag-108m (neutral)	438	8.2E-03	0.0	5.0E+04
I-129 (anion)	15 700 000	3.8	0.0	0.0

3.1.1 Mass transfer coefficients

The dissolved mass transfers between the compartments of the repository system. The mass transfer from a compartment to the next one is proportional to the concentration in the compartment. This proportionality coefficient is called the mass transfer coefficient or the solute decay constant (λ) and it is the inverse of the half-time of the solute in the barrier multiplied by $\ln(2)$. The mass transfer coefficients are calculated based on the equivalent flow rates and pore volumes of the barriers ($\lambda = q/V_p$, (1/a)). The equivalent flow rate is an apparent volumetric flow rate that is combined with the solute concentration in the compartment to obtain the outflow of the solute mass.

From the canister to the bentonite buffer, the mass transfer coefficient can be formulated as (Poteri et al., 2012)

$$\lambda_c = \frac{q_c}{V_c}, \tag{1}$$

where V_c (m^3) is the pore volume of the canister and q_c is calculated as

$$q_c = \frac{q_{ch} q_{hm}}{q_{ch} + q_{hm}}. \quad (2)$$

In Equation (2), the q_{ch} (m^3/s) is the equivalent flow rate through the hole (canister interior side) and q_{hm} (m^3/s) the equivalent flow rate on the bentonite side of the hole. The flow rate through the hole is calculated as

$$q_{ch} = \frac{\pi r_h^2 D_w}{l_c}, \quad (3)$$

where r_h (m) is the radius of the defect hole, D_w (m^2/s) is the molecular diffusion coefficient in water and l_c (m) is the canister thickness. The flow rate on the bentonite side of the hole is calculated as

$$q_{hm} = \frac{r_h r_u}{r_h + r_u} 2\pi D_{eb}, \quad (4)$$

where r_u (m) is the outer radius of the hemispheric volume of bentonite (zero concentration assumed at r_u from the centre of the hole) and D_{eb} (m^2/s) is the effective diffusion coefficient in bentonite.

From the buffer, the solute may transport to tunnel backfill above the deposition hole or to a water conducting bedrock fracture intersecting the deposition hole at the position of the canister defect. Mass transfer in the bentonite buffer is based on solute diffusion and non-constant concentration profile is able to form. With the minimum distance from the canister defect (hole) to the bedrock fracture being the thickness of the buffer, it can be stated that this transient state is short-lived and underestimation of solute mass transport during early transient is not significant in the long run. The effect of the early transient state is investigated further in (Poteri et al., 2012).

The mass transfer coefficient from the buffer to an intersecting bedrock fracture is calculated as (Poteri et al., 2012)

$$\lambda_{bf} = \frac{q_{bf}}{R_{pb} \epsilon_b V_b}, \quad (5)$$

where q_{bf} (m^3/s) is the equivalent flow rate from the buffer to fracture, R_{pb} (-) is the retardation coefficient in the buffer, ϵ_b (-) is the porosity of the buffer and V_b (m^3) is the pore volume of the buffer. The equivalent flow rate is calculated as

$$q_{bf} = 2\pi r_{dh} 2b_v \sqrt{\frac{4 D_w v_{dh}}{\pi^2 r_{dh}}}, \quad (6)$$

where r_{dh} (m) is the radius of the deposition hole, $2b_v$ (m) is the volume aperture of the fracture and v_{dh} (m/s) is the flow velocity in the fracture. The retardation coefficients in the geosphere components of the model are calculated as

$$R_i = 1 + \frac{\rho_i K d_i}{\epsilon_i}, \tag{7}$$

where ρ_i (kg/m^3) is the dry density of the component, ϵ_i (-) is the porosity of the component and Kd_i (m^3/kg) is the distribution coefficient in the corresponding component. The components where the retardation coefficient is calculated are the bentonite buffer, the tunnel backfill and the bedrock. The fracture intersecting the deposition hole around it will transport the solute further into the geosphere.

Mass transfer from the buffer to the tunnel occurs by diffusion along the deposition hole. A delay time is assigned to the transport path that ends up in the fracture intersecting the tunnel. The mass transfer coefficient from the buffer to tunnel is calculated as (Poteri et al., 2012)

$$\lambda_{bt} = \frac{q_{bt}}{R_{pb}\epsilon_b V_b}, \tag{8}$$

where q_{bt} (m^3/s) is the equivalent flow rate from the buffer to the tunnel. The equivalent flow rate is calculated as

$$q_{bt} = \frac{\pi r_{dh}^2 D_{eb}}{s_c}, \tag{9}$$

where s_c (m) is the distance from the top of the canister to the tunnel floor.

From the tunnel, one pathway for the solute to transport is a fracture that intersects the tunnel. The fracture is assumed to intersect the whole tunnel cross section but the groundwater flow is restricted due to low hydraulic conductivity of the tunnel backfill (flow goes around the tunnel section instead of flowing through it). The mass transfer coefficient from the tunnel to the fracture is calculated as (Poteri et al., 2012)

$$\lambda_{tf} = \frac{q_{tf}}{R_{pt}\epsilon_t V_t}, \tag{10}$$

where q_{tf} (m^3/s) is the equivalent flow rate from the tunnel backfill to the fracture, R_{pt} (-) is the retardation coefficient in the tunnel backfill, ϵ_t (-) is the porosity of the tunnel backfill and V_t (m^3) is the volume of the tunnel section. The equivalent flow rate is calculated as

$$q_{tf} = p_t 2b_{vt}\sqrt{\frac{4D_w v_t}{\pi p_t/2}}, \tag{11}$$

where p_t (m) is the length of the intersection of the fracture and tunnel wall, $2b_{vt}$ (m) is the fracture aperture and v_t (m/s) is the flow velocity in the fracture.

In the bedrock, the solute transport is governed by the groundwater flow (advection), sorption on the rock fracture surfaces and matrix diffusion. The mass transfer coefficient describing the spreading of the pulse is formulated based on a mixing tank approximation of the geosphere. The approximation works fluently if the rock layer is not very thin. The mass transfer coefficient is based on the maximum release rate and the upper limit of the half width of the release pulse (see (Poteri et al., 2012) for more information). The equation is

$$\lambda_f = \frac{1}{4.3u^2}, \tag{12}$$

where u describes the transport resistance through the flow path and it's calculated as

$$u = \sqrt{\epsilon_m R_{pm} D_{em}} WL/Q, \tag{13}$$

where ϵ_m (-) is the porosity of the rock matrix, R_{pm} (-) is the retardation coefficient in the rock matrix, D_{em} (m^2/s) is the effective diffusion coefficient in the rock matrix and WL/Q (a/m) is the hydrodynamic control of retention that includes the flow path width W (m), length L (m) and flow rate Q (m^3/a).

The presented mass transfer coefficients are summarized in Table 2. The parameter values for the mass transfer coefficients are presented in Section 4.2.

Table 2. *The equations used to calculate the mass transfer coefficients for the transport branches in geosphere. (Poteri et al., 2012)*

From → / To	Canister	Buffer	Tunnel	Fracture
Buffer↓	$q_{ch} = \frac{\pi r_h^2 D_w}{l_c}$ $q_{hm} = \frac{r_h r_u}{r_h + r_u} 2\pi D_{eb}$ $q_c = \frac{q_{ch} q_{hm}}{q_{ch} + q_{hm}}$ $\lambda_c = \frac{q_c}{V_c}$			
Tunnel		$q_{bt} = \frac{\pi r_{dh}^2 D_{eb}}{s_c}$ $\lambda_{bt} = \frac{q_{bt}}{R_{pb}\epsilon_b V_b}$		
Fracture		$q_{bf} = 2\pi r_{dh} 2b_v \sqrt{\frac{4D_w v_{dh}}{\pi^2 r_{dh}}}$ $\lambda_{bf} = \frac{q_{bf}}{R_{pb}\epsilon_b V_b}$	$q_{tf} = p_t 2b_{vt} \sqrt{\frac{4D_w v_t}{\pi p_t/2}}$ $\lambda_{tf} = \frac{q_{tf}}{R_{pt}\epsilon_t V_t}$	
Biosphere				$u = \sqrt{\epsilon_m R_{pm} D_{em}} WL/Q$ $\lambda_f = \frac{1}{4.3u^2}$

3.1.2 Delay times

In an ideal well-mixed system, the outflow of the solute begins instantly when source mass enters the system. In reality, the transport between the barriers is delayed because the outflow and inflow in the barrier do not occur simultaneously. This is taken into account by estimating delay times for the barriers. The notations in the following equations are the same as before.

The delay time from the canister to buffer is estimated as (Poteri et al., 2012)

$$t_{d,cb} \approx 0.033 \cdot l_c^2 / D_w. \quad (14)$$

The delay time from the buffer to the intersecting fracture is estimated based on the thickness of the bentonite layer between the canister wall and the deposition hole wall (35 cm) and it is calculated as

$$t_{d,bf} \approx 0.033 \cdot R_{pb} l_b^2 / D_{pb}, \quad (15)$$

where D_{pb} (m^2/s) the pore diffusion coefficient in the buffer that is calculated as $D_{pb} = D_{eb}/\epsilon_b$ and l_b (m) is the thickness of the bentonite buffer.

The delay time from the buffer to the tunnel floor is estimated by using a 2.5 m thick layer of bentonite between the top of the canister and the floor of the tunnel (s_c) and it's calculated as (Poteri et al., 2012)

$$t_{d,bt} \approx 0.033 \cdot R_{pb} s_c^2 / D_{pb}. \quad (16)$$

In principle, the delay time for the diffusive transport from the tunnel to the bedrock fracture may be calculated applying the same equation as for the transport in the buffer. However, in the earlier assessments the tunnel section above the deposition hole has been handled as a mixing tank and the delay time has been conservatively assumed to be zero (Poteri et al., 2012). In this thesis, the same assumption is made.

In the geosphere, an advective delay is typical due to water residence time. However, in order to simplify the treatment of the geosphere advective delay is omitted in the calculation (Poteri et al., 2012). As described earlier, the delay times in the system are only translations in time, which delay the beginning of the system response.

The delay time in geosphere is approximated based on the transport resistance in the bedrock and an instant when a small fraction (1/285) of the maximum release is obtained. The delay is estimated as (Poteri et al., 2012)

$$t_{d,f} = 0.1u^2. \quad (17)$$

The delay times for the simplified model are summarized in Table 3.

Table 3. *The equations used to calculate the delay times of individual barriers in the transport branches. (Poteri et al., 2012)*

From → To	**Canister**	**Buffer**	**Tunnel**	**Fracture**
Buffer←	$t_{d,cb} \approx 0.033 l_c^2/D_w$.			
Tunnel		$t_{d,bt} \approx 0.033 R_{pb} s_c^2/D_{pb}$		
Fracture		$t_{d,bf} \approx 0.033 R_{pb} l_b^2/D_{pb}$,	0	
Biosphere				$u = \sqrt{\epsilon_m R_{pm} D_{em}} WL/Q$ $t_{d,f} = 0.1u^2$.

3.1.3 Response functions and release rates

The fact that the solute transport in the components of the simplified system may be presented by solute decay constants (i.e. mass transfer coefficients) or half-times, makes it analogous to a radioactive decay chain. The radioactive decay chain analogy with branches is used to solve the release rates through the system of compartments. The delay times of the system are used to improve the applicability of the model to short lived nuclides by shifting the total response function of the system (described later).

The release rates from one compartment to another are calculated based on the assumption that there is zero concentration in the target compartment. The transport branches of the geosphere in the simplified model can then be formulated with a group of equations (Poteri et al., 2012)

$$\begin{aligned} \frac{dm_c}{dt} + \lambda_c m_c &= \delta_0 \\ \frac{dm_b}{dt} + (\lambda_{bf} + \lambda_{bt}) m_b &= \lambda_c m_c * \delta_{t_{d,cb}} \\ \frac{dm_t}{dt} + \lambda_{tf} m_t &= \lambda_{bt} m_b * \delta_{t_{d,bt}} \\ \frac{dm_f}{dt} + \lambda_f m_f &= \lambda_{tf} m_t * \delta_{t_{d,tf}} + \lambda_{bf} m_b * \delta_{t_{d,bf}}, \end{aligned} \tag{18}$$

where * means convolution, $\delta_\tau = \delta(t-\tau)$, with δ the Dirac delta function and values of τ are the delay times described in Section 3.1.2. The delay time from the tunnel to fracture $\delta_{t_{d,tf}} = 1$ at all times as the delay time is assumed to be zero. The solute decay constants (or mass transfer coefficients) are described in Section 3.1.1. The initial conditions are $m_c(0) = 0, m_b(0) = 0, m_t(0) = 0$ and $m_f(0) = 0$. The convolution with the Dirac functions creates a translation by time τ (i.e. delay) (Poteri et al., 2012).

The analytical solutions for the transport branches are called response functions of the system and they can be obtained by using analogy of a radioactive decay chain. The general form of the radioactive decay chain equations without the delay times or branching can be formulated as Bateman equations (Bateman, 1910)

$$\begin{cases} \dfrac{dN_1}{dt} = -\lambda_1 N_1 \\ \vdots \\ \dfrac{dN_i}{dt} = -\lambda_i N_i + \lambda_{i-1} N_{i-1} \\ \vdots \\ \dfrac{dN_k}{dt} = \lambda_{k-1} N_{k-1} - \lambda_k N_k \end{cases} \tag{19}$$

that form a single branch of a radioactive decay chain. A solution to a chain with initial condition $N_i = 0$ for every $i \neq 1$ is described as

$$N_n(t) = N_1(0) \prod_{j=1}^{n-1} \lambda_j \sum_{j=1}^{n} \left(\frac{e^{-\lambda_j t}}{\prod_{p=1, p\neq j}^{n} (\lambda_p - \lambda_j)} \right), \tag{20}$$

where $N_1(0)$ is the amount of nuclide 1 at t = 0 and n denotes a single nuclide in the branch. The solution is not valid if two decay constants are equal but that can be taken care of by slightly changing some of the decay constants. The response function is formulated based on the Bateman's solution for the radionuclide amounts and for that, a multiplication with the corresponding λ_n is conducted to obtain dimensions as (1/a) corresponding to activity of a nuclide. The total delay time is taken into account by introducing a Heaviside step function $H(t-\tau_{tot,i})$ to each branch and performing translation in the exponent $e^{-\lambda_j t} \rightarrow e^{-\lambda_j (t-\tau_{tot,i})}$ where $\tau_{tot,i}$ is the sum of all the delay times related to the transport branch (Poteri et al., 2012). Thereby, the solution for a response function of a single transport branch is

$$f_{r,n}(t) = H(t-\tau_{tot}) \overbrace{N_1(0)}^{=1} \prod_{j=1}^{n} \lambda_j \sum_{j=1}^{n} \left(\frac{e^{-\lambda_j (t-\tau_{tot})}}{\prod_{p=i, p\neq j}^{n} (\lambda_p - \lambda_j)} \right). \tag{21}$$

For a branching chain, the Bateman solution is calculated by solving the response function with total (solute) decay constants of the compartments. Finally, the single response functions need to be weighted and summed to obtain a total response function of a compartment (i.e. for example a barrier). Basically, the branches are calculated in

Equation (18) by using the sum of λ_{bf} and λ_{bt} in the transport chain. The solutions for the buffer-fracture and buffer-tunnel-fracture branches are added together by weighing (multiplying) the different branches with appropriate quotient of $\lambda_{bf}/(\lambda_{bf}+\lambda_{bt})$ or $\lambda_{bt}/(\lambda_{bf}+\lambda_{bt})$ respectively. Whenever there are several branching points in the transport chain, the coefficient for a branch ($c_{n,j}$) is obtained as a multiplication of decay constant fractions in the branching points (amount n). The branching may be summarized by the following two expressions for the branch level n (Poteri et al., 2012)

$$\begin{aligned} \lambda_i' &= \lambda_{i,1} + \lambda_{i,2} + \cdots + \lambda_{i,k} \\ c_{n,j} &= \prod_{i=1}^{n} \frac{\lambda_{i,j}}{\lambda_{i,1} + \lambda_{i,2} + \cdots + \lambda_{i,k}} \end{aligned} \tag{22}$$

where λ_i' replaces λ_n in Equation (21) whenever there is an additional discharge terms $\lambda_{n,k}$ due to branching. In Equation (22), j depicts the specific calculated branch. The branches are also considered in the biosphere analysis in the same way when the transport chains are extended to biosphere compartments (see Section 3.2.2).

The weighted branch-specific response functions are summed to obtain a total response function for a compartment. The solution then corresponds to a response of the system with a unit release to the first barrier. The definite integral of total response function of the system (all branches summed) then approaches unity as $t \to \infty$. The radioactive decay is taken into account in the end after the release rates are obtained.

The total response function is used to obtain radionuclide release rates for the system. The transfer between the barriers occurs due to linear processes (solubility limits handled later), which means the formulation of the response functions simplifies the transport mechanism and provides a way to address the importance of a single barrier in the system. The exponential term related to the smallest decay constant in the summation mostly determines the shape and output of the response function. This means that the barrier, which retards the solute transport the most (the highest half-time), has the most significance for the release rates.

The source of the radionuclides in the system consist of the IRF part and gradual leaching caused by degradation of the fuel. The IRF part of the release rate is obtained simply by taking a product the IRF and the total response function of the system (dimensions Bq/a) because of the convolution with the delta function (see Equation (18)). The gradual leaching part of the release rate of a nuclide is obtained by calculating the superposition using convolution as

$$r(t) = \int_0^t f_t(t-\tau) f_{cd}(\tau) d\tau \tag{23}$$

where, f_t is the total response function of the system and f_{cd} is the source function determined by the gradual leaching from various parts of the spent fuel. Both parts of the release are added together to obtain the total release rate of a radionuclide.

Mathematically the convolution between the source function due to gradual leaching and the total response function is calculated numerically by using convolution theorem and discrete Fourier transform (Arfken et al., 1985). This may produce convergence or accuracy problems for example if the time steps in the approximation are not conveniently chosen. Computationally, these situations are avoidable by choosing various options in calculations and verifying results.

The gradual leaching for the spent fuel occurs in three parts of the fuel. The parts are the fuel matrix, metal alloys and other metal parts. The longest leaching time occurs in the degradation of the fuel matrix and the shortest leaching occurs in other metal parts. Due to three separately degrading components in the fuel, the inventory left over from the instant release fraction gives typically a rectangle shaped source function with three phases of gradual leaching. The source function for gradual leaching is summarized from three parts of the fuel where contribution of each part is

$$f_{cd,i} = N_i \cdot (1 - IRF_i) \cdot R_{deg,i}, \tag{24}$$

where N_i (Bq) is the inventory related to the spent fuel component in question (fuel matrix, zirconium alloys, other metal parts), IRF_i (-) is the IRF part of the inventory and $R_{deg,i}$ (1/a) is the degradation rate of the fuel component.

Finally, the radioactive decay is taken into account in the end of calculation by multiplying the calculated release rates with the appropriate nuclide-specific decay factor $\exp(-\lambda t)$.

3.1.4 Solubility limited nuclides

The release rate due to gradual leaching depends on the degradation rates of the components of spent fuel. The rate is constant but the amount of radionuclides decreases due to radioactive decay. Some nuclides may be solubility limited in canister pore water meaning that all the activity released from the fuel parts is not dissolved into canister pore water. In other components of the system, the solubility limits are cautiously assumed to not limit the release rates as the mathematical model of the system would become more complicated. The limited release rate inside the canister is straightforward to take into account in the source function determined usually by the gradual leaching and IRF part of the inventory. The solubility limited release differs from the gradual leaching by the fact that the release rate is constant and it is determined by the limited maximum concentration in the water phase and equivalent flow rate. The solubility limits of radionuclides are also affected by the stable isotope inventories of the elements in the canister. The values for the solubility limits are presented in Section 4.2.2.

For the nuclides with solubility limit, the solubility limited release rate is formulated as (Poteri et al., 2012)

$$f_{csl} = MN_A\lambda q_c = A_{max}q_c, \tag{25}$$

where f_{csl} is the activity release rate (Bq/a), M the solubility limit (mol/l), N_A the Avogadro's number (1/mol), λ the radionuclide's decay constant (1/s) and A_{max} the solubility limited volumetric activity of the nuclide (Bq/m^3). A_{max} is calculated based on the element-specific solubility limit that is transformed into radionuclide-specific solubility limit M. This is done by calculating a ratio between a radioactive isotope inventory and the total inventory where the stable isotopes are included. M is simply obtained by multiplying ratio with the element-specific solubility limit. In this manner, it is assumed that both the stable isotopes and radioactive isotopes dissolve at equal rate. This is justified as the inventory of radionuclides is produced as activation products due to neutron activation (in NPPs).

In reality, as the contaminated materials dissolve, the ratio of radioactive and stable isotopes changes in time as the radioactive decay decreases the amount of radioactive isotopes in the solute. The radioactive isotopes decay in the solute and both the stable and radioactive isotopes dissolve at equal rate. Therefore, over time the amount of stable isotopes increases in the solute and A_{max} is decreasing in reality. The constant value obtained based on the initial inventory is a value that is the most suitable for long-lived nuclides.

The release due to gradual leaching is calculated as described in the previous section by source function f_{cd} (see Equation (24)). When solubility limit is considered, the total inventory is taken into account. If the $f_{csl} < f_{cd}(0) + \sum_i IRF_i R_{deg,i}$ the solubility limited release rate is applied for duration t_s until the concentration falls below the solubility limit due to decreased inventory. The duration of the solubility limited source t_s is described as (Poteri et al., 2012)

$$t_s = \ln\left(\frac{A_{max} q_c + N(0)\lambda}{A_{max} q_c + A_{max} V_c \lambda}\right)/\lambda\,, \tag{26}$$

where $N(0)$ is the total inventory in the beginning. In reality, the duration for the solubility limited source should be calculated at every time point based on the dissolved inventory at that moment ($N(0)$ is not totally dissolved in the beginning), which would lead to a differential equation. The Equation (26) overestimates the duration of the solubility limited release because, for example a nuclide with a major inventory in the fuel matrix, which degrades in an average time of 1 000 000 years, has a minor portion of the inventory contributing to the duration in reality.

After time t_s, the concentration of the nuclides in the canister falls below the solubility limit and the mixing tank model can be used to represent the tail of the source term. A source that mimics the release rate from a well-mixed canister is described as (Poteri et al., 2012)

$$f_{csl}(t > t_s) = A_{max} q_c \exp(-(t - t_s) q_c / V_c). \tag{27}$$

The solubility limited release rate approximates the release rate from the canister through the hole by assuming a short half-time from the canister is finally taken into account by convoluting the release rate with the response function of the rest of the system. The half-time of the canister is assumed to be small because Equation (25) takes into account the release rate from the canister and the canister volume does not affect the release rate when solubility limit is active.

3.2 Simplified biosphere model description

The biosphere modelling often contains complexity that typically makes the modelling process challenging. The surface environment is an open system that has seasonal cycles and evolves over time. The modelling of the biosphere leads quickly to vast models that have large amounts of data (Posiva, 2014b). With a simplified model of the radionuclide migration in the biosphere and dose assessment, the risk of overestimation (or underestimation) is present, but transparency of the whole transport chain from the spent nuclear fuel canister to exposed human beings is better.

Mathematically, the biosphere model consists of compartments that form objects in the biosphere and are parts of the migration path of nuclides. The compartments describe the relevant objects that evolve in the future and where radionuclides are present. Typically, the compartments are lakes, wells or terrestrial soils. Using compartments, the biosphere can be described mathematically similarly as the transport barriers in the geosphere. In practice, the solutions of the transport branches extend with the biosphere compartments.

The connections between the compartments are described by transfer equations that determine the values of transfer coefficients. Transfer equations describe mathematically the migration processes. For example, diffusion in sediments or water advection between compartments transport the radionuclides. As in the geosphere, the radionuclides transport mainly dissolved in water but also gaseous transport is considered. The transfer equations determine the transfer coefficients in biosphere, which can be used to describe the half-time of the solute in biosphere compartments.

The human individuals are exposed to radionuclides from different compartments by external radiation and internal radiation that occurs via inhalation and ingestion of contaminated water and foodstuff. The dose rates from various sources are proportional to the activity content (concentration) of the relevant soil layer or water volume.

3.2.1 Model structure

The compartment system used for the biosphere model used in the base scenario is illustrated in Figure 7. The release point to the biosphere is the bottom sediment of the lake or directly the well water. The biosphere objects (BSOs) used in the simplified model in the biosphere are lake, well, forest, croplands and a pasture land. The lake has two sediment layers (intermediate and top sediment) in addition to a water volume. The terrestrial objects consist of single top soil layers and there are three types of croplands in the model, each with its own crop type. The sink in the model receives nuclides transferring out of the system.

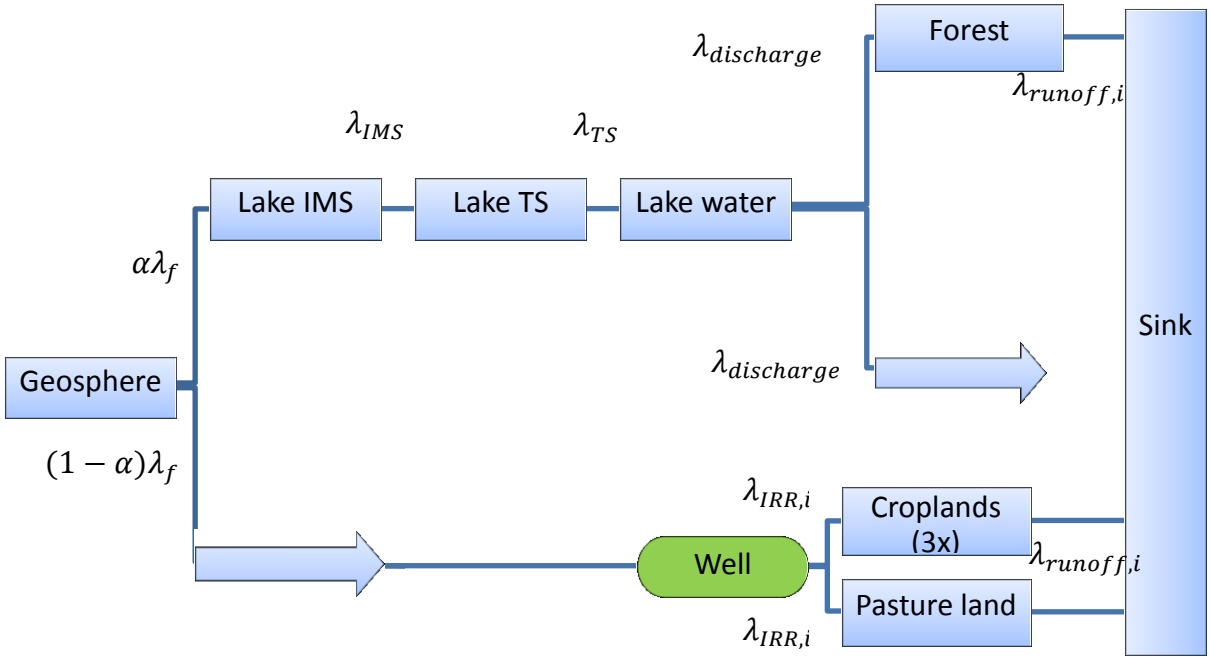

Figure 7. *The objects of the simplified biosphere model and respective mass transfer coefficients presented in a flow chart. IMS denotes intermediate sediment and TS top sediment. The croplands include three croplands with different agricultural foodstuff. The runoff to sink (λ_{runoff}) is applied to all terrestrial objects. Whenever both branches of the biosphere are included, the geosphere mass transfer coefficient receives a coefficient α that divides the mass transfer to two branches. The well is depicted differently as it is not considered as a real compartment (explained in Section 3.2.3).*

The biosphere model has two possible transport branches as illustrated in Figure 7. The branching divides the mass transfer coefficient from the geosphere in defined fractions to two branches. The calculation cases are determined to included either of the branches or both by applying α = 0.5 in the base case. The choice of 50 %/ 50 % division of the geosphere release is hypothetical but there is no good justification for any other division in the base case if both branches are wanted to take into account. The well is only used as irrigation source and therefore, the mass transfer from lake are only considered to forest and sink. The discharge from the lake is cautiously set to be 10 % to the forest and 90 % to sink of the determined discharge distribution in the base case. The choice is hypothetical and it depicts a lake that floods to the forest but the activity is assumed to absorb immediately to the soil layer. The same division for discharge and geosphere release is also used in the reference calculation case in this study.

Similar principle as in the screening model Tier 2 (Posiva, 2014b) is used in selecting the compartment properties for the simplified model. The model is not site-specific as explicit time-dependence for compartment properties cannot be set (the analytical solution is not possible) and choosing a specific location for the radionuclide release would include much uncertainty. To obtain a more site-specific model, the parameters for the properties of the compartments, or biosphere objects, have been derived from the data used in BSA-2012 radionuclide transport calculations (see (Posiva, 2014a) and (Posiva, 2014b)). The scenario in the calculation is not completely fixed because of the stochastically distributed parameters for the biosphere objects. The scenario behind the

simplified model is the expected evolution of the Olkiluoto site in the BSA-2012 reference case (BSA-RC) (Posiva, 2013a).

The transfer processes characterize the migration of nuclides in the biosphere. The nuclides transfer in solutes in the geosphere and therefore, in the biosphere they end up in water circulation. In the biosphere, the water circulation transports the nuclides via the compartments possibly finally to human beings. The simplified biosphere model has limited possibilities to include transfer processes in the biosphere. Due to radioactive decay chain analogy, the backward transfer processes for the compartments cannot be taken explicitly into account. The sedimentation in lakes is an example of such a process. Neglecting sedimentation and resuspension in the lake is a simplifying assumption, which slightly underestimates the release rate from a lake sediment to lake water.

3.2.2 Transport characteristics in biosphere

The radionuclide transport in the biosphere occurs mainly in water that transports between the compartments. The gaseous transport is relevant only for C-14 that is released from contaminated soil as carbon dioxide (CO_2). The carbon dioxide may then be used in photosynthesis in plants that take majority of their carbon from air (Posiva, 2014a).

Several assumptions are made in modelling in order to obtain cautious activity concentrations in the aquatic and terrestrial biosphere objects. Many of the assumptions are based on Tier 2 assumptions in (Posiva, 2014b). The following is a summary of the assumptions:

- The radionuclide inventories in the biosphere compartments are obtained from release rates to the compartments by assuming a (well-mixed) steady-state in the compartment.
- The water from the well or the lake, which ever has the highest activity concentration, is used for drinking water (for humans and animals).
- Sedimentation in the lake is neglected and the whole activity is assumed to be available in dissolved form in the aquatic BSOs.
- The areas of the biosphere objects are determined in a cautious manner to obtain cautious concentrations of activity in soil or sediment layers. Also, cautious distributions coefficients (Kd_i) are selected for the soils and sediments.
- A low well capacity is assumed in order to minimize dilution. On the other hand, the capacity is assumed to be large enough to meet all irrigation needs. This means that the concentration in the well water may be unrealistic as the mixing capacity can be too small to meet up all the drinking water and irrigation demand. Activity losses from the well water by sorption on the well walls are also neglected.
- Food concentrations are estimated by cautious selections for the corresponding concentration ratios (CR_i). In the case of C-14, a specific activity model, which gives conservative estimates of the food concentrations, is used (Avila & Pröhl, 2008).

- Doses are calculated for a hypothetical individual that spends 100 % of the time in the terrestrial ecosystem where the air and soil activity concentrations are the highest.
- The exposed individual has a diet that includes only foodstuff from the contaminated ecosystems (lake, forest, croplands and pasture land).

The transfer equations in the biosphere are used for the mass transfer coefficients between the biosphere objects. The mass transfer coefficients for the biosphere objects are obtained by summing up specific transfer coefficient expressions presented next. The transfer coefficient expression due to advection, runoff or infiltration is described as (Posiva, 2014b)

$$\lambda_a = \frac{Wflux_i}{d_i \cdot \epsilon_i \cdot sat_i \cdot R_i}, \tag{28}$$

where $Wflux_i$ is the advective water flux from sediment/soil layer i (m/a), d_i the thickness of sediment/soil layer i (m), ϵ_i the porosity within layer i (-), sat_i the fraction of water in pore space of sediment/soil layer i (saturated water content) (-), R_i the retardation coefficient in the sediment/soil layer i (-). The retardation coefficient is calculated as

$$R_i = 1.0 + Kd_i \cdot \frac{\rho_i}{\epsilon_i \cdot sat_i}, \tag{29}$$

where Kd_i is the distribution coefficient to sediment/soil matter in layer i (m^3/kg) and ρ_i is the bulk density within sediment/soil layer i (kg/m^3).

The transfer coefficient expression due to diffusion is calculated as (Posiva, 2014b)

$$\lambda_D = \frac{2.0 \cdot D}{d_i^2 \cdot sat_i \cdot R_i}, \tag{30}$$

where D is diffusion coefficient in water (m^2/a). The expression used to calculate transfer coefficient due to outflow or discharge is

$$\lambda_{dis} = \frac{WfluxOut}{A_i \cdot d_w}, \tag{31}$$

where A_i is the area of the object (for example lake) (m^2), d_w the average water depth (m) and $WfluxOut$ is the sum of the discharge from the object (m^3/a). The mass transfer coefficient related to irrigation ($\lambda_{IRR,i}$) concerns only well and irrigated terrestrial objects in the base case. The mass transfer coefficient is calculated as

$$\lambda_{IRR,i} = A_i \cdot irrg/V, \tag{32}$$

where A_i is the area of the irrigation target object (m^2), $irrg$ is the volumetric irrigation amount per unit area in a year ($m^3/m^2/a$) and V is the mixing volume of the irrigation source (m^3). With a well, it is the same as the well mixing capacity.

The mass transfer coefficients in the biosphere are illustrated in Figure 7 in the previous Section. The mass transfer coefficients for the compartments are obtained from the transfer coefficient expressions presented in Equations (28)-(32). From the intermediate sediment of the lake to the upper top sediment (λ_{IMS}) and from the top sediment to lake water (λ_{TS}), the mass transfer is described by the diffusion and water advection (Equations (28) and (30)) (sum of the two). From the lake water compartment, the discharge process is described by Equation (31). In Figure 7, the mass transfer coefficient to forest or sink ($\lambda_{discharge}$) is described by this equation. For all the terrestrial compartments, a small runoff is applied in the model ($\lambda_{runoff,i}$) as mass transfer coefficient. The runoff is calculated with Equation (32).

The mass transfer coefficients in the biosphere are summarized in Table 4. The parameter selection and simulated results for the mass transfer coefficients are presented in Sections 4.2 and 5.1.2. In the biosphere, the equilibrium is achieved much faster than in the geosphere due to openness of the system and annual cycles of nature. Therefore, the well-mixed state in the compartments is obtained fast and the delay times for all the compartments are assumed to be zero.

Table 4. *The expressions used to calculate the mass transfer coefficients for the transport branches in biosphere.*

From To	**→ Lake IMS**	**Lake TS**	**Lake water/Well***	**Forest, Croplands (3x), pasture land**
Lake TS↓	$\lambda_a = \frac{Wflux_i}{d_i \cdot \epsilon_i \cdot sat_i \cdot R_i}$ $\lambda_D = \frac{2.0 \cdot D}{d_i^2 \cdot sat_i \cdot R_i}$ $\lambda_{IMS} = \lambda_a + \lambda_D$			
Lake water		$\lambda_{TS} = \lambda_a + \lambda_D$		
Croplands (3x), pasture land			$\lambda_{IRR,i} = A \cdot irrg/V$	
Sink			$\lambda_{dis} = \frac{WfluxOut}{A \cdot d_w}$ $\lambda_{discharge} = \lambda_{dis}$	$\lambda_{runoff,i} = \lambda_a$

*The discharge only applies for lake water and the target is forest and sink in the base case (10 % and 90 %).

After the mass transfer coefficients for different biosphere objects are obtained, the transport branches from geosphere can be extended to biosphere. Both of the geosphere branches are extended by two biosphere branches in the base case and branching is taken into account in solving the branches for the biosphere compartments. In the base case, the branches are taken into account in the croplands, pasture land and forest in obtaining the response functions and release rates of the biosphere objects. For example, there are three branching points in the radionuclide transport chain to forest soil (buffer-to-tunnel/buffer-to-fracture, geosphere-to-lake/geosphere-to-well, lake-to-forest/lake-to-sink). The total response functions for the biosphere objects are obtained by solving the transport branch by using Equation (21) and adding up the different branches with appropriate weights due to branching (see Equation (22)). The delay times for the branches are determined by the total delay time in geosphere components.

3.2.3 Inventory calculation for the biosphere objects

After obtaining the total response functions for the biosphere objects, the IRF part of the release and gradual leaching are taken into account as described in Section 3.1.3 to obtain the release rates of radionuclides in the biosphere compartments. To obtain

radionuclide inventories for the dose rate assessment, a removing mass transfer coefficient is considered in the biosphere objects except the well. Well is not considered to be an actual compartment in the transport chain of radionuclides as other biosphere objects. It is not assumed have any dispersing effect on the release pulse like other compartments. This means that release rate in the well equals the weighted release rate from the geosphere. The well water is not confined to a compartment like the lake water but it can be still used for drinking and irrigation.

The well does not gather nuclides and the activity concentration is calculated based on the mixing capacity and the release rate as

$$C_w = \frac{r(t)}{W_{cap}}, \tag{33}$$

where $r(t)$ is the release rate (Bq/a) and W_{cap} is the annual well capacity (mixing capacity (m^3/a)).

For other biosphere objects (compartments), the activity inventory is obtained by using the release rate at each time point and the removing mass transfer coefficient as

$$N(t) = \frac{S(t)}{\lambda_{out}}, \tag{34}$$

where N is the radionuclide amount in the compartment (Bq) (see Equation (20)), $S(t)$ is the release rate to the compartment (Bq/a) and λ_{out} (1/a) is the total mass transfer coefficient from the compartment that is calculated as a sum mass transfer coefficients of branches leaving from the compartment.

Based on the radionuclide inventories in the biosphere compartments and corresponding soil masses or water volumes, the concentrations of nuclides ($C_s(t)$ (Bq/kg) or $C_w(t)$ (Bq/m^3)) can be calculated for the dose assessment. The activity amounts are straightforwardly divided by the appropriate water volume (m^3) or soil dry mass ($m = \rho_i \cdot V$) (kg). The dose rates can then be obtained and they are proportional to the calculated concentrations in the related soil layers or water volumes.

In the geosphere, C-14 is handled as non-sorbing organic isotope, which is a conservative assumption. In the biosphere, C-14 is assumed to be in solute inorganic form when it enters the aquatic compartments in the biosphere. This is a conservative assumption as the actual behavior of organic/inorganic C-14 is partly an open issue. When the water from a lake or a well is used for irrigation of terrestrial objects C-14 is assumed to be released to the atmosphere as inorganic carbon dioxide CO_2 immediately. The carbon dioxide with C-14 is then available for uptake of the crops and other vegetation in photosynthesis that is a major path for carbon intake in plants (Posiva, 2014a). C-14 is also available for fish intake in the contaminated water as it is in inorganic form. Therefore, C-14 contribution in the dose assessment in foodstuff is calculated by using a specific activity model (Avila & Pröhl, 2008). The natural presence of C-14 is not taken into account in the model.

In the specific activity model, the usage of contaminated water for irrigation causes an excess of C-14 over stable carbon (C-12) in the growing biomass (Avila & Pröhl, 2008) or fish. The dose exposure can be calculated based on net primary production of the ecosystem and ingestion amount of carbon in the ecosystem. The doses for humans are finally calculated based on the activity release, carbon intake and excess C-14/C-12 ratio (specific activity).

3.2.4 Dose rate calculation

Dose pathways in the model are formulated based on the typical internal and external radiation exposure pathways in safety analyses. For all the nuclides, all dose pathways presented here are calculated based on the activity concentrations in the related soil layer or water volume or air volume. The C-14 is handled differently by using a specific activity model to obtain concentrations in the foodstuff. The dose rates from all the presented biosphere objects are not possible to occur simultaneously such as full external exposure from all croplands. For the total dose rate, a selection of physically possible dose pathways is used and the whole set of analyzed nuclides is taken into account.

After obtaining the concentrations of nuclides in the compartments, the calculation of dose rates is possible. The dose rate via water ingestion by drinking (Sv/a) is calculated as (Posiva, 2014b)

$$E_{dw}(t) = \alpha_{ing} C_w(t) \cdot W, \tag{35}$$

where α_{ing} is the dose conversion coefficient for ingestion (Sv/Bq), $C_w(t)$ the concentration of a radionuclide in water (Bq/m^3) and W is the water ingestion rate (m^3/a).

There are three kinds of crops in the biosphere model and also berries (corresponding to for example lingonberry or blueberry) that can be ingested as foodstuff. The diet of an individual includes cereals, potatoes and field vegetables[2] as crop types. These three kinds form the most portion of crops in an average diet of a Finnish male (Posiva, 2014a). The berries are included in the model more of as a component to observe the possible contribution to the total dose. Also, milk and meat ingestion and the fish ingestion from lake is included in the diet of an individual. The dose rates via ingestion of various foodstuff (excluding milk and meat) (Sv/a) are calculated as (Posiva, 2014b)

$$E_{f,i}(t) = \alpha_{ing} C_i(t) \cdot CR_i \cdot Ing_i, \tag{36}$$

where $C_i(t)$ is the concentration of the corresponding soil or water (Bq/kg or Bq/m^3), CR_i is the corresponding concentration ratio ((µg/kg)/(µg/m^3) or (µg/kg)/(µg/kg)) and Ing_i is the foodstuff ingestion rate (kg/a).

[2] The definition of field vegetables is adopted from BSA-2012. The crop type includes carrot, red beet, swede, turnip, onion and leek and typically consists of 25 % leaf vegetables and 75 % root vegetables. (Posiva, 2014a)

Humans are assumed to have cattle as livestock that drinks contaminated water similarly as humans and eats (possibly) contaminated pasture. The radionuclides end up in the animals and as they produce meat and milk for the humans, they end up to human individuals. The dose rates via ingestion of milk (Sv/a) are (Posiva, 2014b)

$$\begin{aligned} a)\ E_{milk-water}(t) &= \alpha_{ing} C_W(t) \cdot W_{cows} \cdot CR_{milk} \cdot Ing_{milk}\,, \\ b) E_{milk-pasture}(t) &= \alpha_{ing} C_S(t) \cdot Ing_{past} \cdot CR_{past} \cdot CR_{milk} \cdot Ing_{milk}, \end{aligned} \quad (37)$$

where W_{cows} is the water ingestion rate of cows (m^3/d), CR_{milk} is the concentration ratio to cow milk (Bq/l)/(Bq/d), Ing_{milk} is the milk ingestion rate (L/a), $C_S(t)$ is the soil activity concentration (Bq/kg), Ing_{past} is the pasture ingestion rate (kg/d) and CR_{past} is the concentration ratio to pasture (mg/kg)/(mg/kg). The dose rates via meat ingestion (Sv/a) are calculated in a similar fashion as

$$\begin{aligned} a)\ E_{meat-water}(t) &= \alpha_{ing} C_W(t) \cdot W_{cows} \cdot CR_{meat} \cdot Ing_{meat}\,, \\ b) E_{meat-pasture}(t) &= \alpha_{ing} C_S(t) \cdot Ing_{past} \cdot CR_{past} \cdot CR_{meat} \cdot Ing_{meat}, \end{aligned} \quad (38)$$

where CR_{meat} is the concentration ratio to cow meat (i.e. beef) (Bq/kg_{fresh})/(Bq/d) and Ing_{meat} is the ingestion rate of meat (kg_{fresh}/a).

Humans inhale air that contains dust from contaminated ground. The inhalation dose rate (Sv/a) from terrestrial compartments is calculated as (Posiva, 2014b)

$$E_{inh}(t) = \alpha_{inh} C_S(t) \cdot C_{dust} \cdot Inh_{rate} \cdot Exp_{hours}, \quad (39)$$

where α_{inh} is the dose conversion coefficient for inhalation (Sv/Bq), C_{dust} is the dust concentration in air (kg/m^3), Inh_{rate} is the inhalation rate m^3/h and Exp_{hours} is the exposure time (number of hours in a year, h/a).

External irradiation doses occur when individuals spend time on contaminated areas (simultaneously with inhalation). The dose rate (Sv/a) is calculated as

$$E_{ext}(t) = \alpha_{ext} C_{S,V}(t) \cdot Exp_{hours}, \quad (40)$$

where α_{ext} is the dose conversion coefficient for external irradiation (Sv/h)/(Bq/m^3) and $C_{S,V}(t)$ is the soil concentration (Bq/m^3). The inhalation and external exposure are calculated from the same terrestrial object by assuming that the inhalation and time spent for external exposure occur at the same terrestrial site. The cumulative sum of the inhalation dose and external dose is maximized by selecting the object that results in the highest total dose. This is purposely a cautious choice (and assumption).

From the whole set of nuclides, the total radiation exposure (total dose rate) is cautiously maximized by selecting physically possible dose paths for an exposed individual. In practice, the drinking water for humans and animals (livestock) is selected from the water source with the highest activity concentration and combination of inhalation and external irradiation is selected from one terrestrial source.

The C-14 doses from use of the irrigation water are calculated by first obtaining excess C-14/C-12 ratio (specific activity, Bq/kg$_C$) as (Avila & Pröhl, 2008)

$$R_{C-14/C-12} = \frac{C_W(t) \cdot irrg}{h \cdot \lambda_{ex} C_{C-12} + NPP} \tag{41}$$

where $irrg$ is the total volume of irrigation water per unit area used in a year (m^3/m^2/a), h is is the mixing height in air (m), λ_{ex} is the air exchange rate in the mixing layer (1/a), C_{C-12} is the C-12 content in air (kg$_C$/m^3) and NPP is the net primary production in the ecosystem (kg$_C$/m^2/a). The mixing height is calculated as (Posiva, 2014b)

$$h = 2 \cdot \frac{NPP}{veg_p \cdot C_{C-12}}, \tag{42}$$

where veg_p is the vegetation period (i.e. the fraction of the year during which photosynthesis occurs). The air exchange rate in the mixing layer calculated as

$$\lambda_{ex} = v_w / \sqrt{A/\pi}, \tag{43}$$

where v_w (transformed to m/a) is approximated by using a logarithmic wind profile law as

$$v_w = v_{ms} \log\left(\frac{h_{veg}}{z_0}\right) / \log\left(\frac{h}{z_0}\right), \tag{44}$$

where v_{ms} is the measured annual average wind speed (m/s), h_{veg} is the average height of vegetation (m), z_0 is the roughness length (m) and h is the measurement height (m). The ingestion dose from a foodstuff *i* (grown on an irrigated compartment) due to C-14 uptake from air can finally be calculated as

$$E_{ing,i} = R_{C-14/C-12} \cdot C_{ing} \cdot \alpha_{ing}, \tag{45}$$

where C_{ing} is the carbon intake rate of a specific foodstuff (kg$_C$/a).

The C-14/C-12 ratio excess ratio is also calculated in lake water in order to obtain dose rate from fish ingestion. In this case, the excess ratio is (Avila & Pröhl, 2008)

$$R_{C-14/C-12} = \frac{E \cdot r(t)/A}{(DIC \cdot \frac{A_c}{A} \cdot runoff + NPP) \cdot T_{avg}}, \tag{46}$$

where E is the effective release fraction (-), $r(t)$ is the release of C-14 from geosphere (Bq/a), A is the area of the lake, DIC is the concentration of dissolved inorganic carbon (kg$_C$/m^3), A_c is the catchment area of the lake (m^2), $runoff$ is the runoff from the catchment area to the lake (m^3/m^2/a) and T_{avg} is the averaging period (a). Catchment

area of a lake is the area from where the lake gathers the runoff flux. Averaging period is the period for which the average annual dose over lifetime is calculated. It should correspond to the integration period used in the derivation of the dose conversion coefficient used in the calculation.

Due to a non-defined catchment area in the simplified model, the A_c is set to zero. Also, the effective release fraction is conservatively assumed to be one and averaging period is cautiously one year because average annual release rates and dose rates are calculated. The C-14 dose via fish ingestion is calculated similarly as earlier with Equation (45). Other dose paths (drinking water, external irradiation and inhalation) for C-14 are calculated similarly to calculation of those dose paths of other nuclides. The C-14 doses via ingestion of meat and milk, which is contaminated via drinking water for the livestock and pasture ingestion, are not considered in the simplified model as they are not estimated in (Avila & Pröhl, 2008).

4 PROBABILISTIC MODELLING

The probabilistic modelling is included in the analysis by a performing a Monte Carlo simulation. The specific input parameters are considered distributed and they are sampled for each simulation case. The sampling is performed based on the distributions selected for the parameters. With a specific number of simulation cases, the Wilks' method can be used to estimate confidence levels for the obtainable quantities (response functions, release rates, dose rates) with high probability.

4.1 Simulation methods

The parameters for the geosphere and biosphere transport calculations and dose assessment contain various amounts of uncertainty. Instead of applying only one set of cautious parameter values and perhaps conducting a sensitivity analysis, a Monte Carlo simulation is used to calculate the model with many sets of sampled values.

After specific amounts of calculation cases, the results from the simulation are given as confidence levels (or histograms for parameters). The confidence levels give an upper bound for the calculated quantity (response function, release rate, dose rate) under which a specific portion of the results exist. For example, 50 % confidence level sets a level under which 50 % of the obtained results lie (i.e. median). Obtaining confidence levels is performed at every time point so the time series for the confidence levels are obtained.

In the Monte Carlo simulation, the calculation of the model results (e.g. dose rates) is repeated a number of times with randomly sampling the distributed variables. The upper limits for the confidence levels can be determined with high probability by using Wilks' method (Nummi et al., 2012). The method is used to evaluate confidence levels at every time point and it allows to find the minimum number of calculation cases in the simulation required to determine a specific confidence level with a certain probability. Table 5 shows the number of required runs with the probability of the confidence levels set to p = 0.99. In this thesis, 1000 calculation cases are used to determine the confidence levels. In practice, the result quantity, such as total dose rate, is sorted after 1000 runs at every time point. For example, the 95 % confidence level would correspond to a value that is 966th highest after sorting.

Table 5*. Numerical values for i with different combinations of N and with the probability of p = 0.99. (Nummi et al., 2012)*

	Total number of samples *N*			
Confidence level *a*	100	200	500	1000
0.99	-	-	500	998
0.95	100	197	487	966
0.9	97	190	466	922
0.75	86	165	398	782
0.5	63	117	277	538
0.25	36	66	149	283

The parameters in the calculation of the model are sampled based on given (estimated) distributions. For the non-constant parameters, a distribution based on available and earlier data is determined with possible truncation. The sampling procedure takes into account the possible correlations set between the parameters by using NORTA-method (NORmal to Anything) (Chen, 2001). With a given correlation coefficient ρ and a random probability level p (between 0 and 1), the correlated probability level and parameter values are estimated as follows with the help of normal distribution: (ϕ denotes the cumulative distribution function (CDF) of a standard normal distribution N(0,1))

1) Calculate the value of the standard normal probability density function corresponding to the given probability level with inverse CDF as $\phi^{-1}(p)$.

2) Pick a new random number x from standard normal distribution (N(0,1)).

3) Calculate new correlated random number y that is normally distributed as $y = \rho \cdot \phi^{-1}(p) + \sqrt{1-\rho^2}x$.

4) Calculate the value of the cumulative probability density function with the new random number $p_2 = \phi(y)$.

5) Calculate the correlated parameter values by using original p and p_2 as probability levels for inverse CDFs.

The sampling from the assigned distributions is performed by inverse transform by using a random probability level. The choice of the distribution for different parameters depends on the available data and expert judgment. The selections for parameters are presented in Section 4.2 and determination of correlations is handled in Section 4.3. The used distributions are depicted below.

At worst, due to lack of available data, logarithmic uniform (log-uniform) distributions are used with a specific minimum and maximum value. In the log-uniform distribution the logarithm of random variable follows the uniform distribution. The log-uniform distribution is used when the value interval is a few orders of magnitude wide. The maximum and minimum value are used to calculate the inverse of the CDF. The CDF for a log-uniformly distributed random variable x is (Forbes et al., 2011)

$$F(x) = \begin{cases} 0, & x < a \\ \dfrac{\ln(x) - \ln(a)}{\ln(b) - \ln(a)}, & a \le x \le b \\ 1, & x > b. \end{cases} \tag{47}$$

In Equation (47), parameters a and b denote the minimum and maximum values respectively. The inverse CDF for a randomly picked probability level p is

$$F^{-1}(p) = a \cdot \exp((\ln(b) - \ln(a))\, p). \tag{48}$$

With quantities, which had less range between the maximum and minimum value, a uniform distribution is used. The CDF for a uniform distribution with a minimum (a) and maximum (b) is (Forbes et al., 2011)

$$F(x) = \begin{cases} 0, & x < a \\ \dfrac{x-a}{b-a}, & a \le x \le b \\ 1, & x > b. \end{cases} \tag{49}$$

The inverse CDF is used in sampling the values from the distribution and with a probability level p it is

$$F^{-1}(p) = a + (b-a)p. \tag{50}$$

With some data, a triangle distribution is used for sampling because the log-uniform or uniform distribution might overestimate the contribution of the values near the extremes. The requirements for applying the triangle distribution are the minimum (a), the maximum (b) and the mean value (c) for the quantity. The CDF for a random variable x that follows a triangle distribution is (Forbes et al., 2011)

$$F(x) = \begin{cases} 0, & x < a \\ \dfrac{(x-a)^2}{(c-a)(b-a)}, & a \le x \le c \\ 1 - \dfrac{(b-x)^2}{(b-c)(b-a)}, & c < x \le b \\ 1, & x > b. \end{cases} \tag{51}$$

Inverse CDF for a triangular distribution is

$$F^{-1}(p) = \begin{cases} a + \sqrt{(c-a)(b-a)p}, & p \le \dfrac{c-a}{b-a} \\ b - \sqrt{(b-c)(b-a)(1-p)}, & \text{otherwise.} \end{cases} \tag{52}$$

For some data, a logarithmic normal (log-normal) distribution is justifiable. Log-normal distribution is suitable for situations where standard deviation is large compared to the mean value. The justification for a log-normal distribution is enhanced if the parameter is a result of summation of many processes. In nature, the normal or log-normal behavior is observed for many cases (Limpert et al., 2001). With log-normal distributions, negative values cannot be obtained and the distribution is skewed to the right allowing higher probabilities to the values outside a few standard deviations from the mean. Due to possible unwanted, unrealistic realizations log-normal distributions are typically truncated with a minimum and maximum value. The truncation is conducted by repeating the sampling if the obtained value is outside of the acceptable range.

The log-normally distributed values are given by using a realistic value (rv) and a conservative value (cv) or by using a mean and standard deviation. The CDF for the log-normal distribution is (Nummi et al., 2012)

$$F(x) = \frac{1}{2}\left[1 + \mathrm{erf}\left(\frac{\ln x - \alpha}{\sqrt{2}\beta}\right)\right], x > 0 \tag{53}$$

The inverse function for the CDF is

$$F^{-1}(p) = \exp(\alpha)\exp(\sqrt{2}\,\beta \mathrm{erf}^{-1}(2p - 1)) \tag{54}$$

where the parameters α and β are

$$\alpha = \ln(\mathrm{rv}), \qquad \beta = \pm \ln\left(\sqrt{\frac{\mathrm{cv}}{\mathrm{rv}}}\right). \tag{55}$$

Here the cv and rv denote the conservative and realistic value of a parameter. The (+)-sign is used when the conservative value is greater than realistic value and (-) sign otherwise. The realistic and conservative values correspond to $F(\mathrm{rv}) = 0.5$ and $F(\mathrm{cv}) = 1 \pm \frac{\mathrm{erf}(\sqrt{2})}{2} = 0.97725$ or 0.02275. Thus, the realistic value corresponds to the mean value of the distribution and conservative value can be exceeded with a small probability. It must be noted that for some parameters a lower value corresponds to a conservative choice but as a distribution parameter conservative value is in this thesis referred as the value that corresponds to 0.97725 percentile.

The sampling from log-normal distribution can also be based on the geometric standard deviation (GSD) and geometric mean values (GM). For the log-normal distribution, the mean and standard deviation of the logarithm of the data can be obtained from geometric ones as $\mu = \ln(\mathrm{GM})$ and $\sigma = \ln(\mathrm{GSD})$. It must be noted that μ differs from the arithmetic mean obtained on a non-logarithmized data. The value of the inverse cumulative distribution function in this case is

$$F^{-1}(p) = \exp(\mu + \sigma \cdot \Phi^{-1}(p)), \tag{56}$$

where $\Phi^{-1}(p)$ is the inverse of the standard normal distribution at p, namely

$$\Phi^{-1}(p) = \sqrt{2}\,\mathrm{erf}^{-1}(2p - 1) \tag{57}$$

The GM and GSD are often used to cautiously estimate the parameter distributions from experimental data. For any log-normal distribution, about 68 % of the probability mass is distributed over the range of [GM/GSD, GM·GSD] similarly as with any normal distribution 68 % of the values lie between μ-σ and μ+σ.

In addition to the presented distributions, for a normal distribution used also in this study, the sampling is performed based on the (arithmetic) mean value μ and standard deviation σ. The value of the of the inverse cumulative distribution function is given by the logarithm of Equation (56).

4.2 Model parameters

The distributions for the parameters are considered for every parameter in the model that are uncertain or not fixed based on the current design of the repository system. In this section every parameter in the calculation is presented from the canister to the biosphere and dose rate calculation. The distributed parameter values are sampled for each realization in the probabilistic simulation with the methodology presented in Section 4.1. Also, some parameters can be considered correlated and the correlations used in the analysis are presented later in Section 4.4.

The distribution selections presented in the next sections form the base case in this study. In addition to base case, a reference case is formulated. The reference case is formulated from values used as cautious reference case values in (Cormenzana, 2013a) but due to different modelling concepts applied in this study, some values used in (Poteri et al., 2012) are used. The (cautious) values used in (Poteri et al., 2012) are based on an interim safety case report by Posiva on the release and radionuclide transport analysis, the RNT-2008 analysis (Nykyri et al., 2008). Biosphere related parameters, which are not studied in (Poteri et al., 2012) or in (Cormenzana, 2013a), are taken from BSA-2012 reference case (BSA-RC) where applicable.

The distributions for the parameters of the model are chosen based on research done by Posiva Oy and SKB. These two organizations have obtained data from general sources but they have also conducted extensive monitoring to obtain site-specific experimental data. Here, the data are reviewed and partly applied to the model based on the conditions and usability for probabilistic modelling.

The selections for the distributions is widely based on recent research and recommendations. The uniform and log-uniform distributions are used for parameters that have limited range but no other information is available. When a mean value or most probable value (mode) is known in addition to the range, a triangular distribution is used.

Due to lack of knowledge and little experimental data, a log-normal distribution is chosen in some situations. Often some knowledge about a parameter is available from multiple measurements but a definite distribution cannot be assigned. Usually, a geometric mean and geometric standard deviation can be calculated from the samples. Then, a wide range of possible values can be obtained in simulations with the obtained distribution parameters. The truncation limits vary depending on the available data but in this thesis the 1^{st} and 99^{th} percentiles are used as the limits when no other range is not available. This range is also used by SKB (Nordén et al., 2010).

The log-normal distribution is used widely in situations where the overall shape of the distribution is not known or a (geometric) mean value (GM) (i.e. realistic value) and a conservative value can be estimated based on experimental samples. For some parameters a geometric standard deviation (GSD) is used to describe the distribution with the GM value. The sampling from the distributions described with realistic value/conservative value (rv/cv) and GM/GSD is presented in Section 4.1.

In some situations, normality for the parameter is a more justified assumption of the reality than a uniform distribution between a hypothetical range. Like mentioned in the previous section, many processes in nature tend to create random variables that follow normal or log-normal distributions. The parameters used in the calculations are often a result of summation of many processes. The log-normal or normal behavior is then observed in many real situations in nature (Limpert et al., 2001).

4.2.1 General parameters in geosphere transport

In the geosphere, the general parameters for the canister component are presented in Table 6. The parameters choices are based on a probabilistic sensitivity analysis (PSA[3]) report (Cormenzana, 2013a), parameter selection report for the PSA (Cormenzana, 2013b) and the simplified geosphere transport report (Poteri et al., 2012). The parameters related to the dimensions of the KBS-3V design are considered constant for canister and other components in the whole repository system. The sampling from the presented distributions is performed according to the inverse CDFs presented in the previous section.

The defect in the canister is a hole that has a 1 mm diameter in the reference case (Cormenzana, 2013b). In the sensitivity report, the range is simply extended to a maximum value of 3 mm and minimum value of 0.3 mm to obtain the limits for the radius of the hole (r_h).

The pore volume of the canister (V_c) varies due to amount of bentonite that enters the canister through the initial defect. It is difficult to estimate the correct range for the volume but wider range also makes it easier to recognize the significance of the parameter. As a result, the mass transfer coefficient (or solute decay constant) from canister to buffer (λ_c) should get a wide range if the volume would affect the coefficient significantly.

The diffusion coefficient in water (D_w) has a lower limit that is two orders of magnitude lower than the cautious reference case value that is used for the upper limit. It must be noted that the lower limit is close to being physically beyond possible for groundwater.

[3] PSA in this study does not refer to Probability Safety Analysis.

Table 6. *The general parameters for the canister compartment in the geosphere transport. Source reports refer to Posiva's reports (Cormenzana, 2013a) and (Poteri et al., 2012) (WR = working report, POSIVA = Posiva report). Log-uniform distribution is assigned to the quantities that have a minimum and maximum value.*

Quantity and dimension	Symbol	Minimum	Maximum	Reference case	Source
Hole radius (m)	r_h	0.00015	0.0015	0.0005	WR 2013-25, POSIVA 2012-20
Diffusion coefficient in water (m^2/s)	D_w	2.0E-11	1.0E-9	1.0E-9	WR 2013-25
Radius of the hemisphere with zero concentration around canister hole (m)	r_u	0.05		0.05	POSIVA 2012-20
Canister thickness (m)	l_c	0.05		0.05	POSIVA 2012-20
Pore volume of the canister (m^3)	V_c	0.09	0.9	0.7	WR 2013-25

The general and constant parameter choices the buffer compartment are presented in Table 7. Many of the buffer related parameters depend on the KBS-3V design and are taken from the reference report (Poteri et al., 2012).

Table 7. *The general (constant) parameters for the buffer compartment in the geosphere transport. Source reports refer to reports (Poteri et al., 2012) and (Cormenzana, 2013a) (WR = working report, POSIVA = Posiva report).*

Quantity and dimension	Symbol	Value	Source
Deposition hole radius (m)	r_{dh}	0.88	POSIVA 2012-20
Volume of the buffer (m^3)	V_b	15.3	POSIVA 2012-20
Buffer thickness (m)	l_b	0.35	POSIVA 2012-20
Canister distance from the tunnel floor (m)	s_c	2.5	POSIVA 2012-20
Dry density of buffer (kg/m^3)	ρ_b	2760	WR 2013-25

For the buffer part, the parameters related to the intersecting fracture are in Table 8 and they are considered log-normally distributed. The realistic and conservative values with the truncation limits can be seen. The fracture aperture ($2b_v$) distribution is based on the research in (Cormenzana, 2013a). The mean value and conservative value are approximated from a figure that depicts the CDF of the simulated distribution (Figure 15-5 in (Cormenzana, 2013a)) and maximum and minimum are mentioned in the text. The decision of using log-normal distribution is based on the suggestion in (Cormenzana, 2013a)).

The groundwater velocity distribution in the buffer intersecting fracture is determined based on the values used in (Poteri et al., 2012) and (Cormenzana, 2013a). The velocity range between the realistic and conservative value corresponds to range of 2.75E-3 - 0.5 m/a. The value used in (Poteri et al., 2012) is used as a conservative value because the transmissivity used to calculate the value is already an order of magnitude higher than acceptable in the current design. The maximum value is determined to be two orders of magnitude higher than the conservative value and minimum value is set to zero as in (Cormenzana, 2013a). The realistic value is adopted from the calculated maximum value for TDZ-path in (Cormenzana, 2013a). TDZ corresponds to a flow path that leads from the canister, through the buffer and to the deposition tunnel backfill and

to a fracture intersecting the deposition tunnel ("Tunnel Damaged Zone"). The damaged zone is assumed to be primarily below the floor of the deposition tunnel. Therefore, the realistic velocity is a cautious choice for the flow velocity in the fracture that actually intersects the deposition hole due to tighter criteria in the deposition holes. The log-normal distribution is chosen based on the shape of the CDF in the report by (Cormenzana, 2013a) but it's a hypothetical assumption.

Table 8. *The log-normally distributed general parameters for the fracture intersecting the deposition hole. The reference case values in (Poteri et al., 2012) are marked in the cells. Source reports refer to Posiva's published reports (Poteri et al., 2012) and (Cormenzana, 2013a) (WR = working report, POSIVA = Posiva report).*

Quantity and dimension	Symbol	Minimum	Realistic (GM)	Conservative	Maximum	Source
2 x Fracture aperture (m)	$2b_v$	4.0E-6	3.0E-4 **(reference case)**	1.0E-2	1.0E-2	WR 2013-25
Groundwater velocity (m/s)	v_{dh}	0.0	8.72E-11	1.59E-8 **(reference case)**	1.59E-6	POSIVA 2012-20, WR 2013-25

For the tunnel compartment, the constant parameters are presented in Table 9 and the ones related to intersecting fracture are presented in Table 10. Again, the constant parameters are related to the designed KBS-3V concept of the disposal system.

Table 9. *The general (constant) parameters for the tunnel compartment in the geosphere transport. Source reports refer to Posiva's published reports (Poteri et al., 2012) and (Cormenzana, 2013a) (WR = working report, POSIVA = Posiva report).*

Quantity and dimension	Symbol	Value	Source
Perimeter of the tunnel (m)	p_t	16.0	POSIVA 2012-20
Volume of the tunnel section (m^3)	V_t	100.0	POSIVA 2012-20
Dry density of the tunnel backfill (kg/m^3)	ρ_t	2780	WR 2013-25

The bedrock fracture that intersects the deposition tunnel is assumed to have similar aperture properties as the fracture that intersects the deposition hole. The values for the log-normal distributions are presented with the reference case values in Table 10. The groundwater flow velocity in the fracture is again determined based on the reports (Cormenzana, 2013a) and (Poteri et al., 2012). The value used in (Poteri et al., 2012) is again used as a conservative value because of the assumptions of the transmissivity of the fracture. The realistic value is chosen to be the value used as a conservative value in the fracture that intersects the buffer. The decision is based on the fact that the value used for TDZ-path (even the maximum used for the fracture intersecting the deposition hole) is much smaller than the cautious value used in (Poteri et al., 2012) that resulting

distribution is several orders of magnitude wide making it unrealistic. A log-normal distribution is used in probabilistic sampling with truncation limits from zero to a value two orders of magnitude higher than the conservative value (similarly as with the buffer intersecting fracture).

Table 10. *The log-normally distributed general parameters for the tunnel component. The reference case values in (Poteri et al., 2012) are in the column denoted "Ref. case". Source reports refer to Posiva's published reports (Poteri et al., 2012) and (Cormenzana, 2013a) (WR = working report, POSIVA = Posiva report).*

Quantity and dimension	Symbol	Minimum	Realistic (GM)	Conservative	Maximum	Ref. case	Source
2 x Fracture aperture (m)	$2b_{vt}$	4.0E-6	3.0E-4	1.0E-2	1.0E-2	1.0E-3	WR 2013-25, POSIVA 2012-20
Groundwater velocity (m/s)	v_t	0.0	1.59E-8	1.25E-6	1.25E-4	1.25E-6	WR 2013-25, POSIVA 2012-20

The other general parameters for the solute transport in geosphere are presented in Table 11. The hydrodynamic control of retention (WL/Q) is chosen to follow log-normal distribution with the given properties due to results in (Cormenzana, 2013a) (Figure 3-11) and values used in (Poteri et al., 2012). The minimum value from the CDF in (Cormenzana, 2013a) obtained for TDZ-path is chosen as the minimum value and the realistic value is set to the reference case value used by Posiva. The conservative value is approximated to be one order of magnitude higher than the realistic value and the maximum value is set to 1.0E+6 a/m that is approximately 50 % level in the CDF curve for TDZ-path. It must be noted a higher value as a distribution parameter (conservative value) does not correspond to a conservative choice in reality as a lower WL/Q value corresponds to higher release rates (see Equation (12)).

The degradation rates for different inventory parts are adopted from (Cormenzana, 2013a) and they follow log-uniform distribution. For the degradation rates, the limits differ from the reference case values $\pm$ one order of magnitude (except fuel matrix).

Table 11. *Other general parameters related to radionuclide releases and transport in geosphere. The reference case values in (Poteri et al., 2012) are in the column denoted "Ref. case". Source reports refer to Posiva's published report (Cormenzana, 2013a) and (Poteri et al., 2012) (WR = working report, POSIVA = Posiva report). Log-normal distribution is used for hydrodynamic control of retention, rock density is a constant and degradation rates of different fuel parts follow log-uniform distribution in the calculation. (Cormenzana, 2013a)*

		Log-normal distribution					
Quantity and dimension	**Symbol**	**Minimum**	**Realistic (GM)**	**Conservative**	**Maximum**	**Ref. case**	**Source**
Hydrodynamic control of retention (a/m)	WL/Q	1.43E+4	3.76E+4	3.76E+5	1.0E+6	3.76E+4	WR 2013-25
		Constant					
Rock density (kg/m^3)	ρ_m	2700				2700	WR 2013-25
		Log-uniform distribution					
Degradation rate for fuel matrix (1/a)	$R_{deg,1}$	1.0E-8			1.0E-6	1.0E-7	WR 2013-25
Degradation rate for zirconium alloys (1/a)	$R_{deg,2}$	1.0E-5			1.0E-3	1.0E-4	WR 2013-25
Degradation time for other metal parts (1/a)	$R_{deg,3}$	1.0E-4			1.0E-2	1.0E-3	WR 2013-25

4.2.2 Nuclide specific parameters in geosphere transport

The nuclide specific parameters that are used to calculate the solute transport in the geosphere presented next. The distributions used for the parameters are taken largely from the sensitivity analysis report (Cormenzana, 2013a). In the following tables, LU (min), (max) denotes a log-uniform distribution with (min) and (max) as minimum and maximum values respectively.

The solubility limited nuclides are considered in the study by applying solubility limits inside the canister. The data for the solubility limits are adopted from (Wersin et al., 2014b) and determined values are presented in Table 12. For the elements considered, the solubility limit for brackish groundwater is lower than for saline groundwater, but the differences are less than an order of magnitude. Because the brackish groundwater is the most likely groundwater type (Posiva, 2013c), a log-uniform distribution is chosen, which results in more samples being taken from a lower end of the distribution than a uniform distribution. Nevertheless, differences between uniform or log-uniform distributions are small because ratio between minimum and maximum values is small.

The stable isotopes of the elements in the inventory are taken into account by calculating a coefficient for the solubility limit of the element. In reality, the element-specific solubility limits are not directly applicable unless the whole inventory consists of radioactive elements. In the canister, the three components all have different degradation rates and varying content of radioactive/stable isotopes. For the coefficients

for solubility limits, the fraction of the radionuclide inventory of the total inventory is calculated. The total inventory includes the stable isotopes and therefore, a minimum total inventory for the fastest degrading fuel component (other metal parts) is used. For the coefficient (i.e. the fraction of radionuclides), the radionuclide inventory is the total inventory of radionuclides including also other, more slowly degrading components of the fuel. In this manner, a cautious value for the solubility limit coefficient is obtained. The total inventories for the stable and radioactive isotopes of the elements are presented in Table 12. The coefficients are finally used to multiply to element-specific solubility limit in order to obtain a solubility limit for the radionuclide.

For the Mo-93 and Nb-94, the total inventories (stable and radioactive isotopes) are determined based on the maximum values of inventory in the other metal parts inventory. This choice is based on the fact that high values of inventories for Mo-93 and Nb-94 are only possible if the fuel has high content of Mo and Nb in their composition before irradiation. Both isotopes are mainly activation products, which means the majority of the inventory is produced from stable isotopes (Mo-92 and Nb-93). Therefore, the usage of minimum inventories for total inventory values is unrealistic when combined with high inventory of radioactive isotopes. However, the minimum total inventories are used in the reference case calculation (Cormenzana, 2013b).

Table 12. *The solubility limits in the canister in the simplified model. LU denotes log-uniform distribution and U uniform distribution with (min, max) as minimum and maximum values respectively. The reference case values in (Cormenzana, 2013a) are in the column denoted "Ref. case". The radionuclide inventory is the total inventory in the spent fuel canister (fuel matrix, zirconium alloys, other metal parts). (Wersin et al., 2014b), (Cormenzana, 2013b)*

Element	Total inventory of element (mol/tU)	Radionuclide inventory (mol/tU)	Coeff. (fraction of radionuclides)	Solubility limit (mol/l)	Solubility limit for radionuclide (mol/l)	Ref. case** (mol/l)
C-14, Cl-36, I-129	-*	-*	-	∞	∞	∞
Se-79,Se	8.09E-1	1.14E-1	1.41E-1	LU (5.90E-11, 5.80E-10)	LU (8.32E-12, 8.18E-11)	8.32E-12
Mo-93,Mo	19.8	6.82E-3	3.45E-4	LU (2.40E-6, 3.10E-6)	LU (8.50E-10, 1.10E-9)	1.34E-8
Nb-94, Nb	3.43	1.15	3.36E-1	LU (1.90E-7, 9.50E-7)	LU (6.38E-8, 3.19E-7)	1.90E-7
Ag-108m, Ag	2.06E+2	8.27E-1	4.02E-3	LU (5.10E-6, 9.90E-6)	LU (2.05E-8, 3.98E-8)	2.05E-8

*The inventory is not presented here as the solubility limit is not applied in the calculation.
**For the reference case, the Mo-93 and Nb-94 the minimum total inventories are used.

In Table 13, the selected values for effective diffusion coefficients (D_{eb}, D_{em}) and porosities (ϵ_b, ϵ_t, ϵ_m) are shown. In the buffer and tunnel backfill, the water types selected for the data reference are saline and brackish (Table 8-4 of recommended

values in (Wersin et al., 2014b)). The values determine the interval with cautious rounding. A log-uniform distribution is used as only single data values are available.

The porosity values are selected by using the data in Table 8-4 of (Wersin et al., 2014b) (also Table 5-2 in (Cormenzana, 2013b). The upper limits are about the values available for the used water types and lower limits are cautiously selected to be the lowest data available for all water types. A lower porosity corresponds to a higher mass transfer coefficient for a compartment, which results in faster transport and possibly higher radiation risks. The effect of "anion exclusion" (Posiva, 2012b) is taken into account by assigning smaller values for anions than for cations.

The effective diffusion coefficient in the bentonite is selected to cover the range for saline and brackish water types for anions. For cations, the values are taken from (Cormenzana, 2013b) as there are not data available to justify any other range. Again, the effect of anion exclusion is taken into account by assigning smaller values for anions than for cations.

Similar parameters are applied to both cations and anions in the unaltered rock. The justification is similar as in (Cormenzana, 2013b): it is assumed that there is not anion exclusion in the unaltered rock. The porosity value range is taken from (Cormenzana, 2013b) and it is based on site averaged site measurement data. The effective diffusion coefficient range is similarly taken from the measured data.

Table 13. *The nuclide specific porosities and effective diffusion coefficients in components of the geosphere transport. LU denotes a log-uniform distribution. All values are taken from (Cormenzana, 2013b).*

Quantity, symbol and dimension	**C-14, Mo-93, Nb-94, Ag-108m**	**Cl-36, Se-79, I-129**	**Reference case**
Porosity of the buffer ϵ_b (-)	0.43	LU (1.0E-2, 0.11)	0.43 (neutral/cation) 0.08 (anion)
Effective diffusion coefficient in bentonite D_{eb}(m^2/s)	LU (2.0E-11, 2.0E-10)	LU (1.0E-12, 1.0E-11)	1.3E-10 (neutral/cation) 7.8E-12 (anion)
Porosity of the tunnel backfill ϵ_t (-)	0.38	LU (1.0E-2, 0.1)	0.38 (neutral/cation) 0.07 (anion)
Effective diffusion coefficient in rock matrix D_{em} (m^2/s)	LU 1.0E-15, 1.0E-12		6.0E-14 (all)
Porosity of the rock matrix ϵ_m (-)	LU 1.0E-3, 2.0E-2		0.005 (all)

The distribution coefficients of the nuclides in the geosphere components are determined based on Posiva's data in report (Wersin et al., 2014b). The reference case values are taken from the PSA report (Cormenzana, 2013a). Similarly as earlier, the brackish and saline water types are used in selecting data. By applying cautiousness, the lowest values are prioritized between the two water types.

The distribution coefficients in the buffer (Kd_{pb}) are presented in Table 14. For Nb-94, the conservative (and maximum) value is chosen based on glacial melt water (the lowest

available data) as the retardation adds delay to solute transport. The log-normal distributions are assigned with the depicted parameter values due to variety of the data and usage before (for example in (Cormenzana, 2013a)). The conservative values are also used as the maximum values for truncation.

Table 14. *The distributions coefficients Kd_{pb} (m^3/kg) in the buffer for sorbing nuclides. The log-normal distributions are used with truncation limits shown. The conservative values are also used as maximum values. The reference case values are taken from (Cormenzana, 2013a) and other values from (Wersin et al., 2014b).*

Nuclide	Minimum	Realistic (GM)	Conservative	Maximum	Reference case
Mo-93	3.6E-4	7.5E-3	3.1E-2	3.1E-2	2.1E-2
Nb-94	0.40	5.4	23.5	23.5	5.4

All non-sorbing nuclides have been assigned zero distribution coefficients in all components of the transport chain based on recommendations in (Wersin et al., 2014b). C-14 is considered to be cautiously bound to organic species that means it's considered as non-sorbing. I-129 is also a non-sorbing nuclide as the data do not show significant sorption for iodine. With Cl-36 and Se-79, the situation is similar and the recommended value of zero is used in the calculations. With Ag-108m, the distribution coefficient recommendation for all the water types except glacial melt water is zero.

For the tunnel backfill, the distribution coefficients for sorbing nuclides (Kd_{pt}) are presented in Table 15. Again, log-normal distributions are assigned based on the selected values. All the other nuclides considered are assigned a zero distribution coefficient due to recommendations in (Wersin et al., 2014a).

Table 15. *The distributions coefficients Kd_{pt} (m^3/kg) in the tunnel backfill for sorbing nuclides. The log-normal distributions are used with truncation limits shown. The conservative values are also used as maximum values. The reference case values are taken from (Cormenzana, 2013a) and other values from (Wersin et al., 2014b).*

Nuclide	Minimum	Realistic (GM)	Conservative	Maximum	Reference case
Mo-93	4.6E-4	9.6E-3	4.0E-2	4.0E-2	1.9E-2
Nb-94	0.3	3.0	20	20	3.0

The distribution coefficients in the rock matrix (Kd_{pm}) are assumed to follow log-uniform distribution because only upper and lower limits in the data are available. The selections are presented in Table 16. The choices for the limits are based on brackish or saline water conditions in the bedrock and the lowest values are prioritized. The minimum value of 1.0E-10 corresponds to a zero distribution coefficient under the expected conditions. A lower value does not significantly change the retardation coefficient value from 1 but and it does not underestimate the retardation significantly.

In addition to anionic nuclides, the values for C-14 and Se-79 are chosen to be zero in the rock matrix. C-14 is assumed to be in a non-sorbing organic form as before. With Se-79, a zero distribution coefficient is a conservative choice as only the Se (IV) species has a non-zero distribution coefficient in brackish water conditions and there are no data

available for other species. The upper limit for Nb-94 is (over) cautiously selected to be the reference case value in order to obtain shorter time constants for the model.

Table 16. *The distributions coefficients Kd_{pm} (m^3/kg) in the rock matrix for different nuclides. The log-uniform distributions are applied. The values for Se-79 and C-14 are zero in the base case and reference case. (Cormenzana, 2013b)*

Nuclide	Minimum	Maximum	Reference case
Cl-36	1.0E-10	1.7E-6	0.0
Mo-93	9.4E-9	9.2E-4	3.0E-4
Nb-94	1.2E-2	4.2E-1	4.2E-1
Ag-108m	1.0E-10	3.8E-8	0.0
I-129	1.0E-10	5.0E-6	0.0

4.2.3 Instant release fractions

The radionuclide release occurs by instant release and gradual leaching. The IRFs (IRF_i) that are used in the simulations are presented in Table 17. The fraction of the radionuclides, which are located at the fuel-clad gap and grain boundaries, are included in the IRFs. Also, the inventory in the "crud" (a deposit of corrosion products on the outer surface of the cladding) is included in the IRF because the release conditions of that inventory are not known (Cormenzana, 2013b).

The values are adopted from the sensitivity analysis report (Cormenzana, 2013a) and similar log-uniform distribution is applied for each IRF. Typically, the reference case values of the BSA-2012 assessment are included in the IRF interval determined in the (Cormenzana, 2013b). Due to lack of data, the lower limits are typically obtained by dividing the upper limit by 10 in (Cormenzana, 2013b). Hypothetical assumptions are also used for other justifications. The justifications for the IRF ranges from (Cormenzana, 2013b) are summarized below:

- C-14 in the fuel matrix:
  - The reference case value is 0.1. Due to scarce data, a broad interval of [0.01, 0.5] is used.
- C-14 in the zirconium alloys:
  - The reference case value is 0.2 and it's based on the current understanding that 20 % of the C-14 of the cladding is in the oxide layer of zirconium based alloys (Cormenzana, 2013b). Due to scarce data, a broad interval of [0.01, 1.0] is used.
- C-14 in other metal parts:
  - Due to scarce data, a very broad interval of [0.01, 1.0] is used with the reference case value being zero.
- Cl-36 in the fuel matrix:
  - The reference case value is 0.1. The used range of [0.02, 0.2] is calculated based on values used in normal distributions by SKB for the PWR fuel in (SKB, 2010) and the upper limit corresponds to roughly $\mu + \sigma$. The BWR fuel has smaller values for the μ and σ.
- Se-79 in the fuel matrix:

  - The reference case value is 0.004. The range of [0.002, 0.02] is calculated based on the normal distributions by SKB for the PWR fuel. The upper limit corresponds to roughly $\mu + 2\sigma$.
- Mo-93 in the fuel matrix:
  - The reference case value is 0.05 and it is used as the upper limit for the range of [0.005, 0.05]
- Mo-93 in zirconium alloys and other metal parts:
  - Zero IRF is used in the reference case. The upper limit for the range of [0.002, 0.02] represents the crud inventory and the value is adopted from SKB.
- Nb-94 in all inventories:
  - Zero IRF values are used in the reference case. The upper limit for the IRF range of [0.003, 0.03] in zirconium alloys and in other metal parts represents the crud inventory and is adopted from SKB.
- Ag-108m in the fuel matrix:
  - The reference case value is 0.05 and it is used as the upper value for the range of [0.005, 0.05].
- Ag-108m in other metal parts:
  - The reference case value is 1.0 but a broad interval of [0.05, 1.0] is used due to lack of the silver release rate from the Rod Control Cluster Assembly (RCCA).
- I-129 in the fuel matrix:
  - The reference case value is 0.05. The upper limit for the range of [0.015, 0.15] is obtained by deciding to explore the effect of high burnup PWR fuel (for example Olkiluoto 3 reactor), for which higher fission gas releases (FGRs) have been obtained than the reference case value. The FGR and IRF have been observed to be correlated.

The zero IRF values that are not mentioned correspond to an empty inventory on that part of the spent fuel.

Table 17. *The instant release fractions (IRF_i) that are used in the calculations. Log-uniform distribution is applied for each interval given by the minimum and maximum values (separated by a comma). The chosen reference case values are presented in the column denoted "Ref. case". (Cormenzana, 2013a)*

Nuclide	IRF fuel matrix	Ref. case	IRF zirconium alloys	Ref. case	IRF other metal parts	Ref. case
C-14	0.01, 0.5	0.1	0.01, 1.0	0.2	0.01, 1.0	0.0
Cl-36	0.02, 0.2	0.1	0.0		0.0	
Se-79	0.002, 0.02	0.004	0.0		0.0	
Mo-93	0.005, 0.05	0.05	0.002, 0.02	0.0	0.002, 0.02	0.0
Nb-94	0.0		0.003, 0.03	0.0	0.003, 0.03	0.0
Ag-108m	0.005, 0.05	0.05	0.0		0.05, 1.0	1.0
I-129	0.015, 0.15	0.05	0.0		0.0	

Use of log-uniform distributions in the model parameters overestimates the probability of boundary realizations (maximum IRF, minimum porosity, maximum diffusion

coefficient etc.). Of course, they are not impossible but the probability in reality tends to be lower with the boundary conditions because uniform distributions are rare in natural conditions.

4.2.4 General parameters in biosphere analysis

The general parameters in the biosphere analysis are related to the dose rate assessment or to the properties of the biosphere objects. For the reference case calculation, mostly mean values for the parameters are chosen in the following tables. The properties of the biosphere objects are to some extent distributed in order to cover the variance due to time development of the biosphere and also overall uncertainty. Some properties for the objects are determined by using UNTAMO data that are used in reference case calculation in the landscape model (BSA-RC) by Posiva (Posiva, 2014b). The data originally contains hundreds of objects so cautiousness is applied in selecting the most relevant and pessimistic ones for averaging. In addition to the recommendations in (Posiva, 2014a), the diet profile of an exposed individual is used to filter out the larger lakes and terrestrial objects that could provide foodstuff for a larger amount of individuals.

The general parameters required for calculating the dose rates are depicted in Section 3.2.3. The ingestion amounts of an exposed individual are presented in Table 18. An assumption is made that the juices made of wild berries are accounted in the total amount of berries. The ingestion amount of drinking water for humans is considered as the only distributed parameter that follows a normal distribution with the provided parameters as arithmetic mean and standard deviation. Although, in the data source a log-normal distribution is suggested for the drinking water intake, a normal distribution is used for simplicity and the difference is negligible due to small range of values. The truncation limits for the drinking water intake are selected to be the 0 m^3/a and 99^{th} percentile (1.63 m^3/a). The truncation limits do not mean that the exposed individual would not drink at all but instead, the variety depicts the usage of other water sources that are not contaminated. Other parameters are not considered distributed for simplicity of the analysis.

Table 18. *The diet profile of an exposed individual and an individual cow used in the dose assessment. The data are taken from (Posiva, 2014a) that is shortly labelled POSIVA 2012-28 in the table. The drinking water ingestion follows a normal distribution with the given parameters being arithmetic mean (AM) and standard deviation (STD) respectively with truncation limits at 0 m^3/a and 99th percentile (min, max).*

Human	Amount	Symbol	Unit	Source
Drinking water	Normal (0.618, 0.434, min = 0.0, max = 1.63) (ref. case 0.6)	W	m^3/a	Mean and standard deviation from POSIVA 2012-28
Fish	10.2	Ing_i	kg/a	28 g/d in POSIVA 2012-28
Berries	27.7		kg/a	18 g/d berries and 58 g/d juices in POSIVA 2012-28
Cereals	65.3		kg/a	179 g/d in POSIVA 2012-28
Field vegetables	45.6		kg/a	125 g/d in POSIVA 2012-28
Potatoes	37.6		kg/a	103 g/d in POSIVA 2012-28
Milk	184		kg/a = L/a	505 g/d in POSIVA 2012-28
Meat	61.0		kg/a	167 g/d in POSIVA 2012-28
Livestock (cows)				
Drinking water	0.11	W_{cows}	m^3/d/individual	POSIVA 2012-28
Pasture	0.11	Ing_{past}	kg/d/individual	POSIVA 2012-28

In addition to ingestion related parameters, the inhalation parameters used are taken from (Posiva, 2014a). The dust concentration in the air set to a constant value of 5.00E-7 kg/m^3. The inhalation rate is set to follow a uniform distribution with minimum and maximum values of 0.7 m^3/h and 2.5 m^3/h respectively (reference case value 1.0 m^3/h). The exposure time for external radiation and inhalation is full time of the year, 8760 h/a.

The aquatic object in the biosphere model is a lake that receives the radionuclides to its bottom sediment. Another water source is a well that can be used for drinking water and irrigation. The mixing volume for the well, namely the annual mixing capacity of the well, is set to 1000 m^3 in the base and reference calculation case in this study. In the BSA-2012 assessment, the minimum capacity for a shallow household well is determined to be 500 m^3/a (Posiva, 2014a). Taking into consideration the irrigation demand in the simplified model (about 1900 m^3 with maximum cropland areas in the base case), the larger capacity is justified although the resulting drinking water related doses (water ingestion, milk-water and meat-water dose paths) decrease.

The lake properties are shown in Table 19. The parameters may be constants or follow a distribution that is provided in the table. The distributions for the lake area, discharge

and average water depth are based on data produced by UNTAMO (Posiva, 2014a) and the procedure in obtaining the distribution parameters is described later. The discharge is set to both a forest and sink with 10 % and 90 % portions respectively in the base case and in the reference case.

Most of the data are taken from the data basis used in BSA-2012 assessment (Posiva, 2014a). A triangular distribution is used for the advective water fluxes between the sediments (denoted "Water flux up" in the table) because the minimum, maximum and mode are available in the data basis report (Posiva, 2014a). The saturated water content values are partly obtained from the Posiva's landscape model by considering also the data used in biosphere object "EjjG" (see (Posiva, 2013a) for further information) that describes an aquatic ecosystem in the reference case BSA-RC. The bulk densities of the lake sediments are chosen to represent a clay sediment as a top sediment and a fine mineral soil sediment as the intermediate sediment.

Table 19. *The lake object parameters in the biosphere analysis. A part of the data are distributed: TR denotes a triangular distribution with parameters (minimum, mode, maximum), LU denotes a log-uniform distribution with parameters (minimum, maximum), U denotes a uniform distribution with parameters (minimum, maximum). The most of the data are available in (Posiva, 2014a) that is labelled POSIVA 2012-28 in the table. The chosen reference case values are presented in the column denoted "Ref. case".*

Parameter and unit	Symbol	Value	Ref. case	Source
Lake water				
Average water depth (m)	d_w	TR (0.684, 1.30, 1.86)	0.7	Processed data from UNTAMO.
Area (m^2)	A	TR (5 000, 10 400, 15 100)	10 000	Processed data from UNTAMO.
Discharge (m^3/a)	$WfluxOut$	LU (9.83E+1, 1.03E+5)	3180	Corresponds to 3.12E-6 m^3/s and 3.27E-3 m^3/s. Processed data from UNTAMO.
Top sediment				
Water flux up (m/a)	$Wflux_i$	TR (1.0E-3, 2.5E-2, 6.9E-2)	2.5E-2	POSIVA 2012-28
Depth (m)	d_i	0.3	0.3	POSIVA 2012-28
Porosity (-)	ϵ_i	U (0.34, 0.76)	0.56	POSIVA 2012-28
Saturated water content (-)	sat_i	0.56	0.56	Reference case object (EjjG) data. (Posiva, 2014b)
Bulk density (kg/m^3)	ρ_i	TR (160, 260, 650)	260	POSIVA 2012-28
Intermediate sediment				
Water flux up (m/a)	$Wflux_i$	TR (0.001, 0.021, 0.056)	0.021	POSIVA 2012-28
Depth (m)	d_i	0.7	0.7	POSIVA 2012-28
Porosity (-)	ϵ_i	U (0.23, 0.61)	0.43	POSIVA 2012-28
Saturated water content (-)	sat_i	0.56	0.56	Reference case object (EjjG) data. (Posiva, 2014b)
Bulk density (kg/m^3)	ρ_i	U (810, 2 200)	1 800	POSIVA 2012-28

Lake area estimation

The procedure in obtaining the minimum and maximum values for the lake area is the following:

1. From the reference case data, select the lake objects for averaging that
    a. exist for over 1000 years (have at least four time points in UNTAMO)
    b. are at some point over 1 ha ("minimum" lake area in (Posiva, 2014a)).
    c. are not so large that they could produce fish for over 10 individuals. In practice, the maximum area for averaging is about 11.5 ha that is calculated based on the consumption of fish and estimated production (fresh fish production in lakes 8.85 kg_{fresh}/ha, (Posiva, 2014a))
2. Calculate the average lake area at every time point from the selected lakes.

3. Calculate the geometric mean of average lake sizes over time. The geometric mean is considered to be a more cautious estimate for the average value over time because generally the mean value is smaller than arithmetic mean.
4. Calculate the difference of averages to the geometric mean to see the behavior of the average lake area over time. The same behavior could be observed by plotting the absolute values of average lake area values.
5. Obtain the minimum and maximum lake areas from a rather "stable" period and perhaps use the geometric mean as a mode value for the distribution. This approach leads to either a triangular or a uniform distribution. In the base case, a uniform distribution is used.

Average water depth estimation

With the average water depths, the procedure in determining the distribution parameters is rather similar as with the lake area. The selected lake objects for area estimation are used again for obtaining average time series. The following steps are used in excluding some of the selected lake objects and obtaining the estimate for average water depth.

1. The average of the average water depths is calculated for each time point and a geometric mean is obtained over time. The average values that are approximately below 0.7 m (minimum average water depth for a lake in (Posiva, 2014a)) are excluded from the geometric mean.
2. Due to the fact that no "stable" period is not obtained for average water depth, the minimum and maximum are obtained by selecting the minimum and maximum values from the averages that are used to calculate geometric mean.
3. Finally, a triangular distribution is used for average water depth with the mode of the calculated geometric mean.

Lake discharge estimation

The lake in the model has a discharge that removes the water from the lake to a sink (out of the system) or to a terrestrial compartment. The discharge rates are determined by using a similar type of averaging as with the average water depths and lake areas. Again, the same objects that are used in calculating the lake area parameters are selected at first. The procedure in excluding some of the objects includes the following steps:

1. The average value for discharge is calculated for each time point and a geometric mean over time is determined. The maximum discharge for averaging is set to 0.5 m^3/s (minimum mean discharge for a river in (Posiva, 2014a)) because the analysis is cautiously limited to lakes that have a lower turnover rate.
2. A uniform distribution is selected for the discharge rate because the range of discharge values is about three orders of magnitude. The maximum value is obtained from the beginning of a "stable" period at about 5500 years and the minimum value from the last time point because the average discharge rates are decreasing.

The biosphere model includes croplands, a pasture land and a forest as terrestrial objects. The croplands are divided into three most significant crop types in the diet of a Finnish average man (Posiva, 2014a). The crop types included in the model are cereals, potatoes and field vegetables. The parameters describing general properties of croplands in the model are presented in Table 20. The common parameters for all objects are listed

in the upper section of the table. Most of the parameters are taken from the data basis used in BSA-2012 biosphere assessment. By the bulk density, the terrestrial objects are fine mineral soil -based layers (like the intermediate sediment the lake). The runoff flux from the objects is pessimistically selected to have the values related to surface runoff in BSA-2012 (sub-surface runoff is higher than surface runoff). The data from UNTAMO are processed with a procedure described next.

Table 20. *The general parameters for the terrestrial objects in the biosphere model. The reference labels refer to reports (Posiva, 2014a) and (Posiva, 2013b). U denotes a uniform distribution with the minimum and maximum values provided in the brackets. The chosen reference case values are presented in the column denoted "Ref. case".*

Quantity and unit	Symbol	Value	Ref. case	Source
Irrigation (m/a)	$irrg$	0.03	0.03	POSIVA 2012-28
Depth (m)	d_i	0.3	0.3	POSIVA 2012-28
Runoff water flux (m/a)	$Wflux_i$	U (0.014,0.021)	0.018	POSIVA 2012-28
Saturated water content (-)	sat_i	0.54	0.54	POSIVA 2012-30
Bulk density (kg/m^3)	ρ_i	U (810, 2 200)	1 800	POSIVA 2012-28
Porosity (-)	ϵ_i	U (0.23, 0.61)	0.43	POSIVA 2012-28
Cropland for Cereals				
Area (m^2)	A	U (1910, 10 300)	6 110	Processed data from UNTAMO.
Cropland for potatoes				
Area (m^2)	A	U (8 880, 23 200)	16 030	Processed data from UNTAMO.
Cropland for field vegetables				
Area (m^2)	A	U (3 800, 13 000)	8 370	Processed data from UNTAMO.
Pasture land				
Area (m^2)	A	U (7 150, 15 100)	11 100	Processed data from UNTAMO.
Forest				
Area (m^2)	A	U (1 060, 12 930)	6 990	Processed data from UNTAMO.
Runoff water flux (m/a)	$Wflux_i$	U (0.004, 0.008)	0.007	POSIVA 2012-28
Bulk density (kg/m^3)	ρ_i	U (110, 2800)	1200	POSIVA 2012-28

Estimation terrestrial object areas

The areas for the terrestrial objects (croplands, pasture land and forest) are obtained from the reference case UNTAMO data set in a similar fashion as with the lake parameters. The following procedure is conducted in obtaining the areas:

1. The areas for all terrestrial objects are determined by averaging the area of reference case objects at every time point for a specific object type. The following rules for selecting the objects are used:
    a. The objects, which are too large at many time points, are excluded because smaller area is a cautious choice due to higher concentrations in the soil. The maximum area for cereals is 2 ha (typical crop size minimum (Posiva, 2014a)), for potatoes 5 ha (typical crop size median and many croplands larger than 5 ha in the dataset (Posiva, 2014a)) and for field vegetables no an explicit limit is used (all data under 5 ha). For pasture land and forests, no limits for the area are applied.
    b. The objects, which exist less than 1000 years, are excluded but also objects that disappear at some time point are excluded.
2. A geometric mean over the time points is determined. Some exclusions are made in calculating the geometric mean:
    a. For cereals, an area smaller than about 130 m^2 is considered too small to feed one individual (the maximum yield about 5000 kg/ha/a and ingestion amount of 65.335 kg/a (Posiva, 2014a)). Also, averages over 2 ha are excluded to ensure a cautious estimate.
    b. For forests, 1000 m^2 is used for a minimum area in calculating geometric mean. This limit is chosen because the majority of the time series had values over 1000 m^2 and a more realistic value is wanted.
3. The differences between the averages and geometric mean value are plotted in order to observe the development of crop areas. Due to significant rise in average area due to land uplift a uniform distribution for the areas is applied.
    a. For cereals, the minimum and maximum values for the distribution are picked from the data set with the smallest geometric mean. The maximum value is chosen from the end of the time points and minimum from the point that has similar difference to the geometric mean as the maximum value (symmetrically).
    b. For potatoes, a data set with a more stable (and cautious) period is used to determine the minimum and maximum value. From the time points involved in the geometric mean, the minimum and maximum areas are chosen for the uniform distribution.
    c. For field vegetables, the minimum and maximum values are chosen from the data set with the smallest geometric mean. The minimum and maximum are the minimum and maximum values of the time point included in the geometric mean.
    d. For the forest and the pasture land, the minimum and maximum values are chosen from the time series of average areas included in the geometric mean.

The C-14 dose assessment by using a specific activity model is presented in Section 3.2.4. The required general parameters are presented in Table 21. The parameters are mostly adapted from BSA-2012 assessment and the distributions are determined from

the data available in (Posiva, 2014a). The normal distributions used for net primary productions in the ecosystems are recommendations taken from the report. The triangular distributions are chosen for mostly average vegetation heights as only nominal, minimum and maximum values are available.

Table 21. *The parameters required in specific activity model to calculate dose exposure from C-14. N denotes a normal distribution with (mean, standard deviation) as parameters (min and max denote the truncation limits), TR denotes a triangular distribution with parameters (minimum, mode, maximum) and U denotes a uniform distribution with parameters (minimum, maximum). The chosen reference case values are presented in the column denoted "Ref. case". (Posiva, 2014a)*

Parameter and unit	Symbol	Value	Ref. case
Fraction of year during which photosynthesis occurs (-)	veg_p	1.0*	1.0
Height at which the annual average wind speed is measured (m)	h	20.0	20.0
Concentration of stable carbon in air (kg_C/m^3)	C_{C-12}	2.06E-4	2.06E-4
Average annual wind speed (m/s)	v_{ms}	U (3.6, 4.4)	4.0
Cereal cropland			
Net primary production (kg_C/m^2)	NPP	N (0.26, 0.02), min 0.22, max 0.28	0.26
Roughness length (m)	z_0	0.09	0.09
Average height of vegetation (m)	h_{veg}	TR (0.6, 0.85, 1.3)	0.85
Potato cropland			
Net primary production (kg_C/m^2)	NPP	N (0.55, 0.05), min 0.44, max 0.61	0.55
Roughness length (m)	z_0	0.06	0.06
Average height of vegetation (m)	h_{veg}	TR (0.51, 0.6, 0.73)	0.6
Field vegetables cropland			
Net primary production (kg_C/m^2)	NPP	N (0.54, 0.06), min 0.46, max 0.61	0.54
Roughness length (m)	z_0	0.04	0.04
Average height of vegetation (m)	h_{veg}	TR (0.2, 0.4, 0.7)	0.4
Forest			
Net primary production (kg_C/m^2)	NPP	TR (0.16, 0.33, 0.49)	0.33
Roughness length (m)	z_0	1.4	1.4
Average height of vegetation (m)	h_{veg}	TR (0.05, 0.25, 0.8)	0.25
Lake			
Net primary production (kg_C/m^2)	NPP	0.680	0.680

* The justification for the full-year photosynthesis is presented in (Avila & Pröhl, 2008).

The ingestion amounts of carbon are calculated based on the carbon concentrations in different foodstuff and the ingestion amounts determined earlier. The data used for C-14 dose assessment are summarized in Table 22.

Table 22. *The ingestion amounts of carbon for C-14 dose assessment based on the diet of an individual. c_{carbon} denotes carbon concentrations in dry weight in the vegetation or of livestock products (fresh). C_{ing} denotes the calculated values of carbon ingestion based on the diet of an individual. Normal distributions are used in sampling with the given truncation limits (minimum and maximum) and parameters (AM = arithmetic mean, STD = standard deviation). The fish ingestion amount is constant in the calculation (see bottom part of the table). The chosen reference case values are presented in the column denoted "Ref. case". (Posiva, 2014a)*

Amounts	Minimum	Maximum	AM	STD	Ref. case
Cereals (65.3 kg/a)					
c_{carbon} (kg_C/kg)	0.41	0.53	0.45	0.03	0.45
C_{ing} (kg_C/a)	26.8	34.6	29.4	1.96	29.4
Field vegetables (45.6 kg/a)					
c_{carbon} (kg_C/kg)	0.38	0.47	0.40	0.03	0.40
C_{ing} (kg_C/a)	17.3	21.4	18.3	1.37	18.3
Berries (27.7 kg/a)					
c_{carbon} (kg_C/kg)	0.38	0.53	0.43	0.03	0.43
C_{ing} (kg_C/a)	10.5	14.7	12.2.	0.832	12.2.
Potatoes (37.6 kg/a)					
c_{carbon} (kg_C/kg)	0.38	0.53	0.44	0.03	0.44
C_{ing} (kg_C/a)	14.3	19.9	16.5	1.13	16.5
	Fish (10.2 kg/a)				
c_{carbon} (kg_C/kg)	0.108				
C_{ing} (kg_C/a)	1.10				

4.2.5 Nuclide specific parameters in biosphere analysis

The nuclide specific parameters in the biosphere calculation are the distribution coefficients in the various soil layers, diffusion coefficients in water, concentration ratios to various foodstuff and dose coefficients. Diffusion coefficients and dose coefficients are the ones that are not considered distributed in the calculation. Truncated log-normal distributions are assigned based on minimum, maximum, geometric mean and geometric standard deviation for distribution coefficients. The sampling from the log-normal distribution is described in Section 4.1 (see Equation (56)). The truncation limits are calculated to be the 1st and 99th percentile if the data do not provide the limits to avoid physically impossible realizations. For the reference case calculation, mostly (geometric) mean values for the parameters are chosen in the following tables because the values are used in BSA-2012.

The dose coefficients for the radionuclides used in the calculation cases are presented in Table 23. The data are taken from (Posiva, 2014a).

Table 23. *The dose coefficients for ingestion, inhalation and for external exposure due to spatially uniformly distributed radionuclides on the ground surface and to an infinite depth. Mo-93 marked with '+d' indicates that the ingestion/inhalation dose coefficient(s) contribution from radioactive progeny is included. (Posiva, 2014a)*

Nuclide	**Ingestion dose coefficient α_{ing} (Sv/Bq)**	**Inhalation dose coefficient α_{inh} (Sv/Bq)**	**External dose coefficient α_{ext} (Sv/h)/(Bq/m^3)**
C-14	5.8E-10	5.8E-9	2.1E-19
Cl-36	9.3E-10	7.3E-9	4.8E-17
Se-79	2.6E-9	6.8E-9	3.0E-19
Mo-93+d	4.6E-9	4.1E-9	9.4E-18
Nb-94	1.7E-9	4.9E-8	1.8E-18
Ag-108m	2.3E-9	3.7E-8	1.7E-13
I-129	1.1E-7	3.6E-8	1.8E-16

The diffusion coefficients D for free water diffusion are given in Table 24. The coefficients are applied in all biosphere objects and calculation cases. The values are taken from (Posiva, 2014a) and because of limited data distributions are not used.

Table 24. *The diffusion coefficients for free water diffusion used in the biosphere analysis. Due to limited data, the coefficients are constants. (Posiva, 2014a)*

Nuclide	**Diffusion coefficient (m^2/s)**
C-14	1.2E-9
Cl-36, I-129	2.0E-9
Se-79, Mo-93, Nb-94	1.0E-9
Ag-108m	1.7E-9

The distribution coefficients used in the biosphere objects are chosen based on a review in (Posiva, 2014a). C-14 is not sorbing in the biosphere and therefore zero value is used. The log-normal distributions are applied for all distribution coefficients in the biosphere in the base case. Due to sparse data, the truncation limits are calculated to be the 1st and 99th percentiles. The reference case selections are the geometric mean values.

Table 25. *The values for distribution coefficients (K_d) in dry weight in the overburden for the radionuclides (Bq/kg)/(Bq/m^3). Calculated truncation at 1st and 99th percentiles is denoted with the minimum and maximum values (italic). GM denotes geometric mean and GSD geometric standard deviation. The chosen reference case values are presented in the column denoted "Ref. case". (Posiva, 2014a)*

Nuclide	Minimum	Maximum	GM	GSD	Ref. case
Lake (top and intermediate sediments)					
Cl-36	*2.8E-03*	*2.5E-2*	8.4E-3	1.6	GM
Se-79	*1.6E-01*	*14*	1.5	2.6	
Mo-93	*1.8*	*1.3E+2*	15	2.5	
Nb-94	*3.6*	*5.1E+2*	43	2.9	
Ag-108m	*3.6E-01*	*9.0*	1.8	2.0	
I-129	*1.2E-01*	*4.1E-1*	0.22	1.3	
Croplands and pasture land (top layer)					
Cl-36	*1.1E-04*	*1.1E-1*	3.5E-3	4.4	GM
Se-79	*1.3E-02*	*1.1*	1.2E-1	2.6	
Mo-93	*1.5E-03*	*4.4*	8.0E-2	5.6	
Nb-94	*5.3E-01*	*75*	6.3	2.9	
Ag-108m	*2.9E-02*	*7.6*	4.7E-1	3.3	
I-129	*6.2E-03*	*1.6E-1*	3.1E-2	2.0	
Forest (top layer)					
Cl-36	*9.7E-04*	*6.8*	8.1E-2	6.7	GM
Se-79	*1.3E-02*	*6.3*	2.8E-1	3.8	
Mo-93	*4.9E-03*	*74*	6.0E-1	7.9	
Nb-94	*6.0*	*1.5E+2*	30	2.0	
Ag-108m	*8.1E-02*	*31*	1.6	3.6	
I-129	*1.6E-03*	*22*	1.9E-1	7.7	

For the concentration ratios, the data and distribution parameters determined in (Posiva, 2014a) are applied. For C-14, the specific activity model is used instead of concentration ratios. There are gaps in the available data (only nominal or GM value available) and therefore, for some parameter values the geometric standard deviations are adopted from (Nordén et al., 2010). When the truncation limits are not provided in (Posiva, 2014a), the range of between 1st and 99th percentiles is adopted. The parameters for the distributions for the concentration ratios to cow milk are presented in Table 26.

Table 26. *The concentration ratios (or transfer factors) from intake to cow milk (Bq/l)/(Bq/d). GM denotes geometric mean and GSD geometric standard deviation. Log-normal distributions are used with the calculated truncation limits at 1st and 99th (values italic). The bolded values are obtained from (Nordén et al., 2010). The chosen reference case values are presented in the column denoted "Ref. case". (Posiva, 2014a)*

Nuclide	Minimum	Maximum	GM	GSD	Ref. case
Cl-36	*3.6E-3*	*9.0E-2*	1.8E-2	2.0	GM
Se-79	1.5E-3	1.6E-2	4.0E-3	2.1	
Mo-93	4.3E-4	5.2E-3	1.1E-3	2.3	
Nb-94	*6.9E-9*	*2.4E-5*	4.1E-7	**5.8**	
Ag-108m	*3.3E-6*	*7.5E-4*	5.0E-5	**3.2**	
I-129	4.0E-3	2.5E-2	5.4E-3	**2.9**	

The concentration ratios to cow meat are presented in Table 27. The data are sparse so many GSD values are adopted from SKB and truncation limits needed to be determined.

Table 27. *The concentration ratios (or transfer factors) from intake to livestock (cow) meat (Bq/kg$_{fresh}$)/(Bq/d). GM denotes geometric mean and GSD geometric standard deviation. Log-normal distributions are used with truncation at 1st and 99th percentiles (values italic). The bolded values are adopted from (Nordén et al., 2010). The chosen reference case values are presented in the column denoted "Ref. case". (Posiva, 2014a)*

Nuclide	Minimum	Maximum	GM	GSD	Ref. case
Cl-36	*1.4E-4*	*2.1*	1.7E-2	**7.9**	GM
Se-79	*1.5E-3*	*5.3*	8.8E-2	5.8	
Mo-93	*6.7E-5*	*1.5E-2*	1.0E-3	**3.2**	
Nb-94	*2.1E-9*	*3.2E-5*	2.6E-7	**7.9**	
Ag-108m	2.0E-3	6.0E-3	3.0E-3	**1.3**	
I-129	2.0E-3	3.8E-2	6.7E-3	3.2	

The concentration ratios to pasture biomass are presented in Table 28. For Ag-108m, only single value is provided in (Posiva, 2014a).

Table 28. *The concentration ratios from soil to the standing pasture biomass in dry weights (mg/kg)/(mg/kg). GM denotes geometric mean and GSD geometric standard deviation. Log-normal distributions are used with the shown truncation limits. The bolded value for Ag-108m is used as a constant in the calculation. The chosen reference case values are presented in the column denoted "Ref. case". (Posiva, 2014a)*

Nuclide	Minimum	Maximum	GM	GSD	Ref. case
Cl-36	3.0	3.6E+2	75	2.1	GM
Se-79	6.5E-3	11	1.0	3.4	
Mo-93	3.0E-2	46	1.0	5.2	
Nb-94	4.3E-3	51	2.0E-2	6.5	
Ag-108m	**2.4E-2***				
I-129	3.0E-2	10	0.24	6.3	GM

*Only single value provided in (Posiva, 2014a).

The concentration ratios to various crop types in the simplified model are presented in Table 29. A major portion of the truncation values are provided in (Posiva, 2014a).

Table 29. *The concentration ratios from soil to edible parts of crops of dry weight per dry weight of soil (µg/kg)/(µg/kg). GM denotes geometric mean, GSD geometric standard deviation. Log-normal distributions are used with truncation limits shown (calculated 1st and 99th percentiles in italic). The chosen reference case values are presented in the column denoted "Ref. case". (Posiva, 2014a)*

Nuclide	Minimum	Maximum	GM	GSD	Ref. case
Cereals					
Cl-36	6.7	19	6.8	1.8	GM
Se-79	3.1E-02	3.5E-01	3.1E-02	3.4	
Mo-93	6.3E-01	34	7.2E-01	4.8	
Nb-94	8.2E-04	3.7E-02	1.4E-03	6.0	
Ag-108m	1.6E-02	3.9E-01	1.1E-01	2.2	
I-129	6.3E-04	1.5E-01	1.4E-03	3.4	
Potato					
Cl-36	10	18	13	5.2	GM
Se-79	15	34	20	1.2	
Mo-93	2.3E-02	4.4	7.0E-01	2.8	
Nb-94	4.3E-04	51	4.0E-03	6.5	
Ag-108m	5.7E-04	3.7E-02	3.7E-02	3.5	
I-129	*9.5E-04*	*11*	1.0E-01	7.4	
Field vegetables					
Cl-36	5.0	1.4E+03	23	3.8	GM
Se-79	2.9E-01	2.4	5.1E-01	1.7	
Mo-93	4.4E-02	2.7E+02	7.2E-01	4.1	
Nb-94	2.5E-03	51	6.4E-03	3.5	
Ag-108m	2.0E-04	1.3	3.7E-01	3.3	
I-129	1.6E-04	6.0	2.6E-02	3.7	

The concentration ratios to berries are presented in Table 30. The minimum value for GSD is provided commonly to all nuclides and used in the calculation.

Table 30. *The concentration ratios from soil to berries of fresh weight per dry weight of soil (µg/kg)/(µg/kg). Truncation limits of the log-normal distributions are calculated at 1st and 99th percentiles (in italic). The chosen reference case values are presented in the column denoted "Ref. case". (Posiva, 2014a)*

Nuclide	Minimum	Maximum	GM	GSD	Ref. case
Cl-36	*4.4E-2*	*7.3*	5.7E-1	3.0	GM
Se-79	*7.8E-4*	*1.3E-1*	1.0E-2		
Mo-93	*1.6E-3*	*2.6E-1*	2.0E-2		
Nb-94	*1.9E-5*	*3.1E-3*	2.4E-4		
Ag-108m	*4.7E-5*	*7.7E-3*	6.0E-4		
I-129	*1.6E-4*	*2.6E-2*	2.0E-3		

The concentration ratios to freshwater fish are presented in Table 31. For I-129, the forage fish group is selected for the concentration ratio as the most cautious choice.

Table 31. *The concentration ratios from freshwater to edible parts of fish of fresh weight (µg/kg)/(µg/m^3).The chosen reference case values are presented in the column denoted "Ref. case". (Posiva, 2014a)*

Nuclide	Minimum	Maximum	GM	GSD	Ref. case
Cl-36	8.9E-3	1.2E-1	1.1E-1	1.3	GM
Se-79	1.0E-2	9.4	1.6	3.7	
Mo-93	4.0E-6	2.0E-2	9.0E-3	3.9	
Nb-94	6.9E-3	3.0E-2	3.0E-2	2.7	
Ag-108m	4.0E-4	2.1E-1	1.1E-1	1.5	
I-129	3.3E-2	4.0E-1	2.9E-1	2.5	

4.3 Determination of correlations

4.3.1 Base case

The correlations between parameters of the model can justified logically or they can be hypothetical for modelling purposes and sensitivity analyses. In the calculation, the correlated probability levels in random sampling are calculated based on the correlation coefficient between the parameters (see Section 4.1). In this section, the naturally correlated parameters due to chemical similarity or logical reasons are presented. The default selections for correlation coefficients in the base calculation case of the base scenario are presented and the possible effects on mass transfer coefficients and total results are considered.

First, in the general geosphere related parameters, the parameters related to the fracture parameters are considered correlated. The effect of fracture aperture is investigated for Posiva's model in (Cormenzana, 2013a) and the conclusion is that the parameter does not have significant effect on the results within the used range of values (same range in the base case). Therefore, any correlations for the fracture apertures should have no significant effects on the results. In base case, the fracture aperture $(2b_v, 2b_{vt})$ is considered to be fully correlated ($\rho = 1$) with the groundwater velocity in the fracture (v_{dh}, v_t). Between one another, the fractures are independent. The justification is hypothetical and it adds conservatism to the model as the values of mass transfer coefficients proportional to both of the parameters.

The effect of the correlated values for the fracture apertures and groundwater velocities is that the equivalent flow rates to the fractures are also correlated and they increase compared to the situation where the parameters are independent. Therefore, the mass transfer coefficients from buffer to fracture and from tunnel to fracture are partly correlated due to equivalent flow rates and it decreases the variance of the output (release/dose rates).

Next, common correlations between chemically similar nuclides are considered. A division between anionic (Cl-36, Se-79, I-129) and cationic or neutral species (C-14,

Mo-93, Nb-94, Ag-108m) helps in determining chemically similar nuclides. However, it must be pointed out that the behavior of Nb-94 and Ag-108m is not well known to be certain about the group correlations (SKB, 2010). The group correlations are assessed in variant calculation cases of the base case that are presented later.

In the geosphere, common parameters for all anions or cations are the porosities and effective diffusion coefficients in various components of the repository system. The full correlations ($\rho = 1$) are used for anions and similarly for cations for the effective diffusion coefficient in bentonite (D_{eb}) and for the porosity in the buffer (ϵ_b) and in the tunnel backfill (ϵ_t). However, there are no correlations between the parameters themselves in the base case because of limited knowledge. This may result in an unrealistic situation when low porosity of the buffer for anionic nuclides is combined with high diffusion coefficient values in the buffer. Setting these parameters correlated is handled in variant calculation cases.

The common parameter distributions for all nuclides are used for the effective diffusion coefficient in the rock matrix (D_{em}) and porosity of the bedrock (ϵ_m). The parameters have an observable correlation based on measurement data in (Cormenzana, 2013b). In the base case, the correlation coefficient is set hypothetically to 0.5 and the parameters are picked commonly for all nuclides. The value of the correlation coefficient is varied in variant calculation cases.

Due to chemical similarity, the anions and cations could have similar retardation coefficients within the group in the geosphere release barriers due to correlated distribution coefficients. However, because of the uncertainty related to the values of the distribution coefficients and low sorption of the anions, the distribution coefficients are assumed to be independent in the base case. Otherwise, the retardation coefficients in the geosphere components would be correlated for different nuclides and mass transfer coefficients would also be partly negatively correlated to distribution coefficients for all nuclides. Depending on the dominating nuclides, the effect of correlated distribution coefficients varies and it's examined in the variant calculation cases.

Similarly, the considerations of correlations between similar species can be extended to biosphere parameters. In the biosphere analysis, the possible correlations among anionic or cationic nuclides are related to distribution coefficients or concentration ratios to various foodstuff. The nuclide groups of anionic and cationic nuclides would logically have correlated properties as in the geosphere barriers. The distribution coefficients between various nuclides could be correlated but in the base case, they are cautiously independent due to limited knowledge. A negative correlation between a concentration ratio and a distribution coefficient is investigated with minor experimental data to back up the assumption (Avila et al., 2010). The correlations for the concentration ratios and distribution coefficients are investigated in the variant calculation cases.

The effect of correlated distribution coefficient among chemically similar nuclides is that more of the nuclides retard in the soil layers meaning that the inventories in layers increase. Larger inventories result in increased doses from the layers which provide

foodstuff. The effect is reduced with negatively correlated concentration ratios to foodstuff.

In the lake object of the biosphere model, the sediment densities (ρ_i) can be connected. The correlations for the densities of the lake sediments may be justified by the comparing the two-sediment modelling to natural sedimentation in lakes. The more dense materials end up deeper than the less dense materials because the sediment becomes tighter (due to gravity). Therefore, a positive correlation with (hypothetical) correlation coefficient value of 0.5 ($\rho = 0.5$) is used.

Also, the lake discharge ($WfluxOut$) and average water depth (d_w) can be considered correlated but the justification is hypothetical and vaguely based on the data used to determine the distributions for the parameters. By comparing to the real lakes, usually larger lakes have larger discharge rates. Also, in the UNTAMO data of the reference case area, the average water depth decreased over time similarly as the average lake area and average discharge rate. However, the correlation choice between water depth and discharge is purely hypothetical and the parameters are independent in the base case. The effect of the correlation is that it decreases the variance of the mass transfer coefficient from lake water to forest (or sink) as the water depth is in the denominator of the mass transfer coefficient and discharge is in the nominator. The discharge rate however dominates the numerical value of the term together with the lake area so the significance of the correlation may be low. The correlation between the discharge rate and average water depth is varied in the variant calculation cases.

For the base case of the base scenario in the simplified model, the summary of the correlations is presented in Table 32. The base case correlations are varied and further investigated in the variant calculation cases presented next.

Table 32. *The correlations between the model parameters in the base case of the simplified model.*

Parameter	Symbol	Description of correlation	Coefficient
General			
Fracture aperture	$2b_v, 2b_{vt}$	With groundwater velocity.	1
Groundwater velocity	v_t, v_{dh}	With fracture aperture.	1
Nuclide-specific			
Effective diffusion coefficient in bentonite	D_{eb}	Independent nuclide groups (anions and cations) for each parameter. Independent among themselves.	1 (within the group)
Porosity of the buffer	ϵ_b		
Porosity of the backfill	ϵ_t		
Porosity of the rock matrix	ϵ_m	All nuclides correlated.	1 (among nuclides)
Effective diffusion coefficient in the rock matrix	D_{em}	Partial correlation to porosity of the rock matrix.	0.5 (with porosity)
Biosphere			
Top sediment bulk density	ρ_i	Correlation based on general sedimentation.	0.5
Intermediate sediment bulk density			

4.3.2 Variant calculation cases

In variant calculation cases, the correlations are used more extensively for the parameters of the model than in the base case. The base case correlations are assumed to exist and changes to model correlations are conducted. In the calculation cases, the mass transfer coefficients are analyzed first and then, the total dose rates are calculated depending on the observed results. The results are compared to the base case results and the possible differences are observed.

The diffusion coefficient in the geosphere water (D_w) and pore volume of the canister (V_c) are only in some cases connected. In case of low penetration of the water to the canister interior, the pore volume in the canister is low and therefore the diffusion coefficient is extremely low inside the canister. Therefore, some positive correlation for the parameters can be justified. However, as the diffusion coefficient is common for also other parts of the repository system the correlation would only be hypothetical. The effect of the correlation is not clear as the diffusion coefficient is in the nominator and the pore volume of the canister in the denominator of the mass transfer coefficient from the canister. The values of D_w are however significantly lower than other dimension-related parameters, which could decrease the effect on the results. Also, the mass transfer coefficients from the buffer and the tunnel to fracture would be affected although the combined effect on the whole system is not clear. The issue is investigated in calculation case 1.

In the geosphere fractures, the hydrodynamic control of retention (WL/Q), fracture aperture ($2b$) and water travel time (t_w) in a fracture are connected with the equation (Nummi et al., 2012)

$$\frac{WL}{Q} = \frac{WL}{2bvW} = \frac{t_w}{2b} \tag{58}$$

There exists two fractures in the model that intersect the deposition hole and the deposition tunnel. The WL/Q value used in the model depicts the flow resistance in the rest of the geosphere and therefore any correlations with the intersecting fracture apertures are partly hypothetical and they do not exist in the base case. However, due to rock formations it could be possible that when either of the fracture apertures is larger, also the overall flow resistance is lower in the geosphere (assuming the travel time remains constant). The effects of negatively correlated fracture apertures and WL/Q values are investigated in the calculation case 2. As in the base case, the groundwater velocities in the fractures are still fully correlated to fracture apertures. The effect of correlated WL/Q values is that whenever the mass transfer coefficients for the buffer to fracture and tunnel to fracture parts are large, the mass transfer coefficient from the geosphere to biosphere is also larger and the delay time smaller. Therefore, the correlation would increase conservatism to the model and probably result in higher dose rates.

The IRF values for the chemically similar nuclides have been suggested in (SKB, 2010). In calculation case 6, the effect of correlated IRFs for Cl-36, Se-79 and I-129 are examined. All these nuclides have instantly releasing inventory in the fuel matrix and only Cl-36 has also inventory in the zirconium alloys. Only IRFs related to fuel matrix are considered to be correlated.

All the suggested correlations in this section are analyzed by making the simulations with correlations and comparing to the results obtained with the default assumptions (i.e. base case) presented in the previous section. The summary of the correlations examined in the variant calculation cases is presented in Table 33. The formulated calculation cases are summarized after that.

Table 33. *The correlations between the model parameters in the variant calculation cases of the simplified model. In the results, the calculation cases are separated by choosing a correlation coefficient at a time for examination.*

Parameter	Symbol	Description of correlation	Coefficient
Diffusion coefficient in water	D_w	Correlation hypothetical when water partly penetrates the canister interior.	1
Pore volume of the canister	V_c		
Fracture aperture	$2b_v, 2b_{vt}$	With groundwater velocity.	1
Hydrodynamic control of retention	WL/Q	Negative correlation to fracture aperture.	-1
Effective diffusion coefficient in bentonite	D_{eb}	Independent nuclide groups (anions and cations) but parameters correlated among themselves.	1
Porosity of the buffer	ϵ_b		
Porosity of the backfill	ϵ_t		
Instant release fraction	IRF	IRF in fuel matrix correlated for Cl-36, Se-79 and I-129.	1
Porosity of the rock matrix	ϵ_m	All nuclides correlated/independent.	[0,1] (among nuclides)
Effective diffusion coefficient in the rock matrix	D_{em}	Partial correlation to porosity of the rock matrix.	[0,1]
Average water depth	d_w	Correlation based on data (hypothetical).	[0,1]
Lake discharge	$WfluxOut$		
Top sediment bulk density	ρ_i	Correlation based on general sedimentation.	[0,1]
Intermediate sediment bulk density			
Distribution coefficient	$Kd_{pb}, Kd_{pt}, Kd_{pm}, Kd_i$	The correlations inside nuclide groups (anions, cations)	1
Concentration ratio	CR_i	Negative correlation to the distribution coefficient in the corresponding soil layer.	-1

The following calculations cases are separately examined and in all cases, the base case correlations are assumed to exist:

1. The full positive correlation between the diffusion coefficient in water in geosphere (D_w) and pore volume of the canister (V_c).
2. The full negative correlation between the hydrodynamic control of retention (WL/Q) and either one of the bedrock fracture apertures ($2b_v, 2b_{vt}$) in the simplified model. The correlation with both fractures separately is examined.
3. The anionic and cationic groups are not considered and nuclides have independent effective diffusion coefficients in bentonite and rock matrix (D_{eb}, D_{em}) and porosities of the buffer, backfill and rock matrix (ϵ_b, ϵ_t, ϵ_m). The inverse case where all parameters are commonly correlated within nuclide groups (anions/cations) is also examined.

4. Effective diffusion coefficient in the rock matrix (D_{em}) is considered to be correlated to the porosity of the rock matrix (ϵ_m) with correlation coefficients 0 and 1 (in base case 0.5). This calculation case is also combined with case number 3 and partly with 9 by applying correlated distribution coefficients in the geosphere barriers.
5. The IRFs for anions (Cl-36, Se-79, I-129) in the fuel matrix are fully correlated.
6. Average water depth (d_w) and discharge ($WfluxOut$) from the lake are correlated with coefficient 1 (in base case independent).
7. The bulk densities (ρ_i) in the intermediate and top sediment correlated with coefficients 0 and 1 (in base case 0.5).
8. The anionic and cationic/neutral nuclides have correlated distribution coefficients in the buffer, backfill, rock matrix and biosphere soil layers (Kd_{pb}, Kd_{pt}, Kd_{pm}, Kd_i).
9. Concentration ratios to foodstuff (CR_i) in biosphere fully negatively correlated to distribution coefficients in the corresponding soil layers. This case is also combined with the changes in case number 8.

5 RESULTS

In the following sections, the results from various calculation cases obtained by simulating the simplified model are presented. First, the mass transfer coefficients and delay times for the simplified model are analyzed with default parameter selections (i.e. distributions and constant values) and correlations of the base case of the model. The approximations for the resulting distributions of solute mass transfer coefficients in compartments and delay times are presented. Also, the solute half-times corresponding to the mass transfer coefficients (i.e. solute decay constants) are considered in order to obtain a more comprehensible picture of the solute transport in the various compartments of the model.

The results from the base case with the default parameter selections and correlations are presented. The resulting dose rates during the first 10 millennia and release rates during next 100 millennia are calculated. Also, the contributions of various dose paths and different nuclides are analyzed. The deterministic calculation case with reference case parameters is also examined and all results are compared to BSA-2012 reference case results by Posiva.

Even though, the possible correlations between parameters can be justified to some extent, also testing of correlations is conducted by using variant calculation cases. The aim is to find out how the mass transfer coefficients (or compartment half-times) and shape of the output varies along with various parameter correlations and distributions. The effects of various distribution shapes on the model results are analyzed by changing the assumed distributions for those parameters that contribute most to the uncertainty of the model. The base case results are used as a basis for the comparisons.

With the various analyses and comprehensive picture of the simplified model, the most significant parameters in the model can be also distinguished. In addition, the significance of various uncertainties can be estimated. With the obtained results, the further research focus can be directed towards crucial aspects of the long-term safety of the disposal system.

5.1 Compartment decay constants and half-times

The decay constants of the solute in the compartments are described by the mass transfer coefficients. The compartment half-times can be calculated from the mass transfer coefficients by using the relation $t_{1/2} = \ln(2)\,/\lambda$. The barrier, which retards the solute transport most efficiently, has the smallest mass transfer coefficient (solute decay constant) and therefore, the longest half-time for the solute. As known, the term related to the smallest mass transfer coefficient also dominates the shape and magnitude of a response function related to a transport branch. Therefore, the smallest mass transfer coefficients are important and especially their distributions. In the end, the most significant parameter uncertainties need to be identified in order to further optimize work in the analysis and research.

The distributions for the mass transfer coefficients and delay times can be approximated by simulating a sufficient number of realizations and observing the shape of a

histogram. Based on the shape of the histogram, one can approximate the relevant parameters for fitting a probability density function (PDF) of a relevant distribution into the histogram data. The distribution characteristics in this study in most cases are obtained by taking the logarithm from the data and calculating mean and standard deviations. Then, a geometric mean (GM) and geometric standard deviations (GSD) can be determined for example for a log-normal distribution as described in Section 4.1. In some cases, also maximum-likelihood method (MLE) can be used. For the log-normal distributions, the difference between the fitting result obtained with GM/GSD calculated from the data or with the MLE-method is minor.

Another way to approach the distributions of the mass transfer coefficients is to use algebraic methods and equations that define the values of the transfer coefficients. In many cases, the summation, division, multiplication and subtraction are well defined for specific distributions. For example, the sum of normal distributions results in a normal distribution and the product of log-normal distributions results in log-normal distribution (Leemis & Mcqueston, 2008). The correlations change the variance of the resulting distribution as for example for any two random variables X and Y the variance after summation is $Var(X+Y) = Var(X) + Var(Y) + 2Cov(X,Y)$, where $Cov(X,Y)$ is the covariance between the two variables ($\neq 0$ if correlated) (Benjamin & Cornell, 1970). With algebraic methods, the resulting distribution for a mass transfer coefficient can be determined in exact form compared to the simulations where only a numerical result is available at best.

To obtain a quantitative measure for the goodness of the fit, a one-sided p-value of a Kolmogorov-Smirnov test (K-S test) is provided based on the data and fitted distribution (Massey, 1951). In the one-sided test, both alternatives that the empirical CDF is less or greater than the CDF of the hypothesis are applied and the highest p-value is presented. The p-values from a two-sided K-S test are not relevant as only rough approximations are aimed for the distributions. A high p-value (in general over 0.1) indicates that the null hypothesis may not be rejected (i.e. estimated CDF and empirical CDF are close) and low p-values suggest that the fit result is not good as the null hypothesis should be rejected. A level of significance is not selected in this study because the quality of the fitting process is not the focus of the study and rather rough estimates of the distributions are only needed for comparing the time constants of the compartments. The focus is on the uncertainties related to the parameters that contribute most to the uncertainty of the final results (i.e. total dose rate or release rates).

5.1.1 Geosphere transport

The first three mass transfer coefficients in the geosphere transport are the transfer coefficients from canister to buffer (λ_{cb}), from buffer to fracture (λ_{bf}) and from buffer to tunnel (λ_{bt}). The mass transfer coefficients are presented in Table 34 with expressions without constants, algebraically simplified expressions, most significant distributed parameters and examples of estimated distribution parameters with 10 000 realizations. The most significant parameters are presented in an arbitrary order. With estimated distribution parameters, also one-sided p-values are provided. The p-values vary between simulations but generally a higher p-value (over 0.1) indicates that the distribution is a good approximation of the empirical data.

Table 34. *The algebraic simplifications of the three geosphere mass transfer coefficients and the estimated distribution parameters. The distributions are denoted as: LU a log-uniform distribution with (minimum, maximum),* N_{log} *a log-normal distribution with (GM, GSD) and* C *a constant. The highest values from a one-sided K-S-test are provided.*

Mass transfer coefficient	Expression (without constants)		Simplified expression	Most significant parameters	Estimated distribution (example)
λ_{cb}	$q_{ch} = r_h^2(LU)D_w(LU)$ $q_{hm} = D_{eb}(LU)$ $q_c = \frac{q_{ch}q_{hm}}{q_{ch}+q_{hm}}$ $\lambda_c = \frac{q_c}{V_c(LU)}$	Anions	$q_c = \frac{r_h^2(LU)D_w(LU)D_{eb}(LU)}{r_h^2(LU)D_w(LU)+D_{eb}(LU)}$	r_h, D_w, D_{eb}, V_c	N_{log} (1.6E-7 1/a, 5.0) p ≈ 0.01
		Cations/neutrals	$q_{hm} \gg q_{ch}$ $q_c \approx q_{ch} = r_h^2(LU)D_w(LU)$ $\lambda_c = \frac{q_c}{V_c(LU)}$	r_h, D_w, V_c	N_{log} (2.2E-7 1/a 6.2) p ≈ 0.02
λ_{bf}	$q_{bf} = 2b_v(N_{log})\sqrt{D_w(LU)v_{dh}(N_{log})}$ $\lambda_{bf} = \frac{q_{bf}}{R_{pb}(C,N_{log})\epsilon_b(LU,C)}$	Anions	$\lambda_{bf} = \frac{q_{bf}(\approx N_{log})}{\epsilon_b(LU)}$	$2b_v, v_{dh}, \epsilon_b, D_w$	N_{log} (6.9E-6 1/a, 19) p > 0.1
		Cations	$\lambda_{bf} = \frac{q_{bf}(\approx N_{log})}{R_{pb}(N_{log})}$ $(\approx N_{log})$	$2b_v, v_{dh}, Kd_{pb}$	N_{log} (Mo-93) (1.1E-8 1/a, 18) p > 0.1
		Neutrals	$\lambda_{bf} = q_{bf}(\approx N_{log})$	$2b_v, v_{dh}, D_w$	N_{log} (5.3E-7 1/a 17) p > 0.1
λ_{bt}	$q_{bt} = D_{eb}(LU)$ $\lambda_{bt} = \frac{q_{bt}}{R_{pb}(C,N_{log})\epsilon_b(LU,C)}$	Neutrals	$\lambda_{bt} = \frac{q_{bt}(LU)}{\epsilon_b(LU)}$	D_{eb}, ϵ_b	N_{log} (1.9E-4 1/a, 2.6) p ≈ 0.003
		Cations	$\lambda_{bt} = \frac{q_{bt}(LU)}{R_{pb}(N_{log})}$ $(\approx N_{log})$	D_{eb}, Kd_{pb}	N_{log} (Mo-93) (6.2E-6 1/a, 2.5) p ≈ 0.05
		Neutrals	$\lambda_{bt} = q_{bt}(LU)$	D_{eb}	LU (9.3E-5 1/a, 9.3E-4 1/a) p > 0.1

The mass transfer coefficient from canister to buffer (λ_{cb}) results in two different distributions for anions and cations/neutrals. With all nuclides, the expression has only log-uniformly distributed independent parameters. For cations, the diffusion coefficient in bentonite (D_{eb}) is about one order of magnitude higher than for anions and therefore,

the resulting equivalent flow rate on the bentonite side of the canister hole is much larger than on the inner side. In both cases, the log-uniform parameters exist in the final expression both in the nominator and denominator. The resulting distribution even in the simple ratio case of two uniform distributions has diverging mean and moments and therefore, the result is not any conventional distribution.

Based on simulated data and histograms, log-normal distributions are used in fitting a PDF into the data. The resulting distribution parameters reveal that log-normal approximations are rather good ones. With base case parameter selections, the resulting histogram for the λ_c for C-14 (neutral) is presented in Figure 8 together with the cumulative percentages. The results for anions are not presented at this point due to similarity.

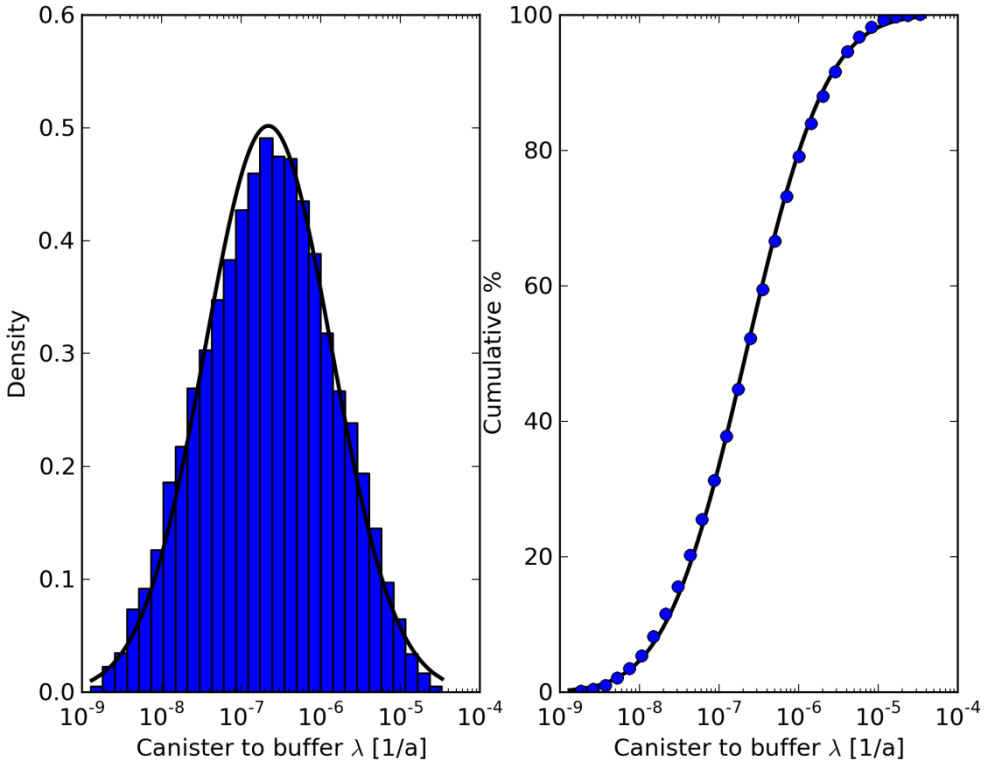

Figure 8. *On the left, the histogram of 10 000 realizations for mass transfer coefficient from canister to buffer for C-14. On the right, the cumulative percentages corresponding to histogram bars are presented. The black line corresponds to a log-normal distribution fitted to the data (GM = 2.2E-7 1/a, GSD = 6.2). All the cationic nuclides had similar mass transfer coefficient distributions from canister to buffer with the parameters of the base case.*

The mass transfer coefficient from the buffer to the intersecting fracture (λ_{bf}) receives three different distributions for anions, cations and neutral elements. The equivalent flow rate is a multiplication of a log-normal variable ($2b_v$) and square root of a product of log-uniform and log-normal parameters (D_w and v_{dh}), which follows roughly a log-normal distribution if only products of a log-normal distributions is considered (Leemis & Mcqueston, 2008). For anions, the resulting mass transfer coefficient is a ratio of the

roughly log-normal equivalent flow rate and log-uniform porosity of the buffer (ϵ_b), which is not a conventional distribution.

With cations, the result is a ratio of log-normal distributions that results in a log-normal distribution as $\log(X/Y) = \log X - \log Y$ where $\log X$ and $\log Y$ are normally distributed as *X* and *Y* are log-normally distributed. The summation (or subtraction) of normally distributed random variables results as a normal distribution (Leemis & Mcqueston, 2008), which means that *X/Y* follows a log-normal distribution. However, the explicit expressions for the distribution parameters are not determined as the log-normality of the equivalent flow rate is only an approximation.

For neutral nuclides, λ_{bf} results in a similar distribution as the equivalent flow rate that is roughly log-normal. From the most significant parameters, the groundwater velocity (v_{dh}) and fracture aperture ($2b_v$) are fully correlated, which results in large GSD values for all nuclides. Also, as both parameters are log-normally distributed, the resulting p-values for the fitted log-normal distributions are high (over 0.1).

For mass transfer coefficient from the buffer to tunnel section (λ_{bt}), the resulting equivalent flow rate for all nuclides is log-uniformly distributed due to one distributed parameter, D_{eb}. For anions, the final expression of the mass transfer coefficient is a ratio of log-uniform distributions (porosity of the buffer ϵ_b and equivalent flow rate), which is not a conventional distribution. For cations, the result is a ratio of log-uniform and log-normal distributions (equivalent flow rate and retardation coefficient R_{pb}), which roughly resembles the reciprocal log-normal distribution. The inverse of a log-normal distribution is log-normal due to relation: $\log X \sim N(\mu, \sigma^2)$, $\log(1/X) = -\log X \sim N(-\mu, \sigma^2)$ where X follows a log-normal distribution. For neutral elements, the result is similar as the distribution of equivalent flow rate (log-uniform) because the porosity of the buffer and retardation factor are both constants.

For all nuclides, a log-normal distribution is fitted to the data although for anions, the result is not clearly log-normal. The result resembles a rather symmetric log-triangular distribution but the difference to a narrow log-normal distribution is small. However, the anions also receive the lowest p-values from K-S-test with log-normal distributions but only a rough approximations are needed in this study. The results from a fitted log-normal distribution for anions is presented in Figure 9.

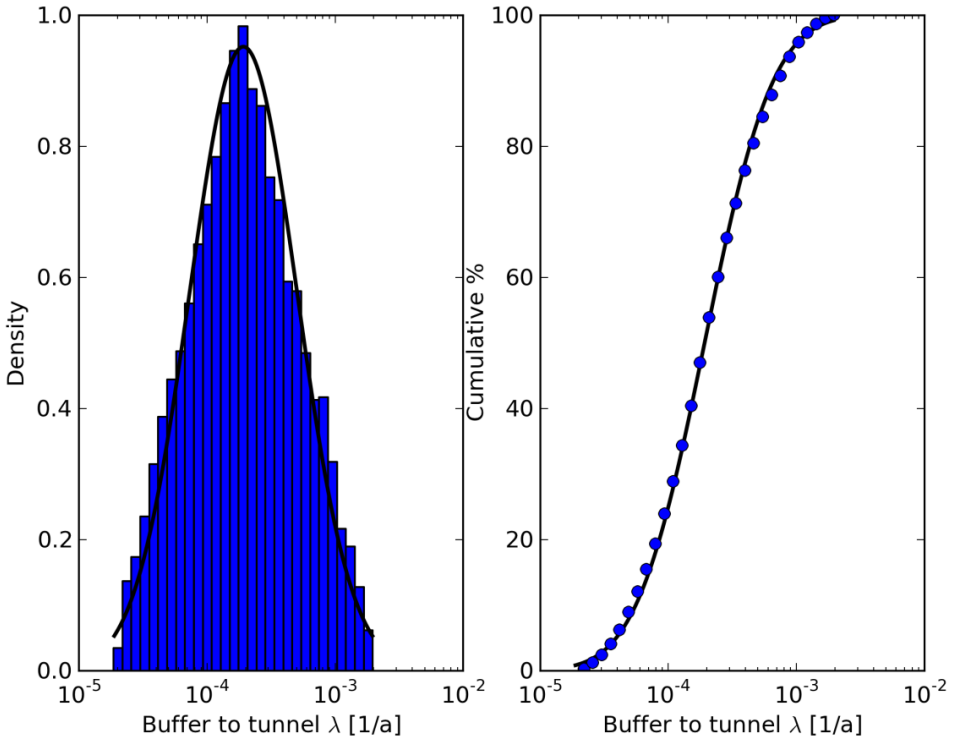

Figure 9. *On the left, the histogram of 10 000 realizations for mass transfer coefficient from buffer to tunnel for Cl-36. On the right, the cumulative percentages corresponding to histogram bars are presented. The black line corresponds to a log-normal distribution fitted to the data (GM = 1.9E-4 1/a, GSD = 2.6). Other anionic nuclides had similar histograms and distribution fittings.*

The results for the last two mass transfer coefficients in the geosphere are presented in Table 35 similarly as earlier. For the mass transfer coefficient from the tunnel section to the intersecting fracture (λ_{tf}), the equivalent flow rate follows similar distribution as the equivalent flow rate for the mass transfer coefficient from buffer to fracture (λ_{bf}). For anions, the final distribution of the mass transfer coefficient is a ratio of roughly log-normal and log-uniform parameters. For cations/neutrals, the result follows slightly different distributions that are approximately log-normal.

Table 35. *The algebraic simplifications of the two geosphere mass transfer coefficients and the estimated distribution parameters. The distributions are denoted as: LU a log-uniform distribution with (minimum, maximum), N_{log} a log-normal distribution with (GM, GSD) and C a constant. The highest values from a one-sided K-S-test are provided.*

Mass transfer coefficient	Expression (without constants)		Simplified expression	Most significant parameters	Estimated distribution (example)
λ_{tf}	$q_{tf} = 2b_v(N_{log})\sqrt{D_w(LU)v_t(N_{log})}$ $\lambda_{tf} = \frac{q_{tf}}{R_{pt}(C, N_{log})\epsilon_t(LU, C)}$	Anions	$\lambda_{tf} = \frac{q_{tf}(\approx N_{log})}{\epsilon_t(LU)}$	$2b_v, v_t, \epsilon_t, D_w$	N_{log} (2.7E-5 1/a, 16) p ≈ 0.06
		Cations	$\lambda_{tf} = \frac{q_{tf}(\approx N_{log})}{R_{pt}(N_{log})}$ $(\approx N_{log})$	$2b_v, v_t, Kd_{pt}$	N_{log} (Mo-93) (3.3E-8 1/a, 16) p > 0.1
		Neutrals	$\lambda_{tf} = q_{tf}$ $(\approx N_{log})$	$2b_v, v_t, D_w$	N_{log} (2.2E-6 1/a, 15) p ≈ 0.06
λ_f	$u = \sqrt{\epsilon_m(LU)R_{pm}\left(C, \frac{LU}{LU}\right)D_{em}(LU)}$ $WL/Q(N_{log})$ $\lambda_f = \frac{1}{u^2}$	Anions	$R_{pm}(LU/LU)$ $(u \approx N_{log})$	$\frac{WL}{Q}, Kd_{pm}, D_{em}, \epsilon_m$	N_{log} (Cl-36) (1.4E-2 1/a, 22) p ≈ 0.003
		Cations			N_{log} (Mo-93) (2.3E-3 1/a, 31) p > 0.1
		Neutrals	$R_{pm}(C)$ $(u \approx N_{log})$	$\frac{WL}{Q}, D_{em}, \epsilon_m$	N_{log} (1.6E-2 1/a, 22) p ≈ 0.02

The p-values for anions and neutrals from K-S tests with log-normal PDFs are slightly lower than for the fitted λ_{bf} distributions because the equivalent flow rate does not follow log-normal distribution as well as earlier. Also, the resulting GSD values are slightly lower than with λ_{bf} distributions. The difference compared to the situation with λ_{bf} is a wider groundwater velocity range with higher realistic and conservative values given as distribution parameters.

The mass transfer coefficient for the geosphere (λ_f) is calculated as a squared reciprocal of a multiplication of log-normal hydrodynamic control of retention (WL/Q) and a square root of log-uniformly distributed parameters. A product of log-normal distribution with log-uniform parameters does not result in a conventional distribution. For all nuclides, the WL/Q dominates the distribution of the mass transfer coefficient and therefore, the expression for u (in Equation (13)) is roughly log-normal. The variance is added by the correlated ($\rho = 0.5$) porosity of the rock matrix (ϵ_m) and

effective diffusion coefficient in the rock matrix (D_{em}) and also, by the distribution of the retardation coefficient.

For all nuclide types, log-normal distributions are used in fitting PDFs to the simulated data. The distribution parameters are estimated by calculating the GM and GSD from the data as before. The lowest p-values are obtained with anions that have low distribution coefficient values in the expression of retardation coefficient. The ratio of log-uniform distributions inside the square root of expression for u is distorting the log-normal result from WL/Q distributions. For cations, a higher distribution coefficient increases the GSD of the final mass transfer coefficient and also, the p-values are the highest. For neutral nuclides, the retardation coefficient has a constant value of unity and p-values for the fitted log-normal distributions are again lower.

Summary of the obtained all approximations of the mass transfer coefficient distributions is presented in Table 36. The most uncertain mass transfer coefficients are the ones related to intersecting fractures and especially geosphere. The most significant parameters in the mass transfer coefficients from buffer to fracture (λ_{bf}) and from tunnel to fracture (λ_{tf}) are the groundwater velocities in fractures (v_{dh}, v_t) and fracture apertures ($2b_v$) that have wide distribution ranges (several orders of magnitude) and they are also correlated. The most significant parameter affecting the geosphere mass transfer coefficient (λ_f) is the hydrodynamic control of retention WL/Q.

Table 36. *Summary of the simulated approximations for mass transfer coefficient distributions with 10 000 realizations and parameter selections and correlations of the base case (in Sections 4.2.1-4.2.5 and 4.3.1). Notations: Cb = canister to buffer, Bf = buffer to fracture, Bt = buffer to tunnel, Tf = tunnel to fracture, Fb = fracture to biosphere, LU = log-uniform distribution, N_{log} = log-normal distribution. The approximated parameters for the distributions are in the brackets (min, max) with LU and (GM, GSD) with N_{log}.*

Nuclide	Cb (1/a, -)	Bf (1/a, -)	Bt (1/a, -)	Tf (1/a, -)	Fb (1/a, -)
C-14	N_{log} (2.2E-7, 6.2)	N_{log} (5.3E-7, 17)	LU (9.3E-5, 9.3E-4 1/a)	N_{log} (2.2E-6, 15)	N_{log} (1.6E-2, 22)
Cl-36	N_{log} (1.6E-7, 5.0)	N_{log} (6.9E-6, 19)	N_{log} (1.9E-4, 2.6)	N_{log} (2.7E-5, 16)	N_{log} (1.4E-2, 22)
Se-79					N_{log} (1.6E-2, 21)
Mo-93	see C-14	N_{log} (1.1E-8, 18)	N_{log} (6.2E-6, 2.5)	N_{log} (3.3E-8, 16)	N_{log} (2.3E-3, 31)
Nb-94		N_{log} (1.6E-11, 19)	N_{log} (8.8E-9, 2.6)	N_{log} (1.1E-10, 17)	N_{log} (3.8E-7, 17)
Ag-108m		see C-14	see C-14	see C-14	see C-14
I-129	see Cl-36	see Cl-36	see Cl-36	see Cl-36	N_{log} (1.2E-2, 21)

The different half-times for the solute in different compartments are presented in Table 37 in the base case. The half-times are calculated from the GM values obtained in the simulations and they have same GSDs as the mass transfer coefficient above. The release is retained most efficiently in the barriers with the longest half-time compared to nuclide-specific radioactive half-life. Without the uncertainties, it can be observed that the most significant barriers are the canister itself and the buffer around it as the half-

times for the solute concentration are the longest for most nuclides. For sorbing nuclides Mo-93 and Nb-94, the most significant barriers are the barriers with bentonite, namely the buffer and the tunnel backfill. Based on the half-times, the Mo-93 and especially Nb-94 releases are extremely low in the analyzed time scope due to the longest half times in all the barriers except the canister. In the canister, the longer half-times for anions occur due to smaller effective diffusion coefficient in the buffer than with cations.

Table 37. *Summary of the approximated solute half-times with parameter selections and correlations of the base case in the geosphere barriers. The values represent the geometric mean values for the mass transfer coefficients. Notations: Cb = canister to buffer, Bf = buffer to fracture, Bt = buffer to tunnel, Tf = tunnel to fracture, Fb = fracture to biosphere.*

Nuclide	Cb (a)	Bf (a)	Bt (a)	Tf (a)	Fb (a)
C-14	3 170 000	1 300 000	2360	311 000	44.2
Cl-36	4 360 000	100 600	3610	25 900	48.3
Se-79					44.3
Mo-93	see C-14	62 200 000	112 000	21 000 000	299
Nb-94		43 700 000 000	78 800 000	6 570 000 000	1 840 000
Ag-108m		see C-14	see C-14	see C-14	44.5
I-129	see Cl-36	see Cl-36	see Cl-36	see Cl-36	55.0

5.1.2 Biosphere transport

The solute transport in the biosphere is defined with mass transfer coefficients presented in Section 3.2.2. The values for mass transfer coefficients are calculated based on expressions in Table 4 and base case parameter selections in Section 4.2. The expressions for the transfer coefficients without constants, simplified expressions and resulting distribution approximations are presented in Table 38 with most significant parameters for each coefficient.

Table 38. *The algebraic simplifications of the biosphere mass transfer coefficients and the estimated distribution parameters. The distributions are denoted as: LU a log-uniform distribution with (minimum, maximum), N_{log} a log-normal distribution with (GM, GSD) and C a constant. The highest values from a one-sided K-S-test are provided.*

Mass transfer coefficient	Expression (without constants)		Simplified expression	Most significant parameters	Estimated distribution (example)
λ_{IMS}, λ_{TS}	$\lambda_a = \frac{Wflux_i(TR)}{\epsilon_i(U) \cdot R_i(C, \approx N_{log})}$ $\lambda_D = \frac{1}{R_i(C, \approx N_{log})}$ $\lambda_{IMS} = \lambda_a + \lambda_D$	C-14	$\lambda_a = \frac{R_i(C)}{\frac{Wflux_i(TR)}{\epsilon_i(U)}}$ $\lambda_{IMS} \approx \lambda_a$	$Wflux_i, \epsilon_i$	N_{log} (IMS) (0.43 1/a, 1.2) p ≈ 3E-4
		Other nuclides	$R_i \approx N_{log}$ $\lambda_a, \lambda_D \approx N_{log}$ $\lambda_{IMS,TS} = \lambda_a + \lambda_D$	Kd_i	N_{log} (Se-79, IMS) (4.1E-5 1/a 2.6) p > 0.1
$\lambda_{IRR,i}$	$\lambda_{IRR,i} = A_i(U)$	All	$\sum_i \lambda_{IRR,i} \approx N_{log}$	A_i	N_{log} (1.2 1/a, 1.2 p ≈ 1E-4
λ_{dis}	$\lambda_{dis} = \frac{WfluxOut(LU)}{A(TR) \cdot d_w(TR)}$	All nuclides	$\lambda_{dis} \approx WfluxOut(LU)$	$WfluxOut$	LU (8.7E-3 1/a, 7.2 1/a) p > 0.1
$\lambda_{runoff,i}$	$\lambda_a = \frac{Wflux_i(U)}{\epsilon_i(U) \cdot R_i(C, \approx N_{log})}$ $\lambda_{runoff,i} = \lambda_a$	C-14	$\lambda_a = \frac{R_i(C)}{\frac{Wflux_i(U)}{\epsilon_i(U)}}$ $\lambda_{runoff,i} = \lambda_a$	$Wflux_i, \epsilon_i$	N_{log} (forest) (9.0E-2 1/a, 1.4 p ≈ 0.003
		Other nuclides	$R_i \approx N_{log}$ $\lambda_a \approx N_{log}$ $\lambda_{runoff,i} = \lambda_a$ $(\approx N_{log})$	$Kd_i, Wflux_i$	N_{log} (Cl-36, cereal cropland) (1.1E-2 1/a, 3.7 p ≈ 0.003

The mass transfer coefficient from the intermediate sediment of the lake to the top sediment (λ_{IMS}) and from the top sediment to the lake water (λ_{TS}) is a sum of diffusion (λ_D) and water advection processes (λ_a). For C-14 the retardation coefficient has a constant value of unity and the mass transfer coefficient results in a ratio of a triangular distribution of water flux and uniform distribution of porosity. The result is not a conventional distribution but an analytical PDF is possible to determine by calculating the integral $p_Z(z) = \int_{-\infty}^{\infty} |x| \, p_{X,Y}(zx, x) dx$, where $p_{X,Y}(x, y)$ is a joint PDF (Curtiss, 1941). However, for simplicity of the analysis a log-normal PDF is fitted to the data based on calculated GM and GSD values. The resulting p-value from K-S-test is rather low but as a rough approximation log-normal distribution is suitable.

For other nuclides, the retardation coefficient is roughly log-normal due to log-normal distribution coefficients. The log-normal assumption is a simplification as the expression includes a ratio of uniformly or triangularly distributed density and porosity. As a result, the diffusion and advection mass transfer coefficient expressions follow approximately log-normal distributions as the inverse of a log-normal distribution is log-normal (see previous section). The final mass transfer coefficient is then a sum of log-normal distributions, which does not have a conventional representation. The empirical distribution obtained with simulations is again approximated with a log-normal distribution and the p-values are rather high. The results for mass transfer coefficient from intermediate sediment to top sediment for C-14 are presented in Figure 10. Generally, for the mass transfer coefficient from the top sediment to lake water, the p-values for log-normal distributions are slightly lower. The reason for this is the density of the layer, which is follows a triangular distribution, and affects the retardation coefficient values.

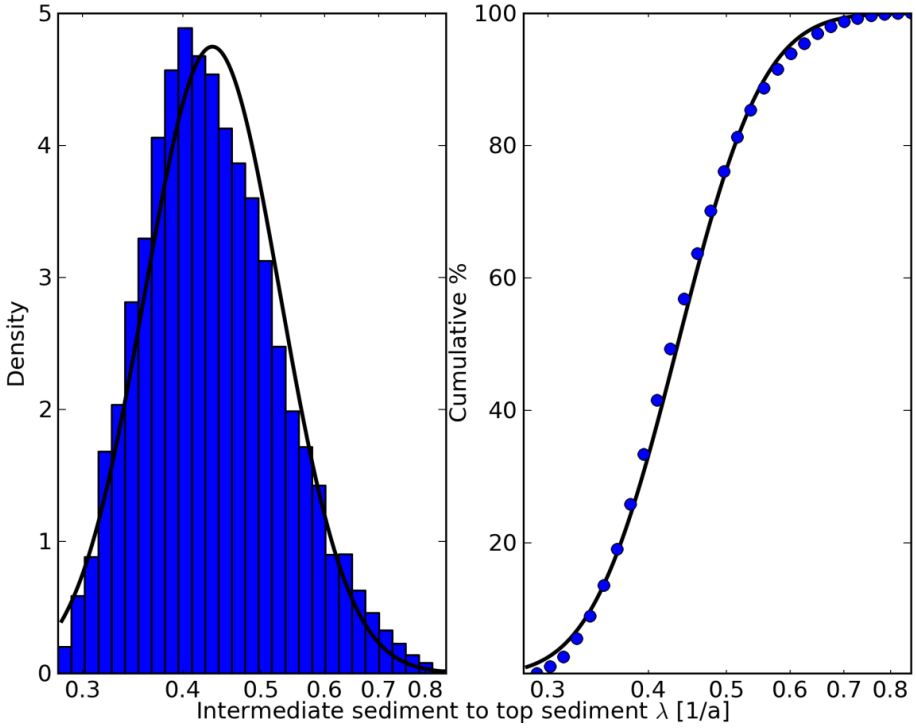

Figure 10. *On the left, the histogram of 10 000 realizations for mass transfer coefficient from intermediate sediment to top sediment of the lake for C-14. On the right, the cumulative percentages corresponding to histogram bars are presented. The black line corresponds to a log-normal distribution fitted to the data (GM = 0.43 1/a, GSD = 1.2).*

The mass transfer coefficient from the well to the irrigated crops ($\lambda_{IRR,i}$) is calculated with Equation (32). The total mass transfer coefficient is calculated as a sum of different irrigation mass transfer coefficients related to different crops. The sum is examined because the single mass transfer coefficients follow uniforms distributions due to uniformly distributed areas of irrigated objects. The resulting distribution is a sum of four translated uniform random variables and a PDF for the distribution can be determined by four consequent convolutions (Benjamin & Cornell, 1970). However,

due to simplicity of the analysis an approximation of a log-normal distribution is used for the mass transfer coefficient as a rough characterization is only needed for comparisons of the mass transfer coefficients. The result for all nuclides is presented in Figure 11. The p-values for the K-S-test are about 1E-4 but the distribution resembles the shape of a log-normal distribution. It must be noted that the difference of a log-normal and normal distribution is negligible if the interval of values is small. Log-normal distributions are used for approximations because it produces positive, physically possible values.

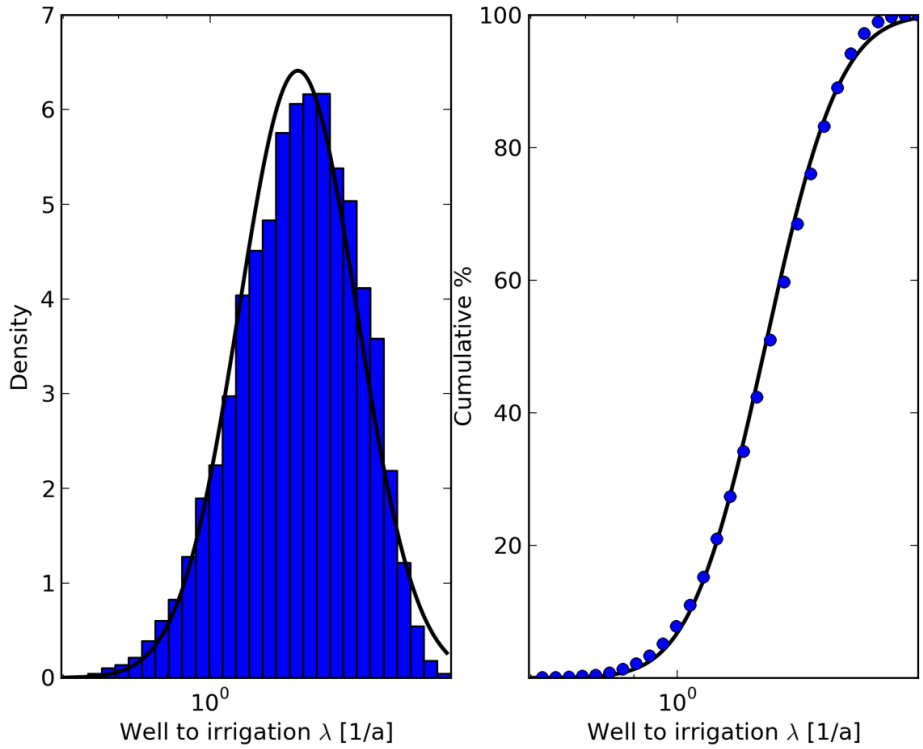

Figure 11. *On the left, the histogram of 10 000 realizations for mass transfer coefficient from the well water due irrigation. On the right, the cumulative percentages corresponding to histogram bars are presented. The black line corresponds to a log-normal distribution fitted to the data (GM 1.2 1/a, GSD 1.2).*

The mass transfer coefficient from the lake water to the sink or forest due to lake discharge (λ_{dis}) follows an approximately log-uniform distribution due to numerically large discharge values compared to area and water depth that follow triangular distributions.

The mass transfer coefficient from the terrestrial objects to sink ($\lambda_{runoff,i}$) for C-14 is a ratio of two uniform random variables that is not a conventional distribution although an analytical PDF is obtainable. For other nuclides, the retardation coefficient is roughly log-normal, which means that the mass transfer coefficient is roughly log-normal as the inverse of a log-normal distribution is log-normal. Thus, the log-normal distribution is used for fitting for other nuclides except C-14. For C-14, the log-normal approximation is determined for the mass transfer coefficient from forest to sink but for croplands no distribution approximation is made due to complex shape of the resulting histogram. The p-values from the K-S-test are in most cases over 0.1 for all nuclides but also worse

p-values are obtained especially for nuclides that have low retardation coefficient values in a soil layer. With C-14, the histogram for the mass transfer coefficient of the cereal cropland is presented in Figure 12. The range for the mass transfer coefficient values for C-14 is from about 0.14 1/a to 0.56 1/a for all croplands.

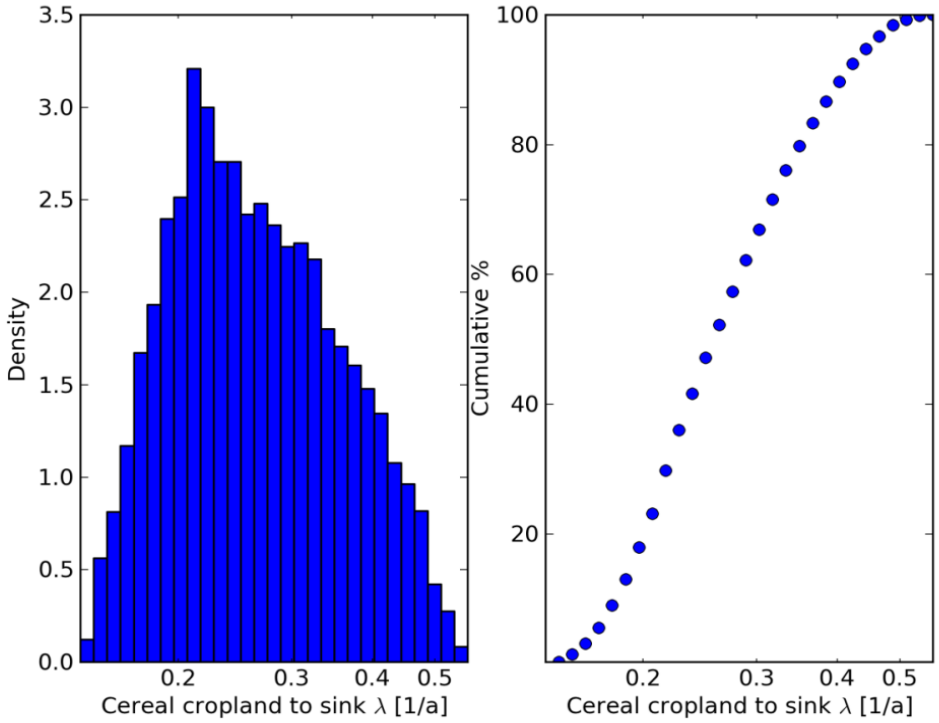

Figure 12. *On the left, the histogram of 10 000 realizations for mass transfer coefficient from the cropland with cereal cultivation to sink for C-14. On the right, the cumulative percentages corresponding to histogram bars are presented. No fitted PDF is provided due to complex shape of the distribution.*

The mass transfer coefficients (or the decay constants) for the biosphere compartments are summarized in Table 39 and in Table 40. Overall, the coefficients in the biosphere have about similar uncertainties (GSDs) for all nuclides and objects compared to the situation in geosphere where larger uncertainties are involved. The coefficients here are approximately log-normally distributed in most cases. The only parameters, which affect the solute mass transfer coefficients and are log-normally distributed, are the distribution coefficients for different nuclides. Also, the larger GSDs are observed for the nuclides that have larger GSD for the distribution coefficient. From other parameters, the water fluxes determine largely the magnitude of the mass transfer coefficient. For example, the water fluxes from the forest to sink are about one order of magnitude less than the water fluxes from other terrestrial compartments and as a result, the mass transfer coefficients are about one order of magnitude smaller for the forest.

The mass transfer coefficients for C-14 and Cl-36 can be observed to be the smallest in all biosphere compartments. The distribution coefficients contribute to this difference compared to other nuclides as the C-14 has zero value and Cl-36 the smallest non-zero values for the distribution coefficients.

Table 39. *The first part of summary of the simulated approximations for mass transfer coefficient distributions in biosphere with 10 000 realizations and parameter selections of the base case. Notations: IMS = intermediate sediment to top sediment, TS = top sediment to lake water, Lake = lake to sink (discharge), Well = well to irrigation targets, Forest = forest to sink , LU = log-uniform distribution, N_{log} = log-normal distribution. The approximated parameters for the distributions are in the brackets (min, max) with LU and (GM, GSD) with $N_{log.}$*

Nuclide	IMS (1/a, -)	TS (1/a, -)	Lake (1/a)	Well (1/a, -)	Forest (1/a, -)
C-14	N_{log} (0.43, 1.2)	N_{log} (1.9, 1.1)	LU (8.7E-3, 7.2)	N_{log} (1.2, 1.2)	N_{log} (9.0E-2, 1.4)
Cl-36	N_{log} (1.1E-2, 1.8)	N_{log} (0.27, 1.7)			N_{log} (2.0E-4, 6.9)
Se-79	N_{log} (4.1E-5, 2.6)	N_{log} (9.4E-4, 2.6)			N_{log} (5.9E-5, 4.3)
Mo-93	N_{log} (4.1E-6, 2.6)	N_{log} (9.4E-5, 2.5)			N_{log} (2.7E-5, 7.9)
Nb-94	N_{log} (1.5E-6, 2.9)	N_{log} (3.3E-5, 2.9)			N_{log} (5.6E-7, 2.8)
Ag-108m	N_{log} (4.9E-5, 2.1)	N_{log} (1.2E-3, 2.1)			N_{log} (1.0E-5, 4.2)
I-129	N_{log} (4.5E-4, 1.6)	N_{log} (1.1E-2, 1.5)			N_{log} (8.4E-5, 7.6)

Table 40. *The second part of summary of the simulated approximations for mass transfer coefficient distributions with 10 000 realizations and parameter selections of the base case. Notations: N_{log} = log-normal distribution. The approximated parameters for the distributions are in the brackets (GM, GSD). All the mass transfer coefficients occur due to runoff to a sink. For C-14 a closed interval of the values is presented.*

Nuclide	Cereal/Potato/Field vegetable cropland or pasture land (1/a, -)
C-14	[0.14, 0.56 1/a]
Cl-36	N_{log} (1.1E-2, 3.7)
Se-79	N_{log} (3.3E-4, 2.6)
Mo-93	N_{log} (5.0E-4, 5.1)
Nb-94	N_{log} (6.3E-6, 2.8)
Ag-108m	N_{log} (8.5E-5, 3.2)
I-129	N_{log} (1.3E-3, 2.0)

The approximated solute half-times for the biosphere compartments are presented in Table 41. The values are calculated by using the GM values in Table 36 and Table 37 and they have the same GSD values. Among the biosphere objects, the intermediate sediment of the lake is the most significant compartment in limiting the radionuclide releases. Based on the half-times, also forest has long half-times but the significance of slow half-time depends on the mass transfer coefficients that transfer the solute to the forest (i.e. discharge from lake in the base case).

Table 41. *Summary of the approximated solute half-times in biosphere compartments with parameter selections and correlations of the base case. Notations: IMS = intermediate sediment to top sediment, TS = top sediment to lake water, Lake = lake to sink (discharge), Well = well to irrigation targets, Forest = forest to sink, Croplands/Pasture land = cropland/pasture land to sink. The geometric mean values for the mass transfer coefficients are used in the calculation except the range given for C-14 in the croplands/pasture land.*

Nuclide	IMS (a)	TS (a)	Lake (a)	Well (a)	Forest (a)	Croplands*/Pasture land
C-14	1.22	0.374	2.75	0.561	7.68	2.62
Cl-36	60.3	2.59			3430	66.5
Se-79	16 800	738			11 800	2 080
Mo-93	168 000	7 400			25 800	1400
Nb-94	476 000	20 800			1 250 000	110 000
Ag-108m	14 200	572			66 900	8 150
I-129	1 560	60.6			8250	544

*Cereal/Potato/Field vegetable cropland

The mass transfer coefficient distributions for three nuclides in the different compartments of the transport chain are presented in Figure 13. Compared to geosphere compartments, the biosphere mass transfer coefficients are significantly higher (and solute half-times lower) and therefore, only three typically lowest mass transfer coefficients in the biosphere are presented. For other nuclides in this study, Cl-36 and Se-79 have similar behavior as I-129 as anionic nuclides, Mo-93 resembles Nb-94 and Ag-108m behaves like C-14 in the geosphere transport.

In general, it can be seen from the overlapping PDFs that the most important barrier in the transport chain varies between the nuclides and calculation cases in the transport simulations. The mass transfer from canister to buffer is the most limiting for other nuclides except Mo-93 and Nb-94 which are efficiently limited by the buffer and tunnel backfill. The largest values for mass transfer coefficients in the geosphere are typically obtained with the geosphere barrier. In some realizations of the system, the geosphere may limit the radionuclide release less than the biosphere objects (soil layers/sediments), which can be viewed as unrealistic if there are (justified) correlations between the mass transfer coefficients in reality. On the other hand, the smallest mass transfer coefficient, which dominates the response function of the system, is typically obtained in the canister or the buffer and there is orders of magnitude difference to geosphere barrier. Also, it can be said that in the reference case, the biosphere mass transfer coefficients resemble the best-estimate ones (about the geometric mean values) due to parameter selections, whereas in the geosphere the mass transfer coefficients are in the over the geometric mean value of the distribution.

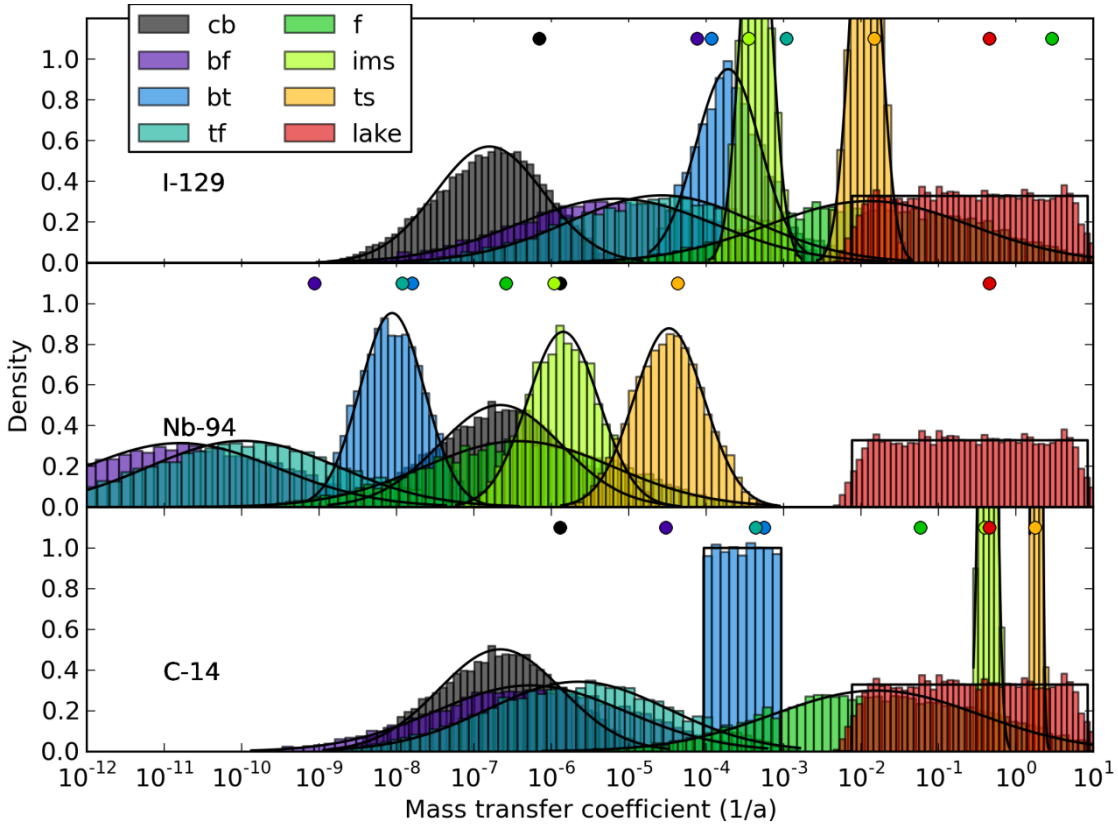

Figure 13. *The distributions of mass transfer coefficients calculated with the parameter selections and correlations of the base case for three nuclides using 10 000 realizations. The fitted distributions are depicted with black lines and the mass transfer coefficients corresponding to reference case parameters are presented as circles. The notation in the legend is: cb = canister to buffer, bf = buffer to fracture, bt = buffer to tunnel, tf = tunnel to fracture, f = fracture to biosphere, ims = intermediate sediment to top sediment , ts = top sediment to lake water, lake = lake discharge. The y-axis is limited to the presented range although densities of some mass transfer coefficients are over the highest value.*

5.2 Delay times

The delay times for the solute transport are simulated and analyzed similarly as the mass transfer coefficients. The base case parameter selections and correlations are presented in Sections 4.2 and 4.3 and they are used in simulations. The summary of the expressions, simplified expressions, significant parameters and approximated distributions are presented in Table 42.

Table 42. *The algebraic simplifications of the geosphere delay times and the estimated distribution parameters. The distributions are denoted as: LU a log-uniform distribution with (minimum, maximum), N_{log} a log-normal distribution with (GM, GSD) and C a constant. The highest values from a one-sided K-S-test are provided.*

Mass transfer coefficient	Expression (without constants)		Simplified expression	Most significant parameters	Estimated distribution (example)
$t_{d,cb}$	$t_{d,cb} = 1/D_w(LU)$	All	$t_{d,cb} = 1/D_w(LU)$	D_w	LU [2.6E-3 a, 0.13 a] p > 0.1
$t_{d,bf}$, $t_{d,bt}$	$t_{d,bf}, t_{d,bt} \approx R_{pb}(C, N_{log})/D_{pb}(LU, \frac{LU}{LU})$	Anions	$t_{d,bf,bt} = 1/D_{pb}(LU/LU)$	D_{eb}, ϵ_b	N_{log} ($t_{d,bf}$) (1.3 a, 2.6) p ≈ 0.004
		Cations	$t_{d,bf,bt} \approx R_{pb}(N_{log})/D_{pb}(LU)$ $(\approx N_{log})$	$D_{eb}, \epsilon_b, Kd_{pb}$	N_{log} (Nb-94, $t_{d,bf}$) (2.9E+4 a, 2.6) p ≈ 0.05
		Neutrals	$t_{d,bf,bt} = \frac{1}{D_{pb}(LU)} = \frac{1}{D_{eb}(LU)}$	D_{eb}	LU ($t_{d,bf}$) [0.28 a, 2.8 a] p > 0.1
$t_{d,f}$	$u = \sqrt{\epsilon_m(LU) R_{pm}\left(C, \frac{LU}{LU}\right) D_{em}(LU)}$ $WL/Q(N_{log})$ $t_{d,f} = u^2$	Anions	$R_{pm}(LU/LU)$ $(u \approx N_{log})$	$\frac{WL}{Q}, Kd_{pm}, D_{em}, \epsilon_m$	N_{log} (I-129) (1.8 a, 21) p ≈ 0.01
		Cations			N_{log} (Nb-94) (6.2E+4 a, 17) p > 0.1
		Neutrals	$R_{pm}(C)$ $(u \approx N_{log})$	$\frac{WL}{Q}, D_{em}, \epsilon_m$	N_{log} (1.5a, 22) p ≈ 0.02

The delay time for the mass transfer from the canister to the buffer ($t_{d,cb}$) includes only one distributed parameter, the diffusion coefficient D_w that is log-uniformly distributed. The inverse of a usual uniform distribution is not a conventional distribution but an analytical form for the PDF is obtainable (Hamming, 1970). The lower and upper limits are $1/a$ and $1/b$ where a and b are the limits for the uniformly distributed variable. When these are multiplied with the constants in Equation (14) the range becomes 2.6E-3 - 0.13 a for all nuclides. The shape of the histogram based on the simulated data is on the other hand close to a log-uniform distribution that is used for approximation. The p-value from K-S-test is about 0.8, which strongly supports log-uniform approximation.

The delay times from the buffer to the fracture ($t_{d,bf}$) and from the buffer to tunnel floor ($t_{d,bt}$) have a similar behavior. For the anionic nuclides, the result is a ratio of two log-uniformly distributed variables D_{eb} and ϵ_b. As noted with the mass transfer coefficients, the shape of the histograms resembles a symmetric log-triangular

distribution but a log-normal approximation is used as a rough approximation. For neutral nuclides, the distribution is an inverse of a log-uniform distribution due to one distributed parameter D_{eb}. The simulated distribution resembles log-uniform distribution as with the canister to buffer delay time. For the cationic nuclides, the log-normal distribution coefficients in the buffer (Kd_{pb}) results in an approximately log-normal distribution of the delay time. The histogram of simulated data for Nb-94 delay time from buffer to fracture is presented in Figure 14 with the fitted log-normal distribution based on GM and GSD values.

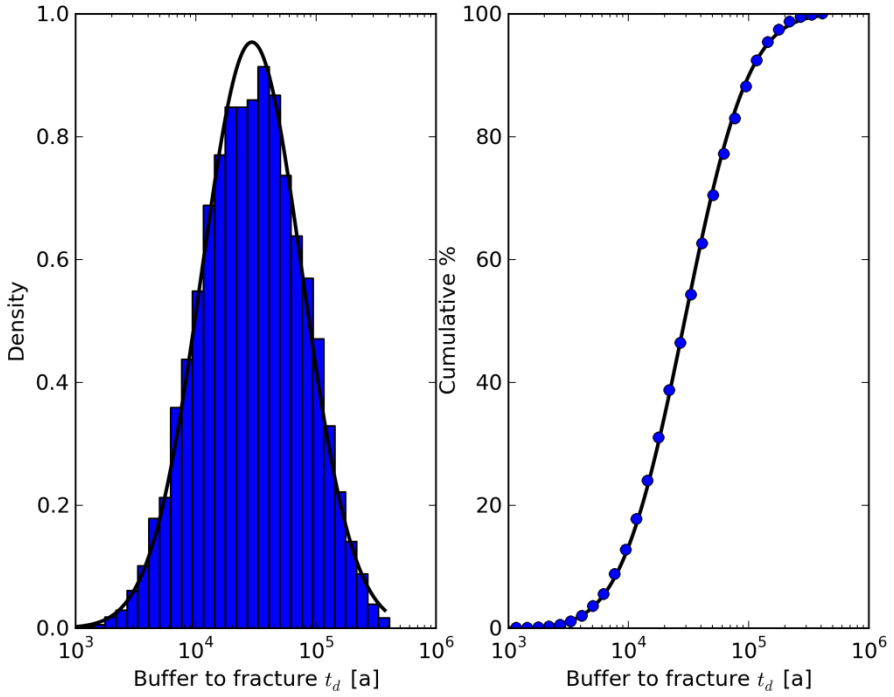

Figure 14. *The delay time for the solute transport from the buffer to the intersecting fracture with 10 000 realizations for Nb-94. A log-normal distribution is fitted to the data (black line) and the obtained values are for GM about 29 000 a and for GSD about 2.6.*

The delay time of the geosphere barrier ($t_{d,f}$) is a result of a multiplication of log-uniform variables and a log-normal WL/Q that has numerically the largest values. The distributions for all nuclides are rather similar in shape due to similar parameter selections in the rock matrix. Log-normal distributions are fitted to the data based on the histograms obtained with simulations.

Summary of the obtained distributions approximations for the delay times are presented in Table 43. With the default parameter selections (i.e. base case), the delay times from the buffer to the tunnel floor are especially large for cationic nuclides. The sorption in the buffer and diffusion length to the buffer floor resulted in a GM value of about 1.5 million years for Nb-94 and about 2100 a for Mo-93. The high delay time for Nb-94 means that the release is strongly limited by the buffer layer above the canister and in practice, no release is transported to the deposition tunnel during the analyzed time scope. It must be noted that the distribution coefficient values are cautiously limited to glacial water maximum values and therefore, only a shortened distance between the

canister and the tunnel floor ($s_c = 2.5$ m) would shorten the delay time in the simplified model.

The most significant and uncertain delay time is the delay from the fracture to biosphere (delay through geosphere) due to the highest GSD values. The delay time has a wide distribution of delay times with parameter selections of the base case. The most significant parameters affecting this delay time are the hydrodynamic control of retention WL/Q, distribution coefficient in the rock matrix Kd_{pm} also the diffusion coefficient in the rock matrix D_{em}. The significant range of the delay times is about seven orders of magnitude, which is a result of all the uncertainties related to the parameters. D_{em} had values between three orders of magnitude, WL/Q had a range of one order of magnitude but the largest numerical values and retardation coefficients varied over one to two orders of magnitude.

Table 43. *Summary of the simulated approximations for delay time distributions with 10 000 realizations and parameter selections of the base case. Notations: Cb = canister to buffer, Bf = buffer to fracture, Bt = buffer to tunnel, Tf = tunnel to fracture, Fb = fracture to biosphere, LU = log-uniform distribution, N_{log} = log-normal distribution. The approximated parameters for the distributions are in the brackets: (min, max) with LU and (GM, GSD) with N_{log}.*

Nuclide	Cb (a)	Bf (a, -)	Bt (a, -)	Fb (a, -)
C-14	LU (2.6E-3, 0.13)	LU (0.28 a, 2.8 a)	LU (14 a, 1.4E+2 a)	N_{log} (1.5, 22)
Cl-36		N_{log} (1.3, 2.6)	N_{log} (68, 2.6)	N_{log} (1.6, 21)
Se-79				N_{log} (1.5, 21)
Mo-93		N_{log} (42, 2.5)	N_{log} (2.1E+3, 2.5)	N_{log} (1.0E+1, 31)
Nb-94		N_{log} (2.9E+4, 2.6)	N_{log} (1.5E+6, 2.6)	N_{log} (6.2E+4, 17)
Ag-108m		see C-14	see C-14	see C-14
I-129		see Cl-36	see Cl-36	N_{log} (1.8, 21)

In the final calculation (i.e. total response functions), the delay times of geosphere barriers are summed to obtain a branch-specific total delay time for both geosphere branches. The simulated distributions for two branches for three nuclides (anionic, cationic and neutral) are presented in Figure 15. Based on the simulations it may be concluded that the delay times are preventing significantly releases of Mo-93 and especially Nb-94 (see Table 43) in the base case of the simplified model. The transfer branch from buffer to fracture begins to affect generally earlier but also with a smaller mass transfer coefficient than the tunnel branch. The Nb-94 delay times suggest that the doses in the biosphere are rare and only occur in minor part of the realizations.

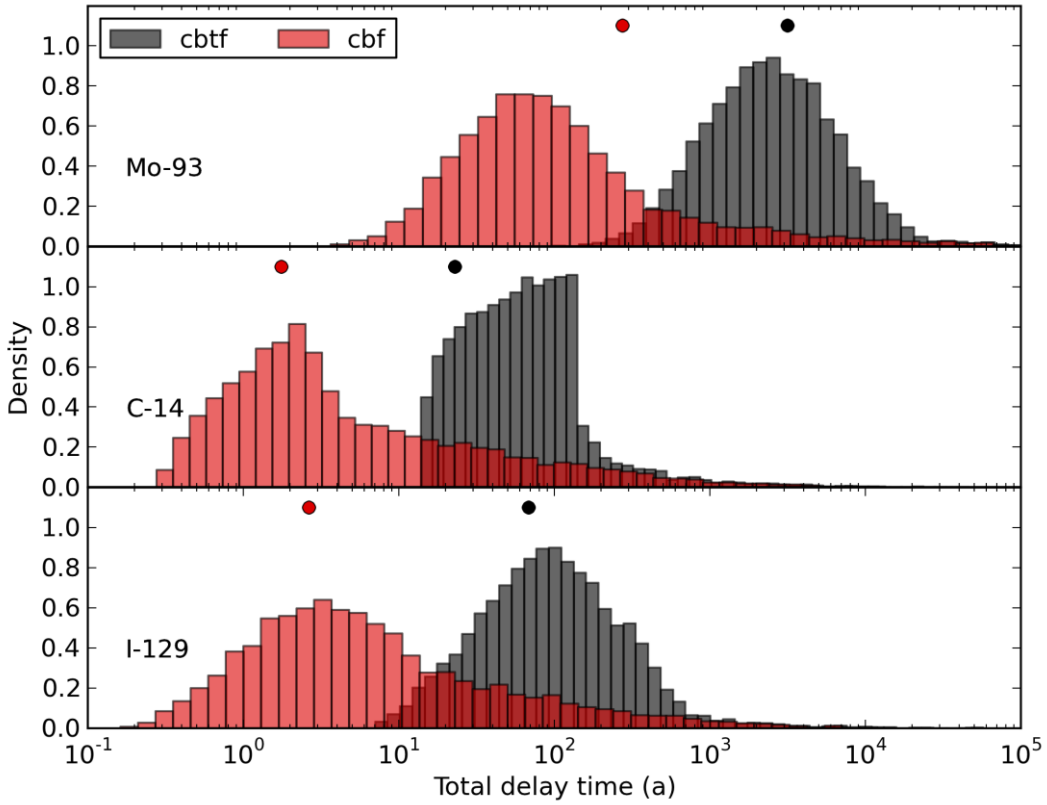

Figure 15. *The total simulated delay times (10 000 realizations) of two geosphere branches for three nuclides that are Mo-93 (cation), neutral (C-14) or I-129 (anion). Cbtf denotes the canister-buffer-tunnel-fracture transport branch and cbf the canister-buffer-fracture branch. The values of delay times obtained in the reference case are market with circles.*

5.3 Base case release rates and dose rates

The calculation cases within the base scenario in this study are calculated with the default parameter selections presented in Sections 4.2.1-4.2.5 and correlations presented in Section 4.3. The geosphere release rates are first calculated with the reference case parameter values in order to compare the deterministic calculation. The results with the BSA-2012 reference case (RC) release rates are presented in Figure 16. The delay time in BSA-2012 RC is for all nuclides 1000 years because the formation of the transport path is assumed to take at least 1000 years. For Nb-94, there are no releases to biosphere due to retardation with reference case parameters in the simplified model. For most nuclides, the simplified model gives similar results as in BSA-2012 RC. The release rate of Mo-93 is about one order of magnitude less in the simplified model than in BSA-2012 RC based on maximum values. Ag-108m is also slightly underestimated by the simplified model. The reason for the underestimations are likely the different modelling concepts but also different solubility limits applied may give a straightforward answer for the differences. However, the shapes of the release rates are similar.

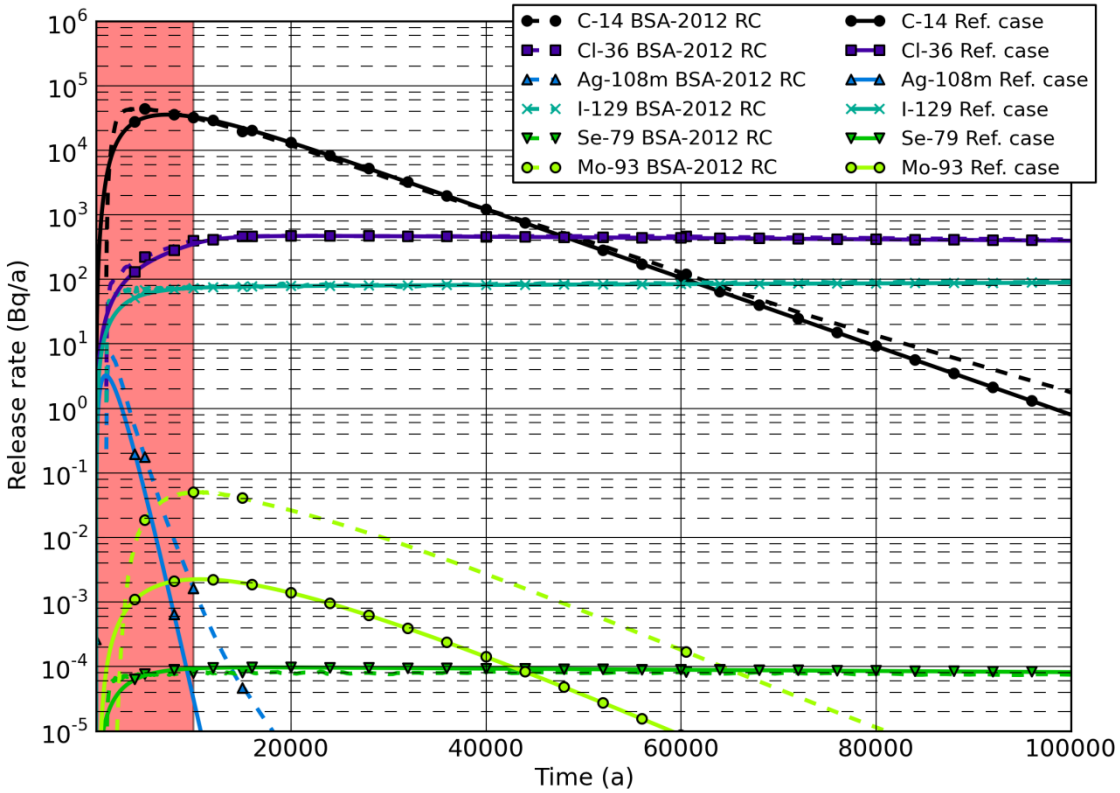

Figure 16. *The reference case calculation results obtained with the simplified model (continuous lines). The BSA-2012 reference case release rates are also presented for comparison (dashed lines). The shaded area is the dose assessment period (i.e. 10 000 years).*

The regulatory constraints for geosphere releases are presented in the YVL Guide by STUK but applied constraints are taken from (Posiva, 2012b) where the regulatory constraints are complemented by a preliminary evaluation from STUK. The release constraint to biosphere for Se-79, Nb-94 and I-129 is 0.1 GBq/a, for C-14 and Cl-36 0.3 GBq/a and for Mo-93 3 GBq/a, which means that in the reference case, the release rates are clearly below the regulatory constraints. For Ag-108m, there is not regulatory constraint provided. The highest release rate during the analyzed time period of 100 000 years is under 0.0001 GBq/a (C-14) and therefore, the base case results are clearly below the constraints. The development of the release rates for the time after 100 000 years is similar for extremely long-lived nuclides (Cl-36, Se-79, I-129). In the end, the radioactive decay will decrease the amount of radionuclides and the curves for all nuclides approach zero as can be observed for other nuclides within 100 000 years.

The geosphere release rates are then simulated by using the parameter distributions and correlations of the base case and 1000 realizations. The shape of the distribution changes in the beginning of the time scope but remains rather unchanged after about 2000 years. The results for a fixed time point at 10 000 years with three most contributing nuclides are presented in Figure 17. The time point of 10 000 years is selected because the maximum release rates regarding dose assessment are then obtained for most nuclides. The reference case values are also marked and it can be concluded that the values are cautiously in the upper half of the resulting distribution but lower than for example 95th percentile.

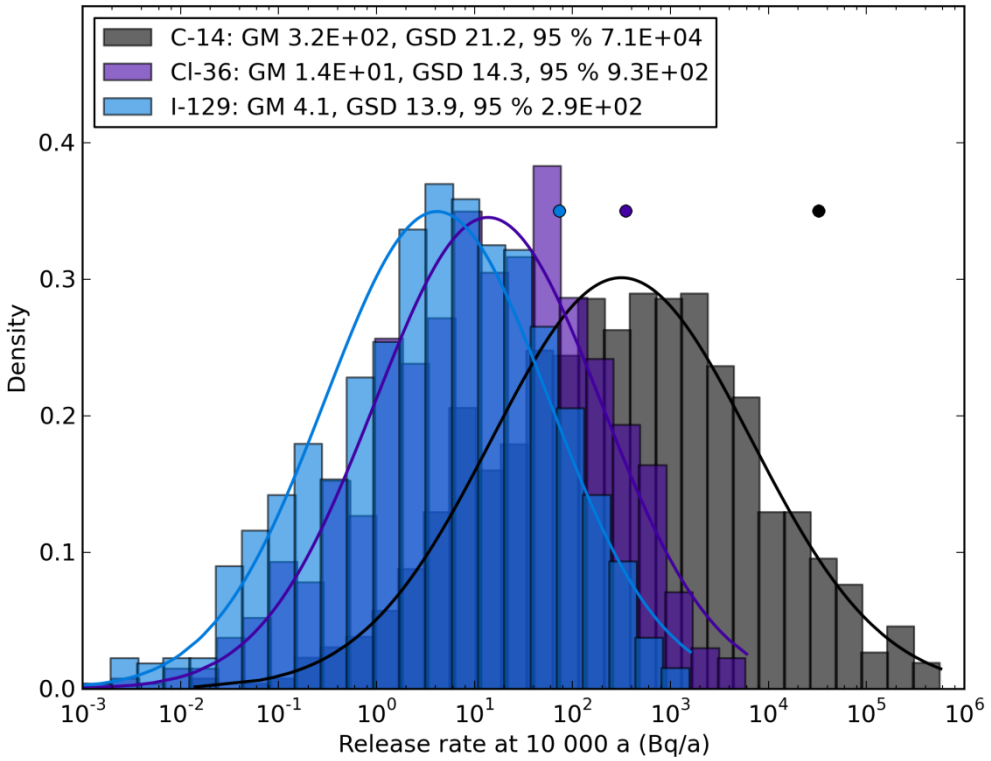

Figure 17. *The simulated release rates (1000 realizations) at 10 000 a in the base case for the three most contributing nuclides. The reference case release rates are marked with corresponding circles and continuous lines represent log-normal distributions fitted to the data. The GM, GSD and 95th percentiles are provided (without units).*

The biosphere calculation and resulting dose rates are performed next. In the base case, the releases in the biosphere occur to the intermediate sediment of the lake (IMS) and well with equal fractions (50 %/50 %). The time series for the total dose rate from the seven nuclides is obtained by using 1000 simulation cases. In every case, all nuclides are summed up for all dose paths and then, the most contributing dose paths are chosen to the total dose rate (i.e. for example choosing the inhalation/external irradiation from object that gives largest contribution). The total dose rate is in this way assessed to comply regulatory requirements of a future agricultural community (an exposed individual) using data relevant to the repository site (see (STUK, 2013) for further information). The confidence levels are determined from the simulated dose rates by applying Wilks' theorem described in Section 4.1.

The results for the total dose rate in the base case are shown in Figure 18 by presenting simulated confidence levels together with the reference case and BSA-2012 RC total dose rates. A best-estimate calculation case with every parameter having (geometric) mean value (CDF = 0.5) is also presented with the most contributing dose path (drinking water from well). The differences between the total dose rate at different confidence levels reflect the uncertainty related to the mass transfer coefficients. There is less than an order of magnitude difference between the total dose rate at 25 % and 50 % confidence levels and slightly less than two orders of magnitude difference between the total dose rate at 95 % and 50 % confidence levels. The dose constraint for

an exposed individual is 0.1 mSv/a regarding long-term safety of nuclear waste (STUK, 2013) and in the 95 % of the calculation cases, the results are about three orders of magnitude lower than the constraint (also 99 % of the cases under the constraint).

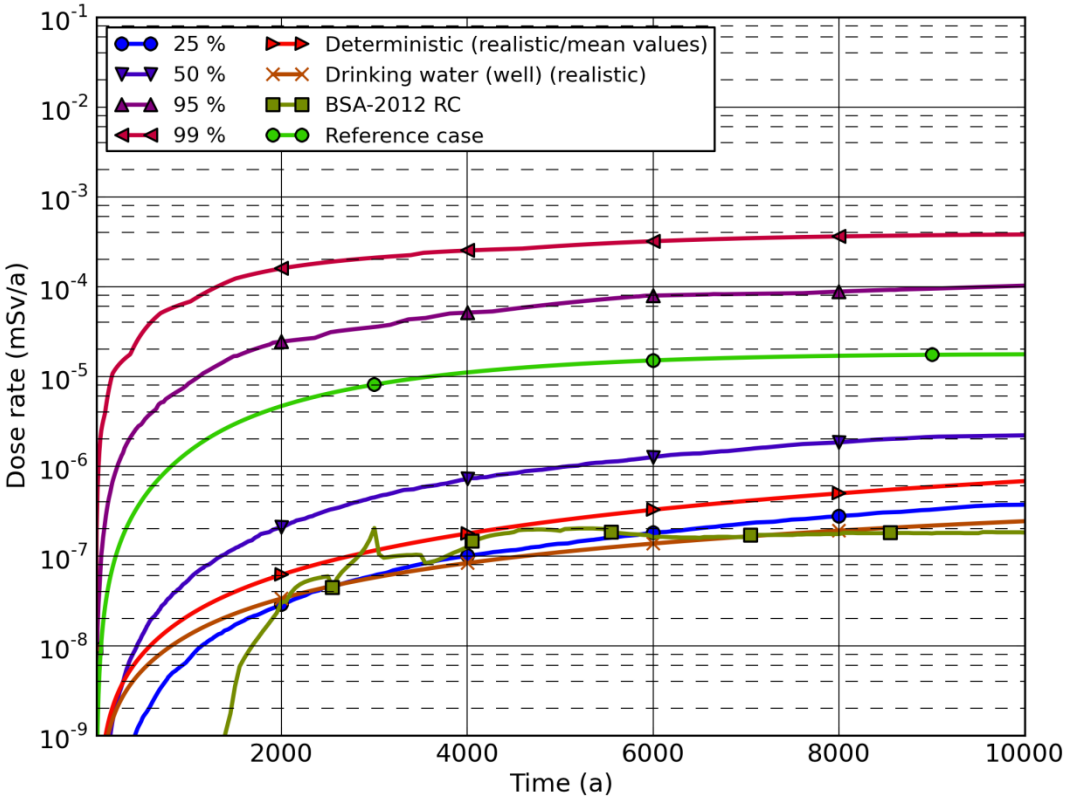

Figure 18. *The calculated total dose rates in the base case. The confidence levels are determined with 1000 realizations. The results from a deterministic case with every parameter having the (geometric) mean value are presented with the dose path from drinking water (from well). The reference case and BSA-2012 reference case results can be seen.*

Based on results in Figure 18, the base case with the simplified model produces rather cautious results. For example, the BSA-2012 RC results are between the total dose rate at 25 % and 50 % confidence levels or under total dose rate at 25 % confidence level during the analyzed time scope. Also, the total dose rate at 95 % confidence level is about one order of magnitude higher than the reference case calculation results with cautious parameter values and the total dose rate at 50 % confidence level is slightly (about 40 %) higher than the deterministic calculation with (geometric) mean values of parameters. The reason for the difference are partly the correlations between parameters as they increase the variance of the mass transfer coefficients (as explained in Section 5.1) and thereby, the resulting dose rates spread over a larger range and confidence levels increase.

All the considered nuclides are simulated separately in order to obtain their individual confidence levels for the total dose rate. The results at 95 % and 50 % confidence levels are presented in Figure 19. The most contributing nuclide in the base case is clearly

I-129. Also, Cl-36 and C-14 contribute significantly but other nuclides have a minor role in the total dose rate of an individual.

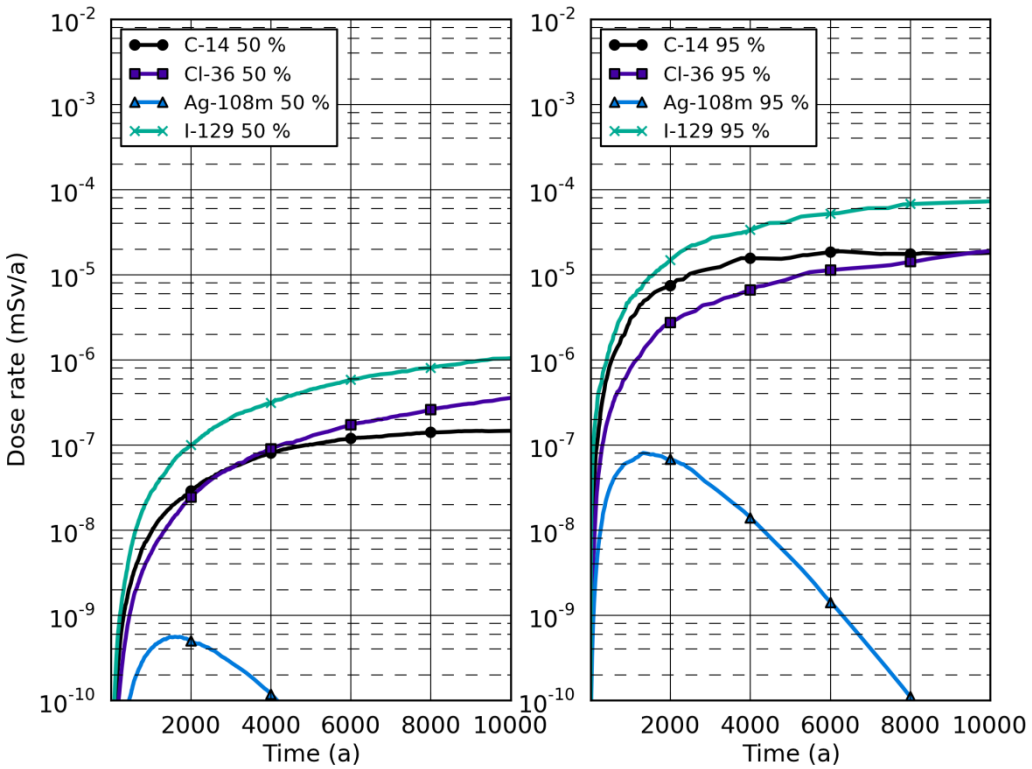

Figure 19. *The simulated total dose rates at 50 % and 95 % confidence levels for single nuclides in the simplified model with 1000 realizations. The rest of the nuclides have dose rates less than 1.0E-10 mSv/a in most of the calculated cases and therefore, the resulting confidence levels are not shown.*

The distributions of the total dose rate at 10 000 years are presented for three most contributing nuclides together with the total dose rate from the whole nuclide set in Figure 20. The difference between the total dose rate at 95 % confidence level and reference case result is now observable more clearly as the reference case results are not in the highest range of the probability mass. The shape of the total dose rate is roughly log-normal for presented nuclides and the total dose rate. The log-normal approximation is similar as for the release rates earlier but the GSD values are increased slightly (about 2 at most) due to uncertainty related to drinking water intake and concentration ratios. Thus, the increase indicates that the uncertainty due to biosphere analysis is rather small. The time dependence of the distribution can be roughly concluded to be rather steady for the most contributing nuclides during the 10 millennia time scope because the confidence levels of the total dose rate have rather steady behavior. The differences between the total dose rate at different confidence levels are similar in Figures 18 and 19 after about 2000 years until the end of 10 millennia. Although the confidence levels of the total dose rate increase, the GSD values of the distributions are rather stable and GM values increase due to increasing release rates (that increase due to response functions).

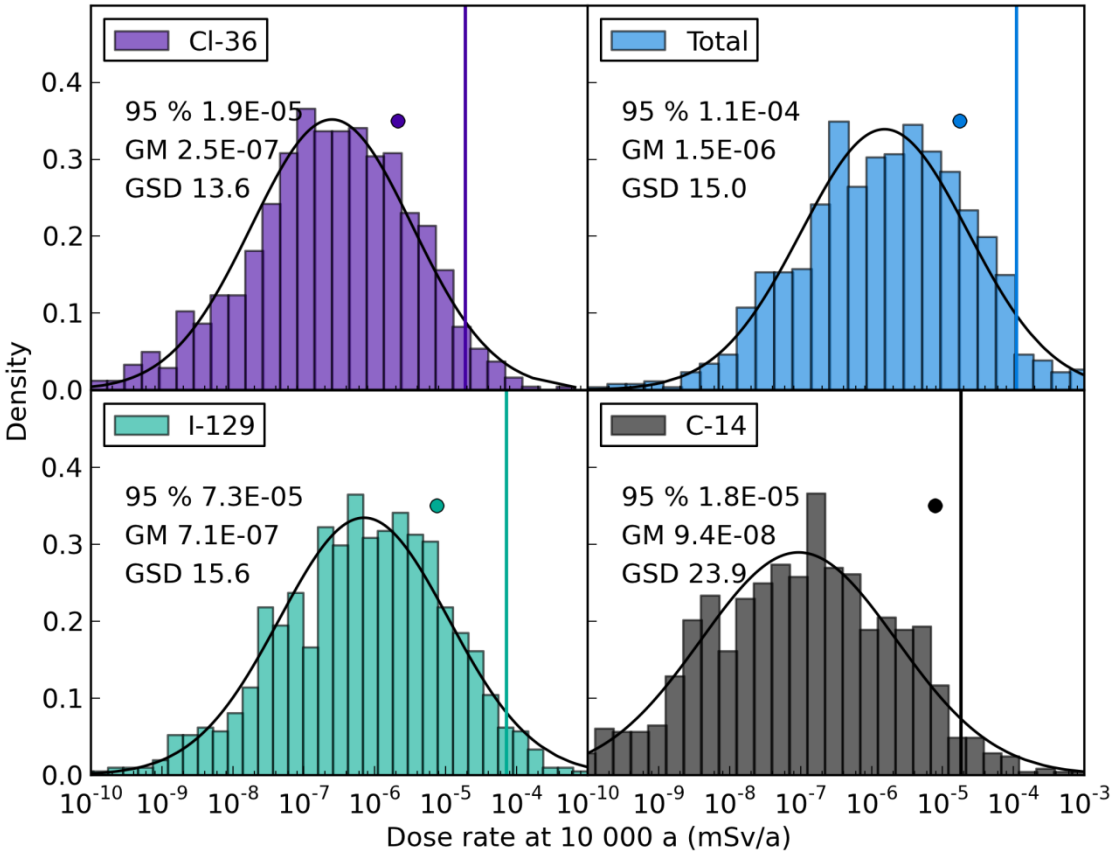

Figure 20. *The simulated total dose rates (1000 realizations, different simulations) for three most contributing nuclides at 10 000 years in the base case. The "Total" includes all the seven nuclides considered in this study. The black lines depict fitted log-normal distributions to the data and vertical lines depict the 95th percentile. The reference case dose rates are marked with circles.*

The most contributing dose paths for I-129 are estimated by calculating a deterministic case with (geometric) mean values of parameters. The results are presented in Figure 21. The largest dose comes from the ingestion of water from well. The second most contributing dose path is the fish ingestion that contributes about equally to the total dose rate near the end of the 10 millennia time period. The milk-water (cows drink well water) dose path and ingestion of potatoes contribute about 10 % each at most to the total dose rate.

For the other nuclides, the most contributing dose paths vary. For C-14, the drinking water from well and fish ingestion are also the most contributing dose paths and others are negligible. For Cl-36, the ingestion of foodstuff from irrigated croplands are contributing the most to the total dose rate (due to generally the highest concentration ratios). For Ag-108m, the external dose basically forms the total dose rate. Based on the dose paths, the concentration factors (and their uncertainty) to the various foodstuff (excluding fish) do not significantly affect the final results from the whole nuclide set unless the ingestion amounts or the factors themselves increase by orders of magnitude. The concentration ratios affect about 10 % to 20 % portion of the total dose rate

depending on the confidence level due to contribution of Cl-36. It can also be concluded that doses due to inhalation or external irradiation are negligible.

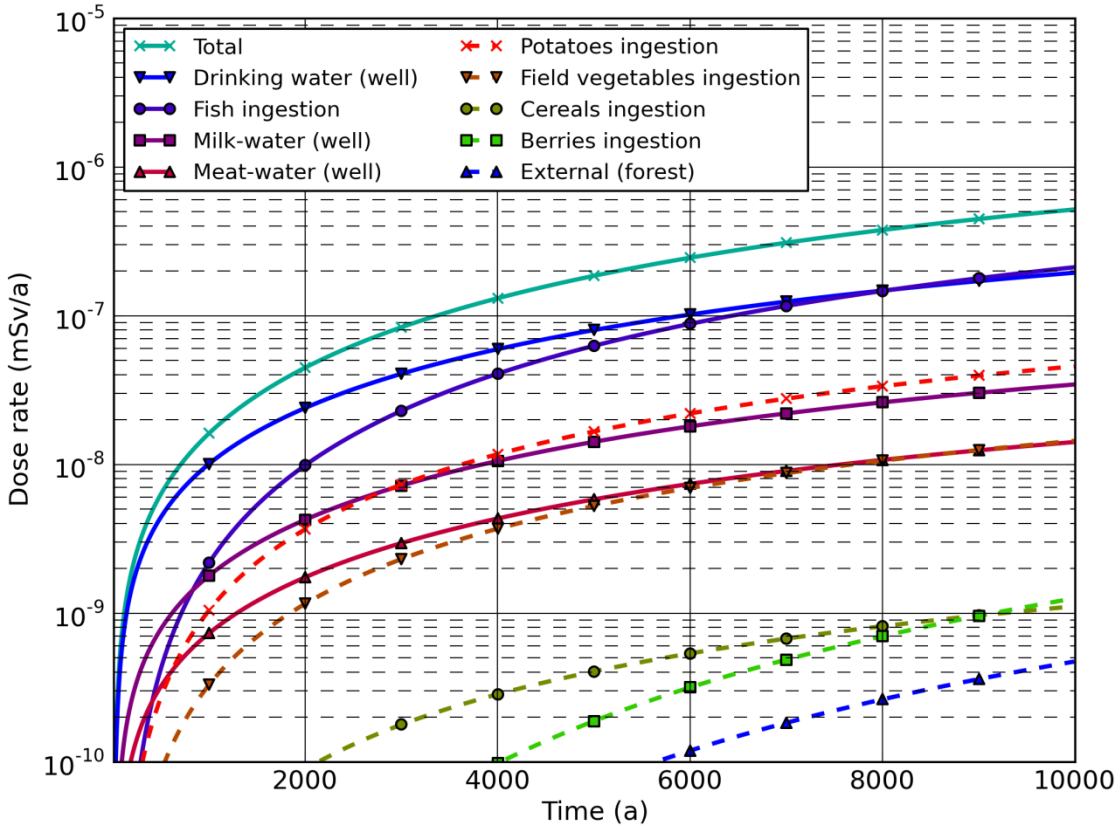

Figure 21. *The results for the most contributing dose paths for I-129 with (geometric) mean parameter values in the base case. The rest of the dose paths (inhalation, meat and milk dose rates from pasture ingestion) are under 10E-10 mSv/a during the analyzed time scope in this deterministic case.*

The results in the base case reflect the limitations of the simplified model. The release rates to biosphere represent well the ones obtained earlier by Posiva. The biosphere calculation overestimates the total dose rate about two orders of magnitude when comparing the reference case total dose rate and BSA-2012 RC results (see Figure 18). This indicates that the biosphere inventories in those compartments, which contribute to the total dose, are significantly larger in the simplified model than in the BSA-2012 RC with the landscape model. Similar derivation for parameters is used and therefore, simplified compartment structure and transport result in a rather cautious estimate of the nuclide transport. On the other hand, the most significant dose path is the ingestion of water (from well), which indicates that the activity concentrations of the compartments should not have a large role in the overestimation.

The overestimation in the biosphere analysis is further confirmed by examining the results with deterministic calculation using (geometric) mean values, reference case results and simulated confidence levels of the total dose rates. The essential differences between the deterministic case with (geometric) mean values and reference case are the geosphere parameters. In the biosphere, almost all the reference case parameter values

are geometric mean values. The cautious geosphere parameters rise the resulting total dose rate by about two orders of magnitude. For the total dose rate at 95 % confidence level in the base case, cautious parameter realizations are likely to be obtained in both geosphere and biosphere. Therefore, the final result is still about one order of magnitude higher than the reference case result. The effect of base case correlations can be observed from the total dose rate at 50 % confidence level that is slightly higher than the deterministic case with (geometric) mean parameter values. The correlations increase also the total dose rate at 95 % confidence level together with the cautious realizations of the biosphere parameters compared to the reference case result.

There are differences also in the dose assessment because the total doses are calculated to an exposed individual in the simplified model, not to a most exposed group as done by Posiva. The individuals in the most exposed group are receiving different doses and the total doses to a most exposed individual could be compared to the results obtained in the simplified model. If, for example, five individuals in the most exposed group of 20 individuals receive the doses similar to ones obtained in the simplified model and the rest receive significantly less, the average total dose can significantly reduce. This dose assessment difference explains a part of the overestimation in the simplified model.

The amount of overestimation in the biosphere analysis varies between nuclides. The final reasons for overestimation are the different dose assessment and well capacity. In addition, as the differences are mainly related to the structure and mathematical description of the compartments, the different behavior of nuclides in the compartments is likely a reason for overestimation. In a more sophisticated model, the sorption occurs in many compartments and transfer processes affect differently to different nuclides resulting in varying radionuclide inventories.

5.4 Effects of varying correlations between parameters

The correlations between the parameters in the base calculation case are presented in Section 4.3 Variant calculation cases are formed from the base calculation case by examining various correlations and observing the changes compared to the base case. The base case (BC) mass transfer coefficients calculated in Section 5.1 are first used in comparisons. If the results vary significantly, the dose rates and/or release rates are calculated and compared to the BC results presented in Section 5.3. Because the time development of the total dose rates is rather stable and they are increasing during the first 10 000 years, the comparisons are made for the distribution shapes at 10 000 years. The calculation cases are variants of the base calculation case and they are presented in Section 4.3.

Case 1

The correlation is first set for the diffusion coefficient in water in geosphere (D_w) and pore volume of the canister (V_c) with a coefficient of 1. By default, the parameters are independent and a positive correlation is justified as the lower limit of diffusion coefficient would correspond to a situation where a little amount of bentonite has entered the canister (and the hole) and the pore volume is low. The correlation affects only the canister to buffer mass transfer coefficient (λ_{cb}) in the system. The resulting

histograms for the mass transfer coefficients for anions and cations are presented in Figure 22. In the base case, log-normal distributions approximated the resulting mass transfer coefficients decently but now, they are not applicable.

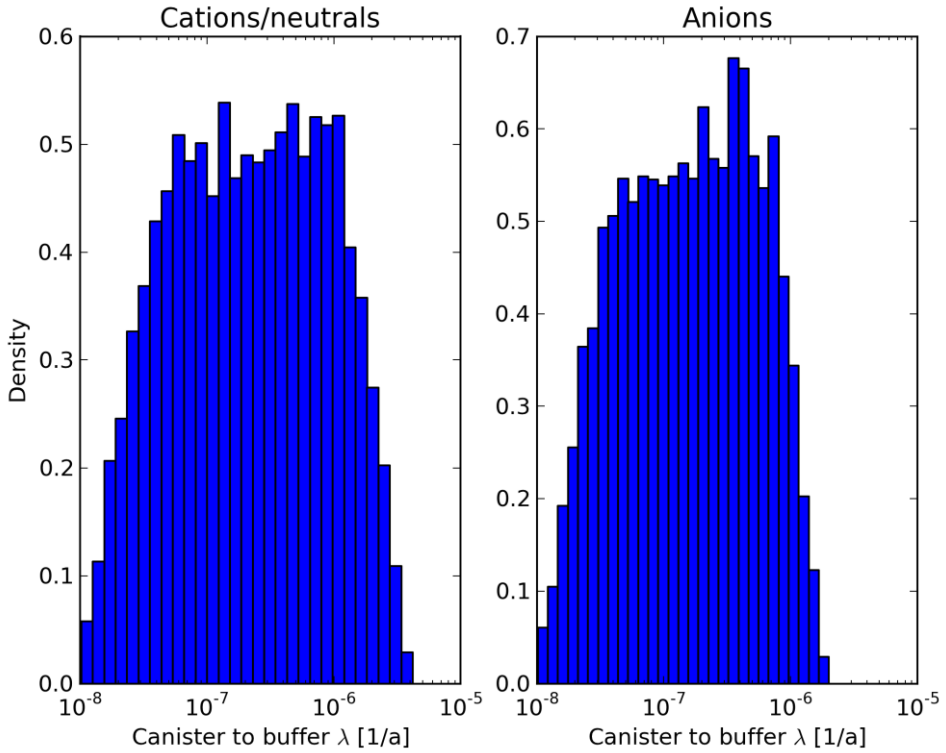

Figure 22. *The resulting mass transfer coefficients (10 000 realizations) for cationic/neutral and anionic nuclides on the left and right respectively with the full correlation between D_w and V_c. In the base case (Section 5.1.1), the mass transfer coefficients could be approximated by log-normal distributions.*

Case 2

In this calculation case, the correlation between the fracture apertures ($2b_v, 2b_{vt}$) and hydrodynamic control of retention (WL/Q) is examined. The negative correlation between either of fracture apertures and hydrodynamic control of retention results in a correlation between either of the mass transfer coefficients related to the fractures (λ_{bf} or λ_{tf}) and the geosphere (λ_f). The distributions of the mass transfer coefficients themselves are not affected as the parameters are not in the same expression. In order to obtain the most cautious case, the correlation is set to -1.

The calculation is divided into two parts for both fractures. With either of the fractures, the changes are similar and therefore, the largest changes the two parts are presented.

Case 3

The case is divided into two parts. At first, the calculation is performed by setting a (full) correlation between effective diffusion coefficient in bentonite (D_{eb}), porosity of the buffer (ϵ_b) and porosity of the backfill (ϵ_t) for both nuclide groups. The porosity of

the rock matrix (ϵ_m) is considered to be independent from other parameters but it is correlated within a nuclide group. The effective diffusion coefficient in the rock matrix (D_{em}) is considered to be similarly correlated to the porosity of the rock matrix as in the base case (ρ = 0.5). The observed changes in the simulated mass transfer coefficients are significant only for the mass transfer coefficient from the buffer to tunnel for anions (λ_{bt}) although also other transfer coefficients are slightly affected. With the correlations set, the distribution for the mass transfer coefficient in the tunnel for anions is log-uniformly distributed around the GM value (same as in the base case) and not roughly log-normal as in the base case.

When the nuclide-specific parameters in the geosphere are considered independent (in base case the biosphere parameters are independent) the anionic/cationic nuclide groups are not taken into account. The simulated results for the distributions of the mass transfer coefficients are not significantly affected when the nuclides are independent. Only the mass transfer coefficient for the geosphere barrier (λ_f) has reduced GSD values by about 5-7.

The resulting GM, GSD and 95th percentile values are in both calculations slightly increased. The results in the correlated case change more compared to the base case and they are presented.

Case 4

The case is calculated in two parts. Due to experimental evidence, the porosity of the rock matrix (ϵ_m) and the effective diffusion coefficient in the rock matrix (D_{em}) are correlated with uncertain correlation coefficient. The full correlation results in slightly increased GSD values for the mass transfer coefficients and delay times of the geosphere barrier (λ_f) compared to base case. Due to minor effect, the final results are not largely affected.

To obtain a cautious estimate with most possible geosphere related nuclide-specific parameter correlations, the case is also partly combined with case number 9 (part two). In case 9, also distribution coefficients are correlated for different nuclide groups. With the full correlations for the geosphere related parameters (base case and D_{em}, ϵ_m, Kd_{pb}, Kd_{pt}, Kd_{pm}), the results reveal increase slight increases for GM, GSD and 95th percentile. However, the increases are not significant compared to the case with independent parameters (case 3 second calculation). Therefore, the nuclide groups within geosphere related parameters do not significantly increase the results.

Case 5

Based on the suggestion by SKB (SKB, 2010), the IRF values in the fuel matrix for anionic nuclides (Cl-36, Se-79 and I-129) are fully correlated. The IRF values only affect the resulting release rates or dose rates as they are only taken into account in the source terms of the calculation.

Case 6

In this case, the average water depth (d_w) and discharge ($WfluxOut$) are considered to be (hypothetically) fully correlated as opposed to base case where they are independent. The effects should be able to be observed in the mass transfer coefficient for the lake water ($\lambda_{discharge}$). With the correlation, any significant changes in the resulting mass transfer coefficient distribution are not seen. The log-uniform distribution for the mass transfer coefficient is dominated by the log-uniform discharge rate.

Case 7

In this case, the bulk densities (ρ_i) in the lake sediment layers (intermediate and top) are considered to be fully correlated as they have correlation of 0.5 in the base case. If the densities are set independent, physically impossible realizations may occur as the top sediment may receive a larger bulk density than the intermediate sediment. With simulations any large effects on the mass transfer coefficient distributions of the sediment layers are not observed (λ_{IMS}, λ_{TS}).

Case 8

In this calculation case, the distribution coefficients are considered to be fully correlated for two nuclide groups in the transport chain compartments where sorption may occur (buffer, backfill, rock matrix and biosphere soil layers) (Kd_{pb}, Kd_{pt}, Kd_{pm}, Kd_i). All the compartments in the chain are considered to be independent between themselves. As the distribution coefficients are used in different expressions of the mass transfer coefficients, the correlations do not have an effect on the resulting transfer coefficient distributions. On the other hand, the correlations make the coefficients partly correlated.

Case 9

The concentration ratios to various foodstuff, which are grown on terrestrial biosphere compartments (croplands, pasture land), can be considered to be negatively correlated to the distribution coefficients in the relevant soil layers. In the base case, the foodstuff except fish have a small contribution when considering the total dose rates (< 30 % of the total dose rate).

The calculation case is divided in two parts. In the first part, the distribution coefficients in the biosphere are independent but negative correlation coefficients are applied for each concentration factor and corresponding distribution coefficient. In the second, case the assumptions of the calculation case 8 are applied also. Then, also the nuclide groups (cations/neutrals and anions) are taken into account by group correlated distribution

factors (part two). The negative correlations to distribution coefficients are set for the concentration ratios of cereals, field vegetables, potatoes, pasture and forest berries. Because in the base case, the correlation ratios do not contribute in the most significant dose paths, the drinking water and fish ingestion amounts are set to zero to obtain a total dose rate based on remaining dose paths (modified base case).

The differences between independent distribution coefficients and correlated ones are not large. Therefore, the nuclide groups seem to have little effect on the final results and the more realistic, correlated case results are presented. The negatively correlated concentration factors decrease the resulting GM, GSD and 95th percentile for the total dose rate compared to the modified base case.

The calculated cases with their shortened descriptions and summarized results are presented in Table 44. The base case is simulated again and compared to the previous Section. Slight changes are observed for GM, GSD and 95th percentile due to random variation for the base case. For other cases, the relative changes compared to the base/modified base case of the 95th percentiles, GM and GSD values at 10 000 years can be seen. In the modified base case, the drinking water intake and fish ingestion are set to zero. The shape of the total dose rate remained approximately log-normal in all cases with 1000 realizations (see previous Section, Figure 20).

Table 44. *The variant calculation cases of the study with shortened description and results. All the results are determined based on simulated data at 10 000 years using 1000 realizations. The relative differences of the cases compared to the base or modified base case are provided. GM denotes geometric mean, GSD geometric standard deviation and ρ the correlation coefficient. The results are in dimensions mSv/a (GSD dimensionless).*

Case	Description	Results
Base	See Sections 4.2.1-4.2.5	95th percentile 1.0E-4* GM 1.4E-6* GSD 13*
1	$\rho = 1$ between D_w and V_c	95th percentile 6.8E-5 (-34 %) GM 1.5E-6 (+7.4 %) GSD 11 (-17 %)
2	i) $\rho = -1$ between $2b_v$ and WL/Q ii) $\rho = -1$ between $2b_{vt}$ and WL/Q	ii) 95th percentile 1.5E-4 (+47 %) GM 1.2E-6 (-16 %) GSD 17 (+32 %)
3	i) $\rho = 1$ between D_{eb}, ϵ_b, ϵ_t and between nuclides of same group (cation/neutral, anion) and $\rho = 1$ for ϵ_m between nuclides of the same group ($\rho = 0.5$ between ϵ_m and D_{em}) ii) Independent D_{eb}, ϵ_b, ϵ_t, D_{em}	i) 95th percentile 1.6E-4 (+60 %) GM 1.5E-6 (+7.1 %) GSD 15 (+13 %)
4	i) $\rho = 1$ between ϵ_m and D_{em} ii) i) and (partial) a combination with case 9. $\rho = 1$ for Kd_{pb}, Kd_{pt}, Kd_{pm} between nuclides of the same group (cation/neutral, anion)	ii) 95th percentile 1.2E-4 (+14 %) GM 1.3E-6 (+7.4 %) GSD 19 (+46 %)
5	$\rho = 1$ between IRF values for Cl-36, Se-79, I-129 in fuel matrix	95th percentile 1.3E-4 (+24 %) GM 1.4E-6 (-1.7 %) GSD 15 (+14 %)
6	$\rho = 1$ between d_w and $WfluxOut$	95th percentile 1.4E-4 (+37 %) GM 1.4E-6 (-0.80 %) GSD 16 (+21 %)
7	$\rho = 1$ between ρ_{IMS} and ρ_{TS}	95th percentile 1.6E-4 (+52 %) GM 1.5E-6 (+3.0 %) GSD 15 (+17 %)
8	$\rho = 1$ for Kd_{pb}, Kd_{pt}, Kd_{pm}, Kd_i between nuclides of the same group (cation/neutral, anion), biosphere objects independent	95th percentile 1.0E-4 (-1.7 %) GM 1.5E-6 (+1.1 %) GSD 14 (+3.8 %)
Modified base	The drinking water intake and fish ingestion zero	95th percentile 4.3E-5 GM 5.1E-7 GSD 14
9	i) $\rho = -1$ between Kd_i and CR_i, drinking water intake and fish ingestion zero ii) Case 8 and $\rho = -1$ between Kd_i and CR_i, drinking water intake and fish ingestion zero	ii) 95th percentile 2.1E-5 (-51 %) GM 3.6E-7 (-29 %) GSD 13 (-5.1 %)

*In Figure 20, the GM is 1.5E-6 mSv/a, GSD 15 and 95th percentile 1.1E-4 mSv/a.

Based on the presented calculation cases, it can be concluded that the base case contains much of the uncertainty and variance in the final results in the simplified model. Any added correlations between the input parameters do not significantly change the GM or GSD values of the final results. The cautious confidence levels (95^{th} percentiles) of the total dose rate change by about 60 % at most which is not a large difference compared to the range of the resulting distributions. Without the drinking water ingestion or fish ingestion, the results decrease about 60 % (95^{th} percentile) which tells that the total dose rate distribution spans over large interval due to uncertainty in the geosphere parameters. Typically, the correlations affect the resulting GSD values more than the GM values, which is expected.

5.5 Effects of varying parameter distributions

The distribution selections for the parameters of the simplified model are presented in Sections 4.2.1-4.2.5. Although many parameters are not log-normally distributed, the time constants receive log-normal distributions for many compartments of the model. In this study, the focus is on the parameter distributions that affect most the total dose rates obtained with the base calculation case.

At first, the parameters, which are related to the mass transfer coefficients with the largest uncertainty in the base case, are examined. The mass transfer coefficients and delay times with the largest uncertainty (approximated GSD values in Section 5.1) may affect much the dose rate distributions as they govern the transport and the resulting distributions of release rates to biosphere. On the other hand, the dose assessment in the biosphere analysis has uncertainty in the drinking water intake and concentration ratios in the base case, meaning that the total dose rate interval of several orders of magnitude is partly result of the dose assessment also.

The mass transfer coefficients with the largest uncertainty are the coefficients from the buffer to fracture (λ_{bf}), from the tunnel backfill to fracture (λ_{tf}) and from the fracture to the biosphere (λ_f) (see Section 5.1.1). On the other hand, the mass transfer coefficient from the canister to the buffer (λ_{cb}) is significant for the final result and therefore, that is also shortly considered in the analysis.

The solute half-time corresponding to mass transfer coefficient for the geosphere barrier (λ_f) and the related delay time ($t_{d,f}$) are not the most significant time constants in the simplified model as observed in Section 5.3. Therefore, a short analysis is conducted as the changes in the uncertainty of the time constants are not likely to affect the final result.

The mass transfer coefficient from the fracture to the biosphere (λ_f) is largely affected by the log-normal distribution of hydrodynamic control of retention (WL/Q). By setting the value of WL/Q constant, the log-normal shapes for the distributions of the mass transfer coefficient are not applicable as only log-uniform parameters exist in the expression. The resulting distribution resembles a log-uniform distribution with rounded edges for most nuclides (not quite log-normal). The GSD values with constant WL/Q vary from about 9 to 20, whereas in the base case the values are in the range of 17-31. The GSD consist now of uncertainty that is nuclide-specifically related to the diffusion

coefficient in the rock matrix (D_{em}), the porosity of the rock matrix (ϵ_m) and distribution coefficient in the rock matrix (Kd_{pm}). The delay time of the geosphere barrier is also dependent on the value of WL/Q and therefore, the GSD values decrease similarly to the range of about 9-20 with constant WL/Q. Like mentioned above, the reductions of the GSD is not likely to have a significant effect on the resulting dose rates or release rates.

Mass transfer coefficients related to fractures in the simplified model

The mass transfer coefficient from the buffer to fracture is examined first (λ_{bf}). The log-normal behavior for the mass transfer coefficient is observed in Section 5.1.1. The log-normal parameters for the mass transfer coefficient are the fracture aperture ($2b_v$) and groundwater velocity in the fracture intersecting the deposition hole (v_{dh}). The GSD values in the base case are about 17-19 for different nuclides (due to correlation of $2b_v$ and v_{dh} and variation of sorption). By setting the v_{dh} as constant with the geometric mean value of the distribution, the simulated GSD values reduced to about 5.5-6.4. The similar simulations are conducted with setting the fracture aperture constant with the geometric mean value. The reduction of the GSD values is again significant as the GSD values are now about 4.

With the mass transfer coefficient from the tunnel to fracture (λ_{tf}), the GSD values decrease also significantly when either the groundwater velocity in the fracture intersecting the deposition tunnel (v_t) or fracture aperture ($2b_{vt}$) is set constant with the geometric mean value. The GSD values in the base case are about 15-17 with different nuclides but the decreased values for GSDs are about 4-6 depending on which of the two parameters are set constant.

When the fracture apertures and groundwater velocities are set independent the GSD values for both mass transfer coefficient distributions are around 7-9. Therefore, the assumed correlation in the base case increases most significantly uncertainty related to the mass transfer coefficients from buffer to fracture and from tunnel to fracture.

Total dose rates with parameter modifications

The changes in the total dose rates of the base case are examined by conducting a simulation with a modified base case. To observe the effects of reduced GSD values for the most uncertain mass transfer coefficients, the examined modifications are applied simultaneously as follows:

- WL/Q value is set constant to the geometric mean value (3.76E+4 a/m)
- Fracture apertures and groundwater velocities in the fractures are set independent.
- Drinking water intake is set to 0.6 m^3/a.

The time development of the resulting confidence levels of the total dose rate is similar as in the base case and the distribution does not change significantly after a few thousand years of the calculation. The modified base case total dose rate distribution at 10 000 years is shown in Figure 23 together with the base case results. The changes

have little effect on the final distribution. Compared to the base case, a slight reduction is observed for GSD (13.1 → 12.4), which results in an about 20 % lower 95th percentile (1.0E-4 mSv/a → 8.1E-5 mSv/a).

In order to reduce the variance of the final result, other significant parameters are examined. One at a time, specific parameters are set constant to the reference case values in addition to the modified base case assumptions. The diffusion coefficient in pore water (D_w) is set constant to 1E-9 m^2/s , the radius of the initial defect (r_h) is set to 0.0015 m, the pore volume of the canister (V_c) is set to 0.9 m^3 and the IRF values for C-14, I-129 and Cl-36 are set to reference case values. The total dose rate distributions at 10 000 years are presented in Figure 23 by using 1000 realizations.

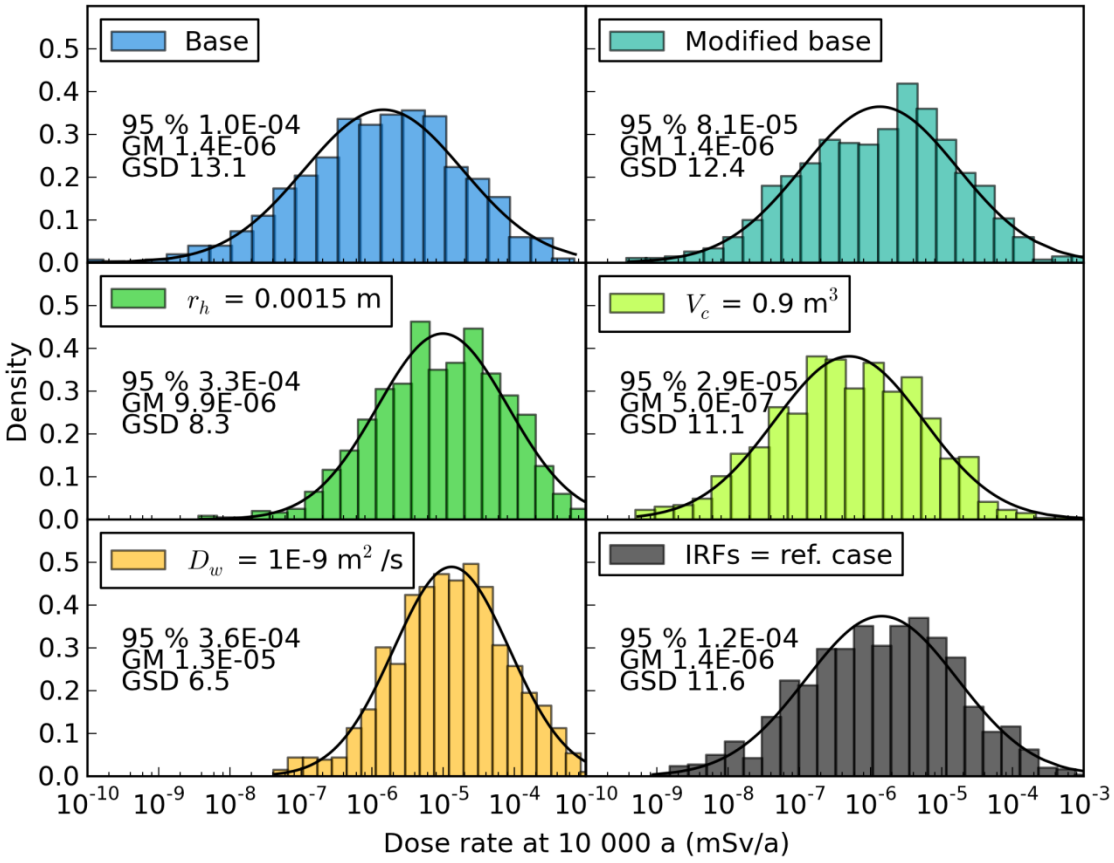

Figure 23. *The simulated distributions for the total dose rate in the base case, in a modified base case and in cases with further parameter modifications. In the modified base case, the groundwater velocities in the fractures (v_{dh}, v_t) and fracture apertures ($2b_v, 2b_{vt}$) are assumed to be independent, hydrodynamic control of retention (WL/Q) has a constant value of 3.76E+4 a/m and drinking water intake is 0.6 m^3/a. The further calculation cases have depicted parameter changes in addition to the modified base case. IRFs only consider the most contributing C-14, Cl-36 and I-129.*

The effects of varying the distributions reveal that although the variances of the most uncertain mass transfer coefficients in the base case are reduced significantly, the total dose rates at different confidence levels still spread over a large interval in the modified base case. Also, IRF values do not significantly affect the distribution of the final result.

The most significant changes to the total dose distribution at 10 000 years are obtained with the radius of the initial defect and diffusion coefficient in the pore water. Although the GM values and GSD values change significantly compared to the modified base case, the 95th percentiles do not change that much. Compared to the original base case, there is about 35 % increase in the 95th percentile which tells that the cautious results remain rather unchanged with varying the most crucial parameter distributions.

6 DISCUSSION AND CONCLUSIONS

The simplified model has been developed for analyzing the entire nuclide transport chain from the spent nuclear fuel through the engineered barrier system and further into the biosphere and to exposed human beings. The model is used to estimate release rates from the geosphere and dose rates in the base case, where the activity is released through a postulated initial defect in the canister. The effects of parameter selections are furthermore investigated in the variant calculation cases. Based on the obtained results, the model transparency and performance is helpful in obtaining cautious results from nuclide transport and dose assessment.

The radionuclide transport model in the geosphere is based on a simplified solute transport model (Poteri et al., 2012). In this study, the model has been extended with a biosphere model and a probabilistic simulation. The biosphere model is modified from a model used for screening evaluation in the biosphere assessment (Screening Model Tier 2 in BSA-2012) of TURVA 2012 safety case portfolio (Posiva, 2014b). However, the overly cautious screening model has been modified in order to obtain a more reasonable model of the biosphere.

The default selection of parameter distributions (or values) has been determined for a base case. The biosphere evolution in time and uncertainty related to release location may be taken into account to some extent with distributed parameters related to the properties of the biosphere objects (soil/sediment layer properties, object sizes). For the geosphere transport, the uncertainty related to the parameters has been adapted to a great extent from the probabilistic sensitivity analysis conducted in (Cormenzana, 2013a) by excluding the unlikely parameter values. For the biosphere, a data basis by Posiva (Posiva, 2014a) has been mainly used but also processed data from UNTAMO tool (by Posiva) has been applied.

The distributions of mass transfer coefficients and delay times have been simulated first to obtain characteristics of the resulting time constants in the system. The smallest mass transfer coefficients correspond to the longest solute half-times in the compartments and therefore, they characterize compartment's ability to retard the nuclide release in the transport chain. With the base case assumptions about the correlations and distribution selections for the parameters, the mass transfer coefficients are usually approximated to be log-normally or log-uniformly distributed. The log-normal distributions are expected because products of various distributions and also log-normal parameters are used in calculating the mass transfer coefficients. With no log-normal parameters involved in the calculation, the results often still resembles a distribution that is roughly log-normal (for example a ratio of log-uniform parameters).

A large uncertainty in a model parameter turns into a large geometric standard deviation (GSD) of the simulated geosphere mass transfer coefficients. At largest, the mass transfer coefficients from buffer to fracture, from tunnel to fracture and through geosphere to biosphere have received GSD values of around 20-30. The ranges for the mass transfer coefficients span over about seven orders of magnitude at largest. The largest uncertainties of the most significant parameters (excluding geosphere barrier) are

partly explained with correlated fracture apertures and groundwater velocities as the GSD values reduced to about 7-9 by setting the parameters independent. The independent and fully correlated cases are the cautious ones for the two parameters as they appear in the nominator of the same expression. In reality, the parameters may even be negatively correlated but the final dose rates or release rates would decrease. For the less significant geosphere barrier, the hydrodynamic control of retention ($WL/\ Q$) dominates the resulting uncertainty.

With any distributions used in the calculation, the simulated mass transfer coefficients appear to approach typically log-normal or normal behavior depending on the range of used parameters. With a narrow interval, the difference of the two distributions is negligible. Typically, the parameters, which receive values differing much from unity, dominates the resulting distribution of an expression. The log-normal behavior of parameters is not self-explanatory but it must be noted that many parameters are a sum or a product of smaller processes or phenomena that in nature often approach log-normal or normal behavior (Limpert et al., 2001).

In the biosphere, the mass transfer coefficients have been estimated based on formulations taken from (Posiva, 2014b) and there are no delay times in biosphere compartments. The transfer coefficients have been generally observed to be higher compared to geosphere barriers. Again, the log-normal (or normal) distributions are good approximations for most of the mass transfer coefficients but also log-uniform distribution have been observed (for lake discharge coefficient). The uncertainty of mass transfer coefficients in the biosphere is significantly lower than in the geosphere barriers. The GSD values ranged from 1 to 8 for all compartments. Sources of uncertainty are mostly related to the distribution coefficients but on the other hand, the magnitude of the mass transfer coefficient is governed by the estimated water fluxes and densities of the sediments or soil layers.

The solute half-times can be compared to radioactive half-lives of the nuclides. If the solute half-time is much larger than the half-life of the nuclide, the nuclide is retained efficiently in the compartment and the attenuation of the release rate is efficient. The half-times of solute in the biosphere compartments are not significant for most nuclides in the biosphere. This means that the solute transport in biosphere occurs fast with the used assumptions and radionuclide releases are in most cases governed by the retention of the nuclides in the engineered barriers. The relative importance between the geosphere barriers varies between the nuclides and the realizations in the probabilistic simulation. For sorbing nuclides (Mo-93, Nb-94), the buffer and tunnel backfill are the most dominating barriers and for non-sorbing nuclides (C-14, Cl-36, Se-79, Ag-108m, I-129), the canister limits the release rate typically in most of the realizations. The most significant compartment attenuating the radionuclide releases in the biosphere is the intermediate sediment layer of the lake in the simplified model.

Due to probabilistic simulation used in the model, the relative importance of the release barriers in the transport chain vary between the realizations. Due to wide distributions of mass transfer coefficients, the smallest mass transfer coefficients in the biosphere may in some cases be smaller than the largest ones in the geosphere barriers, which can be viewed as an unrealistic combination if a correlation can be justified for the mass

transfer coefficients in reality (see overlapping of distributions in Figure 13). However, the most important release barriers are typically canister and buffer and therefore, the "unrealistic" combinations for the less important barriers do not affect the final results significantly. Also, by conducting large number of realizations these "unrealistic" combinations only form a minor part in the total results.

The delay times in the simplified model have been observed to be also approximately log-normally distributed when more than one distributed parameter is involved. The sums of delay times translate the release rate in time and only histograms for the resulting distributions are provided (see Figure 15). For Nb-94, the base case results for the delay times in the barriers are significantly higher than the 10 millennia time scope used for the dose assessment. For other nuclides, the approximated geometric mean values are not significant regarding dose assessment. Large uncertainties are only related to the delay time in the geosphere barrier that had GSD values of around 20 (31 for Mo-93) due to distribution of WL/Q (GSD reduction to 9-20 with constant WL/Q). When the resulting distributions for the delay times are taken into account, the significant releases for Mo-93 and especially Nb-94 can be concluded to be unlikely.

The resulting release rates to biosphere in a reference calculation case have been observed to be similar for most nuclides compared to BSA-2012 reference case (RC) results by Posiva. For Mo-93 an underestimation of one order of magnitude is observed and that indicates overestimated sorption or underestimated solubility limit in the simplified model. Overall, the simplified geosphere model performs well considering the simplifications made as the shapes of the release rates are similar to the ones obtained in BSA-2012 RC. The simulated distributions of the release rates are approximately log-normal for most contributing nuclides during the largest part of the time scope with the base case assumptions about the parameter distributions and correlations (due to mostly log-normal time constants). The resulting GSD values are in the range of about 14-20 for the nuclides with the largest release rates (C-14, Cl-36, I-129). The reference case results are cautious compared to the simulated distributions (higher than the mean value) but clearly lower than the release rate at the highest confidence levels (e. g. 95^{th} percentile).

In the base case of this study, the geosphere releases discharged into a well and a lake. The resulting dose rates have revealed that the simplified model gives a rather cautious estimate of the total dose rate. Although the parameter values have been chosen similarly in the reference case, the BSA-2012 RC results by Posiva are about two orders of magnitude lower than the reference case results with the simplified model. The total dose rate is dominated by I-129, C-14 and Cl-36 and from dose paths, especially drinking water from well and fish ingestion are the most contributing. Also, the simulated results with likely, realistically chosen parameter distributions in the base case result in rather cautious total dose rates at different confidence levels. The overestimation of the dose rates is partly related to the different well capacity and dose assessment conducted for a single individual (not a group). Also, the simplified transport chain and mass transfer in the biosphere is likely to result in higher activity concentrations in the biosphere compartments than in the BSA-2012 RC. The shape of the resulting total dose distributions at 10 000 years in the base case are similar as the release rates (log-normal), which is expected. The GSD values for C-14 and I-129

increased by about 2 compared to the release rate distributions due to distributed drinking water intake. The increase is less (about 1) for Cl-36 because of smaller drinking water contribution in the total dose rate.

The reference case total dose rate is less than one order of magnitude lower than the total dose rate at 95 % confidence level obtained in the base case. The reference parameters in the biosphere represent mostly the geometric mean values for the parameters and the total dose rate at 95 % confidence level of the base case is most likely to represent realizations with cautious parameter values both in the geosphere and biosphere. Thus, the cautious biosphere parameter realizations are likely to contribute to a part of the described difference. The total dose rate at 50 % confidence level with about geometric mean parameter realizations is about one order of magnitude lower than the reference case. Thus, there is less increase with the cautious biosphere parameters than with cautious geosphere parameters and it can be concluded that the uncertainty in the simplified biosphere model has a smaller role in the final results than uncertainty in the geosphere model.

The total dose rate at 50 % confidence level in the base case is slightly higher than total dose rate in the deterministic calculation case with (geometric) mean values (CDF = 0.5). The difference is related to correlations between the parameters. The effect of a correlation between the parameters changes the resulting uncertainty of the mass transfer coefficients and delay times and the final result. If the parameters are multiplied or summed in the modelling process, the uncertainty of the final result typically increases with a positive correlation. If they are subtracted or divided by one another, the uncertainty may decrease or stay the same as without the assumed positive correlation. The effect in both cases depends on the numerical values and ranges of the parameters involved (effects vice versa with a negative correlation). However, if the uncertainty is related to a less significant transport barrier (such as geosphere), the amount uncertainty does not considerably affect the final results.

The variant calculation cases with varying correlations between the parameters reveal that the base case results in the simplified model remain rather unchanged although different distributions for the mass transfer coefficients are obtained compared to the base case. At most, the 95^{th} percentile of the total dose rate is increased by about 60 % of which some portion may be accounted for random variety. The reduction is similarly around 50 % at most based on comparison between the base case and the simulated 95^{th} percentiles of the total dose rate at 10 000 years. The correlations, which affect the final results of the calculation most, are related to the geosphere parameters. No significant reduction has been observed in the total dose rates at the highest confidence levels when the drinking water and fish ingestion are excluded from the dose paths (about -60 %), meaning that the cautious values of concentration factors (and distribution factors) largely contribute at the higher confidence levels. On the other hand, fish ingestion and drinking water are significant when examining the dose rates at other (lower) confidence levels (i.e. reduction is larger). Based on this, the uncertainty and log-normal shape of the final result (i.e. release rates or dose rates) is largely related to geosphere parameters (and the resulting smallest mass transfer coefficients):

The distribution of the final results spans over several orders of magnitude in this study. For example, the difference between the total dose rate at 50 % and 95 % confidence levels in the base case have been observed to be about two orders of magnitude. With reduced variance for the most uncertain mass transfer coefficients in a modified base case, the distribution has been observed to be about the same. Therefore, the difference is related to the parameters required for mass transfer coefficient from the canister to buffer. Reducing the uncertainty related to the parameters in the geosphere in general is a way to reduce the uncertainty of the final result. To conclude, parameters with the largest uncertainty have little effect on uncertainty of the final result and the most important uncertainties are especially related to the dominating mass transfer coefficients (such as diffusion coefficient in pore water).

The parameters that are used for the mass transfer coefficient of the canister are largely affecting the final result. These parameters are for example diffusion coefficients in bentonite and pore water. The fracture related parameters, namely fracture apertures ($2b_v, 2b_{vt}$) and groundwater velocities (v_{dh}, v_t) in the fractures, also affect the resulting uncertainty. For sorbing nuclides, the distribution coefficients in the buffer and tunnel backfill also significantly affect the release rates. The parameters, which govern how the inventory is divided to gradually leaching part and instantly released inventory, are the distributions for the instant release fractions (IRFs). They are also a (minor) source of uncertainty in the simplified model for nuclides that are not solubility limited (i.e. the most contributing C-14, Cl-36, I-129).

The solubility limits chosen in this study reflect the most likely conditions in the repository during most of the time in the future and therefore, saline or brackish water types are used also in determining other parameter values in the geosphere. The uncertainty related to the groundwater composition inside the canister can be considered be a major source of uncertainty in the simplified model depending on the nuclide in consideration. However, the significance of solubility limits is not large as the most contributing nuclides (C-14, I-129, Cl-36) to the total dose are not affected by the solubility limits (and groundwater composition) and other nuclides still have solubility limited release rates.

The simplified model allows usage of various kinds of source functions (with other than constant degradation times) to be considered and implemented with small effort. The biosphere scenario can be also changed given the presented biosphere objects of this study. The model can be extended to cover also other nuclides and other types of repositories if the release barriers may be similarly described as well-mixed compartments by using an equivalent flow rate and a pore volume.

For the future research, it may be concluded that the simplified model is a simple analysis tool compared to more accurate models used by for example Posiva Oy. Because the mathematical model behind the tool is based on a linear, homogenous differential equation system with constant coefficients, a detailed time dependence of the compartments cannot be taken into account. Therefore, more extensive numerical models are still needed for more accurate, time-dependent calculations. However, the simplified model is suitable for situations when the time evolution of the mass transfer

coefficients is negligible and simulated results with different parameter distributions are preferred.

7 SUMMARY

This study is related to the safety analyses of the KBS-3V disposal concept that is planned to be used for the disposal of spent nuclear fuel in Olkiluoto. The model used in the study provides a complementary and parallel analysis tool for analyzing the radiological consequences for humans arising from spent fuel disposal in Olkiluoto. The radionuclide transport modelling is based on Posiva's reference scenario, where an initial canister defect is assumed. In this study, a simplified model of solute transport in geosphere (Poteri et al., 2012) has been extended by developing a simplified biosphere model using the similar principles as in the geosphere modelling. A probabilistic simulation has been used to take into account the uncertainty related to physical quantities used in the model. By simulating the whole transport chain from the repository to the exposed human beings, the most significant release barriers and parameters in the transport modelling have been determined.

The transport of the solute can be described in the simplified model by mass transfer coefficients (or solute decay constants) and delay times. These constants have been simulated at first for the nuclides considered in the study (C-14, Cl-36, Se-79, Mo-93, Nb-94, Ag-108m, I-129). Based on the resulting distribution of the constants (typically log-normal), the releases of the sorbing cations are retained significantly in the buffer and tunnel backfill (geometric mean of solute half-time $\gg$ 1 Ma). For other nuclides, the canister is the most significant barrier in the repository system (geometric mean of solute half-time $\approx$ 3-4 Ma). When compared to nuclide half-lives, in most cases, Mo-93 and Nb-94 have efficiently limited release rates to biosphere due to shorter physical half-lives.

Based on comparison to the results obtained by Posiva with similar parameters, the simplified model overestimates the resulting dose rates by about two orders of magnitude due to different dose assessment (different well capacity and most exposed individual rather than a group). The release rates from geosphere do not differ much from the ones obtained by Posiva for most nuclides but an underestimation of one order of magnitude is observed for Mo-93. The total dose rate is dominated by I-129, C-14 and Cl-36 and from the dose paths, especially drinking water from well and fish ingestion are the most contributing. By changing the parameter correlations (even hypothetical correlations), the observed effects are of minor importance compared to the uncertainty resulting from distributions of the input data. With changing the most uncertain parameter distributions, no significant changes in the distribution of the total dose rate has been observed. The most important parameters affecting the observed log-normal shape and uncertainty of the resulting dose rates or release rates are the diffusion coefficients in bentonite and in pore water and radius of the initial defect and also bedrock fracture apertures and groundwater velocities (all related to canister or buffer).

The methodology of the model can be used also for similar kinds of disposal systems in a transparent and effortless way. The concept of equivalent flow rate and pore volume in determining the mass transfer coefficient is straightforward to extend. With different repositories, any barriers with similar transfer processes may be represented in a similar fashion and comparable calculations may be performed.

REFERENCES

Arfken, G. B., Weber, H. J. & Harris, F. E. 1985. Mathematical Methods for Physicists, 3rd edition. Academic Press Inc., San Diego, California, USA. 985 p. ISBN 978-012-059-820-5.

Avila, R. & Pröhl, G. 2008. Models Used in the SFR1 SAR-08 and KBS-3H Safety Assessments for Calculation of C-14 Doses. Posiva Oy, Eurajoki, Finland. Posiva Working Report 2007-107. 33 p.

Avila, R., Ekström, P.-A. & Åstrand, P.-G. 2010. Landscape dose conversion factors used in the safety assessment SR-site. Swedish Nuclear Fuel and Waste Management Co. (SKB), Stockholm, Sweden. Technical Report TR-10-06. 169 p. ISSN 1404-0344.

Bateman, H. 1910. Solution of a system of differential equations occuring in the theory of radio-active transformations. Proceedings of the Cambridge Philosophical Society, Mathematical and Physical Sciences, v. 15. p.423-427.

Benjamin, J. R. & Cornell, C. A. 1970. Probability, Statistics, and Decision for Civil Engineers. McGraw-Hill Inc., New York, USA. 640 p. ISBN 978-007-004-549-1.

Chen, H. 2001. Initialization for NORTA: Generation of Random Vectors with Specified Marginals and Correlations. INFORMS Journal on Computing, Vol. 13, No. 4. p. 312-331. ISSN 1526-5528.

Cormenzana, J. L. 2013a. Probabilistic Sensitivity Analysis for the "Initial Defect in the Canister" Reference Model. Posiva Oy, Eurajoki, Finland. Posiva Working Report 2013-25. 532 p.

Cormenzana, J. L. 2013b. Selection of Probability Density Functions (Pdfs) for the PSA of the "Initial Defect in the Canister" Reference Model. Posiva Oy, Eurajoki, Finland. Posiva Working Report 2013-61. 84 p.

Curtiss, J. H. 1941. On the distribution of the quotient of two chance variables. The Annals of Mathematical Statistics Vol. 12 No. 4. p. 409-421.

Forbes, C., Evans, M., Hastings, N. & Peacock, B. 2011. Statistical distributions 4th edition. John Wiley & Sons Inc., Hoboken, New Jersey, USA. 212 p. ISBN 978-0-470-39063-4.

Hamming, R. W. 1970. On the Distribution of Numbers. The Bell System Technical Journal, Vol. 49, No. 8. p. 1609-1625.

Keto, P., Mamunul Hassan, M., Karttunen, P., Kiviranta, L., Kumpulainen, S., Korkiala-Tanttu, L., Koskinen, V., Jalonen, T., Koho, P. & Sievänen, U. 2013. Backfill Production Line 2012 - Design Production and Initial State of the Deposition Tunnel Backfill and Plug. Posiva Oy, Eurajoki, Finland. Report Posiva 2012-18. 164 p. ISBN 978-951-652-199-5.

Leemis, L. & Mcqueston, J. 2008. Univariate Distribution Relationships. The American Statistician, Vol. 62, No. 1. p. 45-53.

Limpert, E., Stahel, W. A. & Abbt, M. 2001. Log-normal Distributions across the Sciences: Keys and Clues. Bioscience Vol. 51, No. 5. p. 341-352.

Massey, J. F. 1951. The Kolmogorow-Smirnov Test for Goodness of Fit. Journal of the American Statistical Association, Vol. 46, No. 253. p. 68-78.

Nordén, S., Avila, R., de la Cruz, I., Stenberg, K. & Grolander, S. 2010. Element-specific and constant parameters used for dose calculations in SR-site. Swedish Nuclear Fuel and Waste Management Co. (SKB), Stockholm, Sweden. Technical Report TR-10-07. 123 p. ISSN 1404-0344.

Nummi, O., Kyllönen, J. & Eurajoki, T. 2012. Long-Term Safety of the Maintenance and Decommissioning Waste of the Encapsulation Plant. Posiva Oy, Eurajoki, Finland. Report Posiva 2012-37. 218 p. ISBN 978-951-652-224-4.

Nykyri, M., Nordman, H., Marcos, N., Löfman, J., Poteri, A. & Hautojärvi, A. 2008. Radionuclide Release and Transport - RNT-2008. Posiva Oy, Eurajoki, Finland. Report Posiva 2008-06. 164 p. ISBN 978-951-652-166-3.

Posiva. 2012a. Safety Case for the Disposal of Spent Nuclear Fuel at Olkiluoto - Synthesis 2012. Posiva Oy, Eurajoki, Finland. Report Posiva 2012-12. 277 p. ISBN 978-951-652-193-3.

Posiva. 2012b. Safety Case for the Disposal of Spent Nuclear Fuel at Olkiluoto - Assessment of Radionuclide Release Scenarios for the Repository System 2012. Posiva Oy, Eurajoki, Finland. Report Posiva 2012-09. 435 p. ISBN 978-951-652-190-2.

Posiva. 2012c. Olkiluoto Site Description 2011. Posiva Oy, Eurajoki, Finland. Report Posiva 2011-02. 1028 p. ISBN 978-951-652-179-7.

Posiva. 2013a. Safety Case for the Disposal of Spent Nuclear Fuel at Olkiluoto - Terrain and Ecosystems Development Modelling in the Biosphere Assessment BSA-2012. Posiva Oy, Eurajoki, Finland. Report Posiva 2012-29. 380 p. ISBN 978-951-652-210-7.

Posiva. 2013b. Safety Case for the Disposal of Spent Nuclear Fuel at Olkiluoto - Surface and Near-Surface Hydrological Modelling in the Biosphere Assessment BSA-2012. Posiva Oy, Eurajoki, Finland. Report Posiva 2012-30. 157 p. ISBN 978-951-652-211-4.

Posiva. 2013c. Safety Case for the Disposal of Spent Nuclear Fuel at Olkiluoto - Formulation of Radionuclide Release Scenarios 2012. Posiva Oy, Eurajoki, Finland. Report Posiva 2012-08. 135 p. ISBN 978-951-652-189-6.

Posiva. 2014a. Safety Case for the Disposal of Spent Nuclear Fuel at Olkiluoto - Data Basis for the Biosphere Assessment BSA-2012. Posiva Oy, Eurajoki, Finland. Report Posiva 2012-28. 1446 p. ISBN 978-951-652-209-1.

Posiva. 2014b. Safety Case for the Disposal of Spent Nuclear Fuel at Olkiluoto - Radionuclide transport and dose assessment for humans in the biosphere assessment BSA-2012. Posiva Oy, Eurajoki, Finland. Report Posiva 2012-31. 268 p. ISBN 978-951-652-212-1.

Posiva. 2014c. Safety Case for the Disposal of Spent Nuclear Fuel at Olkiluoto - Dose Assessment for the Plants and Animals in the Biosphere Assessment BSA-2012. Posiva Oy, Eurajoki, Finland. Report Posiva 2012-32. 380 p. ISBN 978-951-652-213-8.

Posiva Oy. 2014a. Safety Case for the Disposal of Spent Nuclear Fuel at Olkiluoto - Data Basis for the Biosphere Assessment BSA-2012. Posiva Oy, Olkiluoto, Finland. Report Posiva 2012-28.

Poteri, A. 2013. Simplifying solute transport modelling of the geological multi-barrier disposal system. VTT Technical Research Centre of Finland, Espoo, Finland. VTT Science 42. 141 p. ISBN 978-951-38-8097-2.

Poteri, A., Nordman, H., Pulkkanen, V.-M., Hautojärvi, A. & Kekäläinen, P. 2012. Representing Solute Transport Through the Multi-Barrier Disposal System by Simplified Concepts. Posiva Oy, Eurajoki, Finland. Report Posiva 2012-20. 92p. ISBN 978-951-652-201-5.

SKB. 2010. Data report for the safety assessment SR-site. Swedish Nuclear and Fuel and Waste Management Co. (SKB), Stockholm, Sweden. Technical Report TR-10-52. 462 p. ISSN 1404-0344.

STUK. 2013. YVL-ohje D.5 Ydinjätteiden loppusijoitus (in Finnish). Radiation and Nuclear Safety Authority, Helsinki, Finland. 19 p. ISBN 978-952-478-904-2.

Wersin, P., Kiczka, M. & Rosch, D. 2014b. Safety Case for the Disposal of Spent Nuclear Fuel at Olkiluoto - Radionuclide Solubility Limits and Migration Parameters for the Canister and Buffer. Posiva Oy, Eurajoki, Finland. Report Posiva 2012-39. 226 p. ISBN 978-951-652-219-0.

Wersin, P., Kiczka, M., Rosch, D., Ochs, M. & Trudel, D. 2014a. Safety Case for the Disposal of Spent Nuclear Fuel at Olkiluoto - Radionuclide Solubility Limits and Migration Parameters for the Backfill. Posiva Oy, Eurajoki, Finland. Report Posiva 2012-40. 166 p. ISBN 978-951-652-220-6.